FLEXIBLE STRETCHABLE ELECTRONICS FOR SPORT AND WELLBEING APPLICATIONS

Wolfson School of Mechanical, Electrical and Manufacturing Engineering

Loughborough University

This dissertation is submitted in partial fulfilment of the requirements for the award of Master of Philosophy

by

Jonathan Flowers

July 2019

I would like to thank my family for their relentless teasing until I finished my thesis.

I wouldn't have done it without you.

"Do or do not... There is no try."

Yoda

ABSTRACT

Wearable electronics are becoming increasingly widespread in modern society. Though these devices are intended to be worn, integrated into clothing and other everyday objects, the technologies and processes used to manufacture them is no different than those that manufacture laptops and mobile phones. Many of these devices are intended to monitor the user's health, activity and general wellbeing, within clinical, recreational and assistive environments. Consequently, the inherent incompatibility of these rigid devices with the soft, elastic structure of the human body can in some cases can be uncomfortable and inconvenient for everyday life. For devices to take the step from a 'wearable' to an 'invisible', a drastic rethinking of electronics manufacturing is required.

The fundamental aim of this research is to establish parameters of usefulness and an array of materials with complimentary processes that would assist in transitioning devices to long term almost invisible items that can assist in improving the health of the wearer. In order to approach this problem, a novel architecture was devised that utilised PDMS as a substrate and microfluid channels of Galinstan liquid alloy for interconnects. CO_2 laser machining was investigated as a means of creating channels and vias on PDMS substrates. Trace speeds and laser power outputs were investigated in order to find an optimal combination. The results displayed upper limits for power densities; where surpassing this limit resulted in poor repeatability and surface finish. It was found that there was an optimal set of trace speeds that ranged from approximately 120mm/s to 190mm/s that resulted in the most reliable and repeatable performance. Due to the complex nature of a materials variable energy absorption properties, it is not possible to quantify a single optimal parameter set.

To understand the performance of these devices in situ, finite element analysis was employed to model deformations that such a device could experience. The aims here were to investigate the bond strength required to prevent delamination, between the silicon-PDMS and PDMS-PDMS bonds, in addition to the stress applied to the silicone die during these deformations. Based upon the applied loads the required bond strengths would need to be at least ~65kPa to maintain PDMS-PDMS adhesion during these tests, while stress on the silicone-PDMS adhesion required an expected

higher ~160kPa, both of which are within the reach of existing bonding techniques that are capable of withstanding a pressure of ~600kPa before failure occurs. Stress on the silicon die did not exceed ~7.8 MPa during simulation, which is well below the fracture stress.

By developing knowledge about how various components of such a system will respond during use and under stress, it allows future engineers to make informed design decisions and develop better more resilient products.

ACKNOWLEDGEMENTS

CONTENTS

LIST OF TABLES

LIST OF FIGURES

LIST OF ABBREVIATIONS AND ACRONYMS

AC	-	Alternating Current
ADPL	-	ANSYS Parametric Design Language
AFM	-	Atomic Force Microscopy
ANT	-	Adaptive Network Topology
ASME	-	American Society of Mechanical Engineers
BHF	-	British Heart Foundation
BS	-	British Standards
CFD	-	Computational Fluid Dynamics
CNC	-	Computer Numerical Control
CNT	-	Carbon Nanotube
CPU	-	Central Processing Unit
CW	-	Continuous Wave
DC	-	Direct Current
ECG	-	Electrocardiography
ECTC	-	Electronic Components and Technology Conference
EEG	-	Electroencephalography
EGaIn	-	Eutectic Gallium Indium
EKG	-	Electrocardiography
EMI	-	Electromagnetic Interference
EN	-	European Norms
FCC	-	Federal Communications Commission
FE	-	Finite Element
FEA	-	Finite Element Analysis
FEGSEM	-	Field Emission Gun Scanning Electron Microscope
FPCB	-	Flexible Printed Circuit Board

FR4	-	NEMA grade for glass-reinforced epoxy laminate material
HCl	-	Hydrogen Chloride
HDI	-	High Density Interconnect
HSFLD	-	Hydrostatic Fluid
IBM	-	International Business Machines
IC	-	Integrated Circuit
IEC	-	International Electrotechnical Commission
IEEE	-	Institute of Electrical and Electronics Engineers
IMEC	-	Organization for R&D in nanoelectronics and digital technologies
IP	-	Ingress Protection
IPC	-	Institute for Printed Circuits
ISO	-	International Organization for Standardization
IoT	-	Internet of Things
MADPL	-	Mechanical ANSYS Parametric Design Language
MIT	-	Massachusetts Institute of Technology
NEMA	-	National Electrical Manufacturers Association
NHS	-	National Health Service
Nd:YAG	-	Neodymium-doped Yttrium Aluminium Garnet
PCB	-	Printed Circuit Board
PDMS	-	Polydimethylsiloxane
PEDOT:PSS	-	poly(3,4-ethylenedioxythiophene) polystyrene sulfonate
PMMA	-	Poly(methyl methacrylate)
PPG	-	Photoplethysmography
PZT	-	Lead Zirconate Titanate (Pb[Zr(x)Ti(1-x)]O3)
R2R	-	Roll to Roll
RF	-	Radio Frequency

RIE	-	Reactive-Ion Etching
RoHS	-	Restriction of Hazardous Substances Directive
SEM	-	Scanning Electron Microscope
SMD	-	Surface Mount Device
SMT	-	Surface Mount Technology
TFT	-	Thin-Film-Transistor
UK	-	United Kingdom
UL	-	Underwriters Laboratories
US	-	United States
USA	-	United States of America
UV	-	Ultraviolet

LIST OF APPENDICES

1 INTRODUCTION

1.1 Foreword

In recent years, the general populous has become more connected than ever, with the inception of smart watches and fitness trackers. Their recent boom in popularity has furthered the need for new manufacturing and design processes to allow the creation of devices that are not physically invasive or bothersome during day to day wear. To achieve this transition from "wearables" to "invisibles", new materials and production processes must be utilised, electronics need to go from hard and rigid to soft and conformal.

Creating truly conformal electronics poses many challenges that are vastly different from those faced by rigid systems, however, these new conformal devices need to be capable enough to lose no functionality when compared to their rigid siblings. Care must be taken to reference relevant physiology in order to correctly analyse use cases and possible sensor requirements thus creating a substantial definition of the problem.

1.2 Problem Identification

The world of electronics today would be completely unrecognisable to the pioneering engineers like Thomas Edison, who began experimenting with thermionic vacuum tubes in the late 19th Century [1]. Engineers have progressed

from measuring the size of components in centimetres to requiring electron microscopes to measure nanometre scale transistors. In the process computers have transitioned from top secret codebreaking machines during World War II [2] to the warehouse sized computers of the space program [3] finally reaching the ubiquitous portable computers that we all carry around in our pockets today. These marvels of modern computing are now worn on our wrists or carried in our pockets which allow us to stay connected to the wider world, providing us with on demand entertainment, schedule our time and act as a source of knowledge. In addition to all the data that are sent to the device, they also record and monitor a wide range of data points. The ability to continually monitor our physical activity levels, heart rate, sleep levels and more, gives us great insight into the health of our populations, especially when these data are paired with machine learning and 'big data' analytics [4], [5]. Chronic diseases such as hypertension, diabetes, cardiovascular disease and chronic obstructive pulmonary disease account for nearly 70% of the total spend on health and social care in England [9]. Fortunately, most of these chronic diseases can be averted with simple lifestyle changes such as eating healthily and being physically active [10], [11]. However, the current paradigm of telling the public to be physically activity "today" in order to reduce the risk of acquiring a chronic disease "tomorrow" (i.e. later in life) does not appear to be working [12]. Indeed, the prevalence of physical inactivity in England is thought to be ~95% [13]. Not being able to see the "return on their investment" in the short term, people may lose motivation for their active lifestyle efforts [14], [15]. According to current research, the ability to show how behaviour is directly affecting immediate health may be the solution to reducing the burden of chronic disease [6], [7]. However, implementing this as a form of treatment or strategy for prevention on a large scale is currently infeasible.

Miniaturisation and cost reduction of electronics has been the natural direction of progress for many years, moving from the large devices that were delivered on trucks, to becoming functioning computers that are given away on the front of

magazines for free [8]. This cost and size reduction has spawned the Internet of Things (IoT) boom, where everything now contains a computer, including the devices people wear. In order to further this ubiquitous adoption of technology the devices that people will need to able to conform to the users' needs and body. Corporations such as Nokia have produced concept designs for such devices [9] before the underlying technology was even proven possible. It was proposed by *Park et al* that miniature non-invasive wearable sensor platforms would be the future of long term clinical monitoring [10]. The key to making these technologies viable lies in making the devices soft, conformal and comfortable for long term wear/use.

The current technologies in this space are too large, obtrusive, invasive, expensive, and/or discretised. Wearables companies are currently attempting to solve some of these problems, however, the devices they produce tend to be limited in what they can monitor and are often not comfortable to be worn all the time. This presents an opportunity for the surging wearable technologies sector to evolve towards the less explored area of "invisibles". An idea that the device a user wears is completely integrated and unnoticeable, during their day to day activities. This could be systems integrated into their clothing, or a lightweight patch with hybrid physiological and behavioural health sensors that could be worn invisibly, continuously would allow a wearer to understand how their lifestyle behaviours (positive or negative) impact their immediate (i.e. acute) health. More specifically, such a hybrid sensor would provide the wearer with acute (i.e. potent) bio-behavioural feedback that may be more motivational in terms of lifestyle behaviour change.

These new disruptive technologies would help catapult healthcare from being centred around hospitals and GP offices into a ubiquitous healthcare environment where personalised data may engage the public to self-monitor and self-manage their own health. By placing onus on the user for their own health and showing

immediate effects of their behaviour on their body, it could motivate them to change and make more informed decision on things like diet and exercise for instance. Especially that it has been found that information alone is unlikely to motivate behavioural change, but being given autonomy to do this could very well achieve this [11].

Developing medical technologies is incredibly expensive [12]. This is due to strict regulation and testing requirements. The technologies can however be developed and marketed towards the health and fitness markets, where standards are much laxer than that of the medical world. This initial market entry point could then be used to bridge the gap between health and wellbeing in the consumer market and the clinical bed space. The current level that athletes compete at is pushing the human body incredibly close to its physical limits [13]. This means that nutrition; training and behavioural programs are becoming highly optimised to the individual, but are generally being done without metrics and feedback from the athletes [14]. This is often due to the expensive nature of the required equipment and the inability to monitor the athlete during peak performance on the field or track. The monitors that are used have been developed as event monitors, as in they are designed for specific points when they will be looking for a specific behaviour. This creates a void for a technology that can become a "life monitor", by monitoring vital signs during events, but also during normal every day activities, which is especially important when looking at athlete recovery. There have been some examples where on body monitoring is beginning to work its way into completive sport, such as Riddell's InSite concussion monitoring system [15], [16] and heart rate monitors used by runners and cyclists [17]. These however still give very limited insight into the athlete's physiological state.

In order to achieve any of the advancements required for long term, comfortable devices, electronics manufacturing and design must take a fundamental shift within many of its processes and material selections when it comes to the PCB. Current

electronics that are manufactured on fiberglass or even Kapton based substrates are unable to deform [18] very much, especially when the deformations are large and repetitive as would be required to conform to the human body. Both the flexibility and stretchability of current systems need to be drastically improved to achieve the transition from "wearables" to "invisibles".

Attempts have been made to transition to the "invisibles" category of technology by companies such as mc10 [19]–[21], however their approach creates expensive to manufacture and slow to bring to market devices, which have prevented the fast and ubiquitous uptake that is normally seen with consumer health monitoring devices. The biggest issues that face many of these emerging technologies, is the approach that seeks to replace conventional silicon foundry processes, which as of writing is the most ubiquitous technique used to manufacture integrated circuits. These new processes often produce devices with lower transistor density and thus increased power consumption [22], when compared to their silicon equivalents.

Many of these new and novel devices may be relatively performant within the scope for which they were designed, however cost is a large factor in how effectively these devices can be utilised in a commercial setting. Almost all of these processes utilise many manual steps (for which automation would be difficult) to manufacture these devices. This makes them unsuitable for any kind of manufacture at scale and thus maintains a high price per unit. The use of batch processes can increase the yield of these manufacturing processes, however, a manufacturing method that utilises continuous manufacturing processes would be optimal.

Devices that can monitor vital signs and health metrics of a person, while being almost invisible and able to be purchased at super low cost require developments to be carried out across manufacturing, design and materials. The new technologies should be able to take advantage of existing design tools and off the shelf discrete components. To achieve this a paradigm shift in design methodology and approach to the assembly and materials structure will need to be developed and researched.

1.3 Research Aims and Objectives

Research into manufacturing methods and the required materials to create soft conformal electronics is being carried out globally by various institutions and corporations. However, many of these processes look to "reinvent the wheel" in reference to the manufacture of integrated circuits, rather than leveraging conventional silicon-based manufacturing processes. Some work into the utilisation of existing technologies has been carried out, however very little has been done to investigate scalability and cost reduction of any of these processes or design concepts.

The project objectives are to investigate the following:

1. Identify a group of materials and techniques that are capable of producing flexible, stretchable electronics at commercial scales and at low cost.
2. Identify the limitations of these materials during use and manufacturing processes.

This project aims to develop a body of knowledge that can be leveraged to create flexible, stretchable electronics at commercial scales for a variety of applications. It aims to write the rules that underpin both design considerations and limitations that bound system design and manufacture, thus enabling commercial applications to develop products through utilisation of this research.

This thesis gives an evaluation of the current market trends and the direction wearable technologies are looking to take in the future, going on to evaluate the various technical challenges required to bring advanced wearables and invisible devices to market . Through this, developing parameters of usefulness, which can be used to focus the research of such devices and understand the requirements that would drive these designs. These parameters were used to develop a set of experiments. The first was to develop a method of manufacturing prototype devices. This approach sought to investigate the use of a CO_2 laser to cut millimetre scale channels into a PDMS substrate. The second study looked at selecting an

appropriate bonding method for PDMS lamination and load distribution into silicon integrated circuits through the use of finite element analysis.

2 BACKGROUND

2.1 Introduction

This project is one that covers a large range of disciplines that range from the manufacture of electronics to human physiology and behaviour research. These topics may be discrete, but the successful manufacture of systems that are able to seamlessly integrate into the life of the user requires true understanding of both the device's environment and use.

2.2 Physiology

Initial research conducted into the work being carried out at Loughborough University's National Centre for Sport and Exercise Medicine helped to create an insight into why all the other sensors used by the group have failed to meet the needs of both researchers and clinicians. After consulting with clinicians and researchers at other institutions, such as Joey Eisenmann at Michigan State University in the US, there are currently no systems on the market that are capable of long term, non-invasive, unobtrusive vital signs monitoring. The requirements from the literature allow a stage to be set for some of the applications for the technology, thus aiding the creation of increasingly specific specifications and requirements for technologies that are researched throughout this project.

Physical inactivity is a problem that is drastically affecting both the UK economy and healthcare system. Physical inactivity accounted for nearly 10% of all deaths worldwide in 2008. This huge number is due to physical inactivity being a large contributing factor that leads to coronary heart disease, colon cancer, breast cancer, type 2 diabetes and premature all-cause mortality [6]. Each of these individual conditions occur more in the UK when compared to the global average. These are

all cases that likely could have been prevented through physical activity. In 2007 Cycling England (UK, disbanded 2011) published figures stating that over £240 million could be saved annually if cycling trips increased by just 20% [23] with another study published in 2012 stating that if the levels of walking doubled the NHS (National Health Service, United Kingdom) would see savings of over £20 billion over the next 20 years [24]. However, a study carried out in 2008 indicates that the population within England generally spends far too much time in sedentary pursuits. In addition to this, "32% of men and 60% of women were not fit enough to sustain walking at 3mph up a 5% incline (i.e. they would require severe or maximal exertion, and were classified as 'unfit')." [25]. This just demonstrates the scale of the problem within England as studies have been carried out that show an increased risk of suffering from non-communicable diseases with physical inactivity. The research estimated increases in the life expectancy in some regions of up to 0.95 years [26]. The Department of Health for England has looked at methods for improving the health and wellbeing for people with long term conditions and found that implementing self-care and behavioural interventions are some of the best ways to treat these conditions [27]. This lines up perfectly with the work being done at Loughborough University's Physical Activity & Public Health Research Group [28]. The health benefits of physical activity have been relatively well documented by multiple groups. These benefits include the prevention of multiple different diseases that include cancer and diabetes [7], [23]. In addition to the physiological benefits there have been multiple studies showing that psychological health is also improved through physical activity [29].

There is one major barrier to using physical activity as a method of treatment. This is the issue of motivation. In order to motivate a person to begin exercising regularly and being active in order to treat these conditions requires a certain amount of persuasion which, at the moment is often done with a behavioural intervention [11]. These interventions need to be carefully constructed in order to motivate the patient into beginning physical activity and convincing them that physical activity will

improve their condition. This has been seen to be even more difficult when using physical activity and behaviour change as a preventative measure [30], [31].

This research into physiology can be utilised as a guide for the capabilities such a device requires and some very real applications that have a need for the technologies being researched within this project.

2.3 The Current Market

There are various research labs and universities all over the world developing flexible electronics each with their own strengths and weaknesses. The main protagonists in this field are MC10 (MC10 Inc, MA, USA), a US company based out of Lexington, Massachusetts, who are currently deemed the market leader and IMEC (Leuven, Belgium) who are currently working to develop various technologies as part of the BioFlex Project. However, as of the time of writing, there are no commercial processes that produce truly flexible and stretchable electronics. When information is released by one of these labs or universities it is usually quite sparse or lacking specifics. Researchers at the University of Massachusetts Amherst are currently developing a patch-based sensor that is designed to gauge stress and fatigue in military personnel [32]. Their processes seem to be investigating printing electrics onto a flexible substrate. From the images provided it seems their attempts are looking at printing the transistors directly onto the substrate. The research is very likely many years from any kind of viable product as tool acquisition is still being carried out and the facility is still in its early stages [33]. The capabilities of the sensors themselves seem to be a lab on chip style device that will be monitoring compounds in the wearers sweat.

The current industry leader for truly stretchable, flexible conformal electronics is MC10. This is a company that has been generating a lot of marketing excitement with their only commercial product being the CheckLight. The CheckLight uses conventional flex-PCB manufacture which is neither new or innovative [34]. The

technologies that they are looking to commercialise are what they call "digital tattoos" which creates very thin, flexible and stretchable electronics [20]. These tattoos however are structured by using very thin three-dimensional or two-dimensional self-similar gold interconnects between every component, down to the individual transistors. The manufacturing methods required to produce these components are incredibly complex and require vastly different tools and processes when compared to the standard methods used currently by the semiconductor industry [19], [20]. MC10 have currently patented the use of electronics that use self-similar serpentine interconnects to monitor tissue condition using two electrodes [35]. This does not detail what data the technology is capable of recording from the skin.

The two organisations mentioned above seem to be some of the biggest players in the field of stretchable conformal electronics, even though both are many years from a commercially viable product that takes advantage of their respective technologies.

2.4 Flexible Technology Designs and Concepts

In order to create a flexible and stretchable piece of electronics it will need to be assembled from multiple components that all perform differing functions and therefore have vastly different packaging requirements. This section on designs and concept work has been further subdivided for the reasons stated above. However, certain aspects such as the design of antennae or sensors themselves are not within the scope of the project but must still be investigated due to a requirement for their integration into a final unit and compatibility with the manufacturing processes used.

In order to realise a device that can be both flexible and stretchable, technologies will have to be developed in a variety of fields. In order to correctly identify what these fields are, a system overview has been outlined. This block diagram breaks down a possible device into a subset of components as can be seen in Figure 2-1.
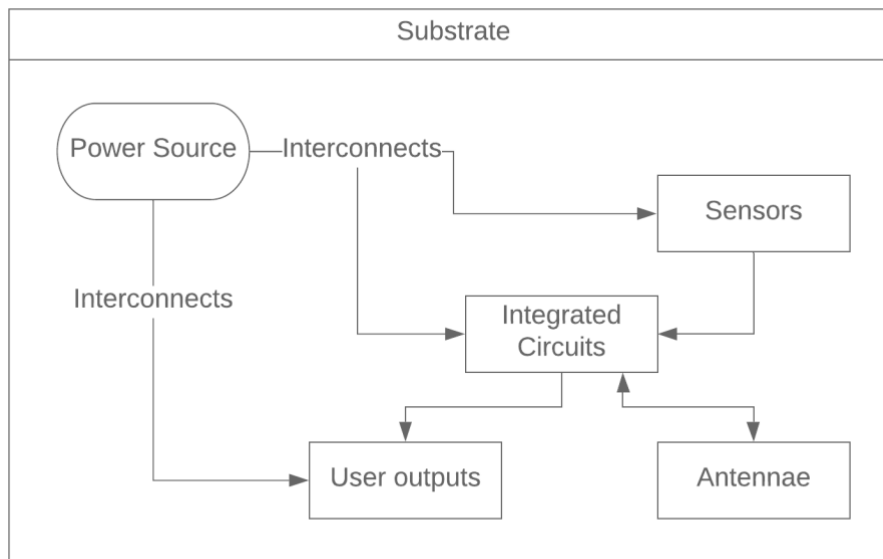
Figure 2-1 Block diagram of an example device

The design of such a system does not end with the device. The correct selection of manufacturing processes are vital to creating a cost effective end product. The processes and flow used to manufacture a device would be vastly different depending on the final design of the system. Each section of the literary review below investigates a section of the block diagram above or a manufacturing process that could be used for one of these devices. All these however must be firmly grounded with the final application in mind. It is therefore important to keep in mind both the physiological applications and use cases in addition to the current market as this research moves forward.

2.4.1 Antennae Design

Even though the design of the actual antennae and RF testing are outside the scope of the project, it is important to be aware of possible designs and use cases as the sensors that are manufactured will require wireless communication with other devices. This means that antennae design must be investigated to ensure

manufacturing processes are compatible with most design and manufacturing methods used for antennae.

There are a wide variety of designs for different kinds of antennae, however many of these are not suited to being flexible. However, research being carried out has been looking into the use of liquid metal alloys in order to create flexible and stretchable antennae. Work carried out by *Cheng et al*. at Uppsala University developed a 2.4GHz unbalanced loop antenna. The team used Galinstan alloy embedded in PDMS to create the antennae, which allowed it to be stretched multi-axially during operation. The team managed to achieve efficiencies of 98% when not stretched and the lowest value during a 40% stretch was 84% efficiency when transmitting at 2.4GHz [36]. Attempts have also been made at developing micro strip patch antennae; however, their efficiencies are much lower than those of the unbalanced loop antennae. The more interesting part of the paper is the use of a series of small PDMS posts in order to create a large area void within the PDMS, which could be used on other applications [37]. Some have used liquid metals to create tuneable antennae that can change their resonant frequency by physically changing its dimensions [38]. However, this would be quite difficult at microfluidic scales due to the use of pumps, which due to Galinstan's viscosity would need to be relatively powerful. Once these antennae are built and attached or inserted into the human body their behaviour will be dramatically different than in air. This is due to impedance mismatch and detuning because of frequency shifts caused by the electrical properties of tissues and structures within the body [39]. The work carried out by *Vidal et al*. investigated using various simulations to quantify this behaviour creating an understanding of how antennae will behave and how performance will be affected, thus allowing the design to account for these caveats. Even though the sensor designs being discussed in this report are non-invasive, the dielectric properties of the tissues could have an effect on antennae performance. This behaviour has had mixed opinions on its effect on transmittance when the antennae

is the skins surface [40], [41], therefore further investigation will be required for the specific use case.

2.4.2 Experimental Production Methods

There is a huge amount of research being carried out in novel production methods for flexible and stretchable electronics; however, some of these are far from being ready to be integrated into a production let alone having functional prototype devices built. Some of these methods will be discussed below.

Savagatrup et al. have been investigating the use of various novel materials for use in molecularly stretchable electronics. The materials were classified and then organised into three distinct groups:

- "Random composites of rigid structures sitting atop or dispersed in an elastic matrix" [42]
- "Deterministic composites of patterned serpentine, wavy, or fractal structures on stretchable substrates" [42]
- "Molecular materials, non-composite conductors and semiconductors that accommodate strain intrinsically by the rational design of their chemical structures" [42]

The investigations completed are very interesting and show promise however, the balance between electrical and mechanical properties has not yet been reached. The technologies are also yet to leave the lab for testing or production.

Other researchers are attempting to use conventional materials, with novel processing techniques. One example of this is *Kim et al.* who is looking to use silicon, gold and other standard materials from the semiconductor industry. The team used transfer printing in order to retrieve material layers and bond them to the required substrate; this method allows the creation of three-dimensional structures, which is especially useful for the self-similar interconnects, which allow the electronics to stretch [43]. However, the performance of the parts produced through these

techniques are heavily lacking when compared to commercially available silicon products. This group seems to be part of MC10.

Another group that seem to be taking a similar approach is the one lead by M. Kaltenbrunner at the University of Tokyo. The group are using a series of layered foils and post-processing steps such as vacuum evaporation and chemical vapour deposition to produce systems that are less than 10μm thick [44]. This makes these systems extremely flexible, but not stretchable. In order to solve this problem, they apply the prefabricated foils to a pre-stretched polymer substrate, which then relaxes creating fine creases in the material. This method has its limitations however, as once the original amount of strain is reached on the substrate, the foil will then have a high load placed on it, making it relatively brittle. In addition to this, it requires all design to be carried out at the transistor level making the implementation of such designs difficult and expensive.

Some proof of concept work has been done with carbon nanotubes to create electronics that are both flexible and stretchable [45]–[47]; however, there are no production facilities that exist which are capable of manufacturing CNT based electronics as can be seen in Figure 2-2. This is due to it being a very young technology that needs to mature before it can be used in commercial systems.
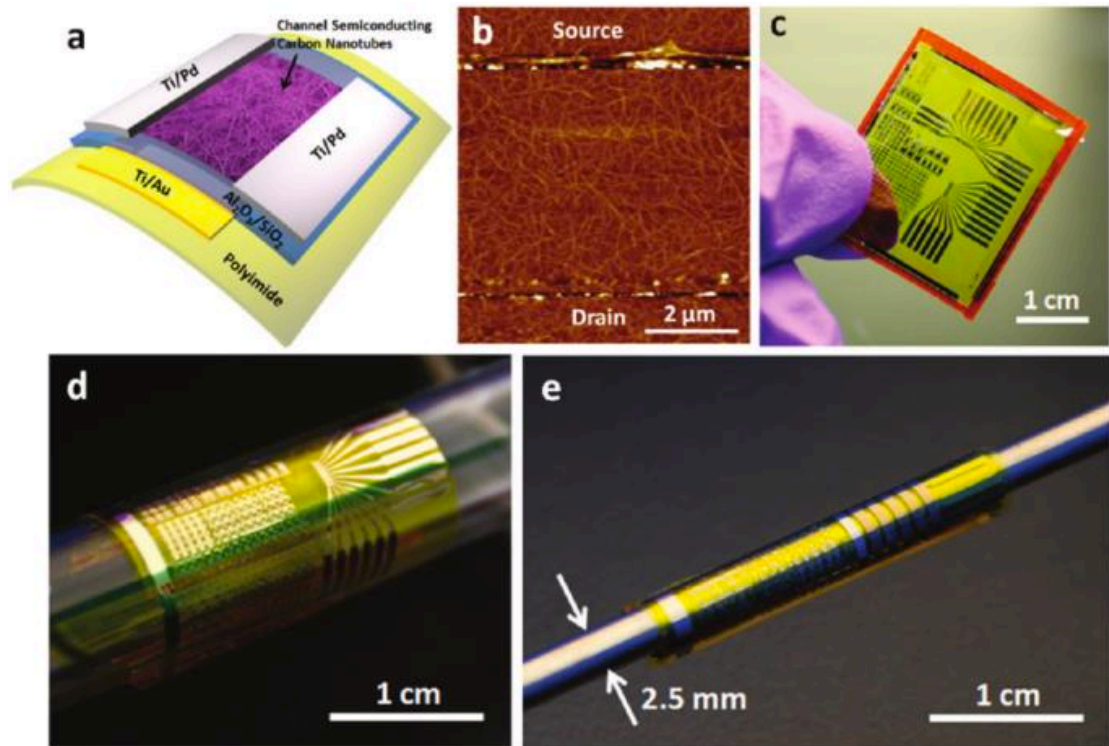
Figure 2-2 Flexible thin-film transistors and integrated circuits using semiconducting carbon nanotube networks. (a) Schematic diagram of a local- gated nanotube TFT on a flexible substrate. (b) AFM image showing the channel of the flexible nanotube TFT, which consists of random networks of semiconducting carbon nanotubes. (c) Photograph of a flexible nanotube circuit with a size of ~2.5 × 3cm². (d,e) Photographs showing the extreme bendability of the flexible nanotube circuits, where the samples are being rolled onto a test tube with a diameter of 10 mm (d), and a metal rod with a diameter of 2.5 mm (e) [46].

One large problem that many of these experimental production methods face are that they are currently unable to match the reliability, speed, density and power efficiency of electronics produced on silicon.

2.4.3 Microfluidics

Microfluidics are incredibly important for any kind of biosensor application due to the need for carrying fluid samples and reactants around the system. Microfluidics

can also be used to carry conductive fluids, which can allow the creation of stretchable and even self-healing wires [48]. Having the ability for the conductive material to heal itself in the case of damage is important for the longevity and reliability for the systems as they are likely to be used in environments that are not stable or forgiving, such as on the body during extreme sports. This means that if a section of the device is overstrained which causes a break in the wire, as soon as the strain is released, the wire will reconnect, restoring conductivity along the wire [49]. Microfluidic channels are normally created by etching or forming the substrate and filling the channels as a secondary step. However another method proposed by Fassler and Majidi is to freeze cast interconnects with the use of moulds then form the substrates around them [50]. This method can however lead to some issues with thermal expansion that are not discussed within the paper. This may also be difficult to implement with a scalable production process due to having to move delicate structures at temperatures below -20°C.

Work carried out by *Hu et al.* at the University of Illinois Urbana-Champaign investigated the use of liquid metal in order to create super flexible interconnects. They used a PDMS and CNT blend in order to create a conductive polymer that acted as a temperature and pressure sensor in addition to a strain gauge. These were then connected with microfluidic channels of Galinstan, which allow the system to be exceptionally flexible, getting close to the mechanical properties of skin. The Young's modulus for the system was measured to be between 0.36MPa and 0.87MPa at 200µm thick, which when compared to human skin is in a similar range (0.1MPa – 1.1MPa at 200µm) [51] as can be seen below (Figure 2-3).
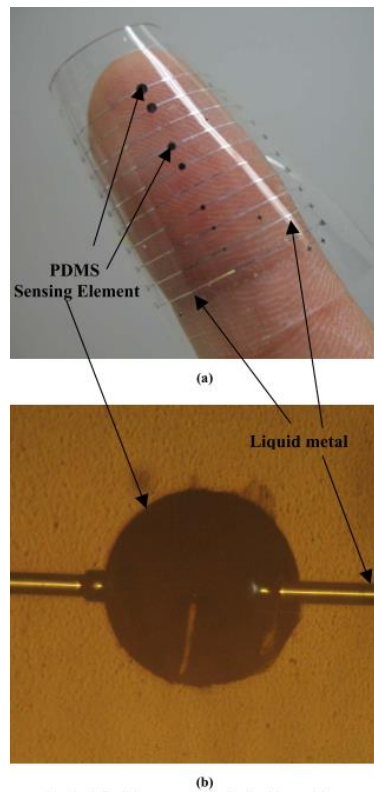
Figure 2-3 (a) Final flexible sensor skin (b) liquid metal in contact with PDMS sensing element in optical microscope (x5 magnification). [51]

The use of Galinstan within microfluidic channels presents a problem, which is the ease at which Galinstan produces an oxide layer on its surface. One possible solution to this problem is the use of an HCl solution, which reduces the Galinstan oxide layer to a more manageable level that makes the material easier to work with [52]. *Li et al.* have been working on this, whereby they have identified issues that Galinstan has for microfluidics, which are mostly due to the almost instantaneous oxidation process that occurs, creating a substance that will wet to almost any surface. Concentrated HCl is used to combat this by preventing the formation of an oxide layer. In order to improve flowability of the Galinstan in microfluidic applications, HCl is run through channels along either side of the Galinstan within the PDMS, thus allowing the HCl to diffuse through and prevent an oxide layer being formed when coming into contact with the PDMS. This may not be practical in complex designs

but a solution that utilises HCl may be found to allow easier filling of Galinstan filled channels.

Another interesting method of manufacture investigated by *Koh et al* [53] is the use of Galinstan as a filler for PDMS. The loading of liquid Galinstan throughout a cured polymer instead of more common conductive solid particles, such as nickel enables the creation of flexible polymer composites without much effect to the cured modulus of the material as can be seen in Figure 2-4. This technique shows promise, allowing loading of up to 70% volume of conductive material. However, it is yet to be seen if by loading PDMS with Galinstan will protect other contact metals from the effects of liquid metal embrittlement.
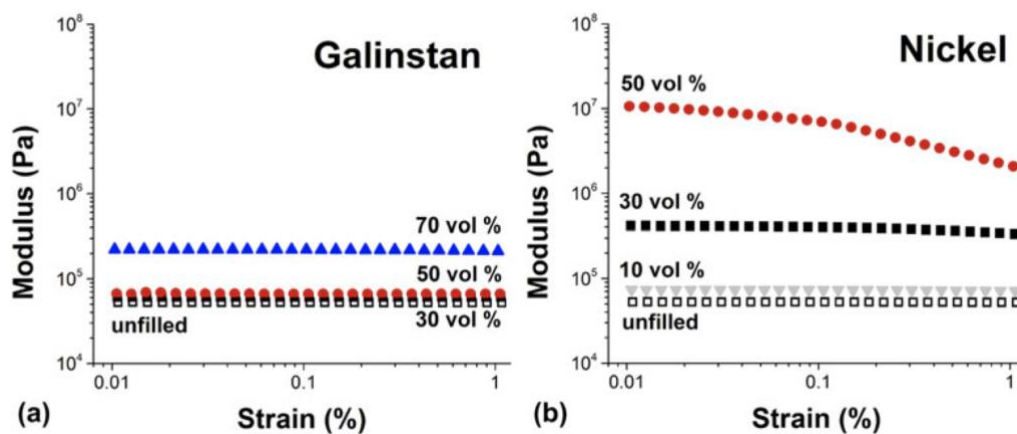
Figure 2-4 Strain-dependent storage modulus obtained at 1 Hz for various concentrations of (a) Galinstan and (b) nickel particles dispersed in V41: T11 PDMS.

2.4.4 Power

The design of batteries and various energy harvesting devices is not covered within the project itself, however, they are a requirement for a wireless sensor and thus investigations into viable power methods and how they could be integrated is required.

All electronics require a power supply of some sort in order to function. The types of power supply can be separated into three groups;

- Energy harvesters that are essentially some kind of power generator that passively generate electricity for the system from the environment.

- Energy storage, which is normally referred to as a battery, which is charged before use or it may generate energy actively through a chemical reaction.

- Hybrid energy storage; this would include both an energy harvesting system and an energy storage solution. This hybridised setup can allow the use of smaller energy harvesting systems in order to increase the longevity in order to increase battery life.

Due to the requirements for this system, multiple solutions may have to be combined in order to maintain the small scale and flexibility of the system. Thermoelectric generators seem quite attractive for on-body sensor systems as they can take advantage of the temperature differential that exists between the skin and the environment. Flexible thermoelectric generators are under development by multiple research groups. One approach, which may be suitable for flexible substrates, taking advantage of co-sputtering to lay down conductive and semi-conductive thin films [54]. However, the efficiencies of these generators are currently quite low. The other approach used various screen-printing techniques to lay down the conductive materials onto a glass fabric. This produced very high quality and efficient generators, achieving a power density of 28mW g-1 [55]. However, due to the use of a glass fabric, these generators would not be capable of stretching at all. The stretch that is applied to the device could also be used to generate power. The use of a printed PZT layer onto PDMS substrate can act as a kinetic energy generator. These generators can be up to 80% efficient [56], but are still in the early stages of development and there is still a lot of classification work to do, in addition to integrating systems to utilise the generated power. A demonstrator of this power generation technology can be seen below (Figure 2-5).

Figure 2-5 Demonstration of band-type flexible TE generator for harvesting thermal energy from human skin: (a) photos of band-type flexible TE generator and (b) electricity generation measured on human skin at an air temperature of 15 ℃. Scale bar, 1 cm. [55]

One of the main problems with the use of batteries is that lithium-based batteries normally require the use of a liquid or gel electrolyte to function efficiently. One approach is to contain the gel within the layers of the battery creating a flexible stretchable battery by creating a matrix of small batteries that are connected using self-similar interconnects [57] in ways reminiscent of the technologies used by *Choi et al* [58] for their laminated heating elements. These batteries achieve very good power and energy densities because they are fundamentally a standard lithium-ion cell [57]. Other methods involve brand new system and even chemistry designs. One such example is the creation of a 3D thin-film battery that is created on a perforated substrate in order to increase the available surface area. This battery uses a Ni cathode current collector, a MoO_yS_z as well as a hybrid polymer electrolyte and a lithiated graphite anode. This cell design achieved a capacity of $2mAh/cm^2$, which is about thirty times greater than that of a similar cell using only a two dimensional structure [59]. This technology appears to be very promising, however it is yet to leave the lab and enter production.

Another interesting power generation method being researched by *Yang et al*, whereby liquid Galinstan is used as an electrode in what they refer to as a Liquid Metal Triboelectric Nanogenerator. The team created a triboelectric nanogenerators in a range of geometries such as pads, bracelets and macroscopic woven structures. The material makeup of these generators utilised PDSM or silicone polymers to encapsulate the devices and claimed a total power output of up to 8.43W/m^3 [60], possibly making these devices appropriate for low power on body sensors. However, a major drawback of these generation systems is their inability to provide continuous power, thus being relegated to that of a battery or capacitor charging system.

2.4.5 Stretchable System Design

There are a variety of ways to create a stretchable system; however, these require modifications to the concepts that are currently employed in the design of electronics.

There seem to be two approaches to this. The first is targeted towards smart textiles, where the electronics are designed so that they can easily be integrated into woven fabrics and clothing. Work being done by *Jang et al.* looks at embedding electronics directly onto stretchable fabrics in order to create breathable electronics. The design uses serpentine interconnects made of copper, which mean that when the material is over stretched it experiences plastic deformation [61], which can lead to breakages, and thus a relatively short lifespan for the system meaning this can cause reliability concerns for more complex designs. In addition, the production method used is completely novel and thus will be very expensive to roll out for large-scale production, especially due to the use of techniques such as reactive-ion etching and requiring manual retrieval of the produced electronics from the glass substrate.

Another group at IMEC is researching the use of serpentine interconnects using conventional fabrication methods, which is very low cost but does not create a truly

flexible system. Electronics are integrated into clothing by stitching and encapsulating in a polymer in order to improve strength and reliability by protecting the fragile systems. The designs use packaged SMT ICs and requires an FR4 Stiffener under each IC to prevent pad separation [62]. A very similar project is being carried out at Ghent University, which uses the idea of creating stretchable electronics by placing non-stretchable components in a 'stretchable matrix'. This method specifically uses standard PCB manufacturing technologies; however, it is all done at macroscopic scales, therefore creating very large structures and systems.

The interconnects used are 'horse shoe shaped' meanders made of copper as can be seen in Figure 2-6, however the team realised these were not reliable and tried to overcome this by using multiple tracks running in parallel. The problem still exists due to plastic deformation occurring within the copper [63]. A similar work, but at a smaller scale is being done by *Jahanshahi et al.* who are doing this without the FR4 backing but then embedding everything within a polymer, such as PDMS for full encapsulation [64]. This faces the same essential problems as all the other groups that are using serpentine interconnects.
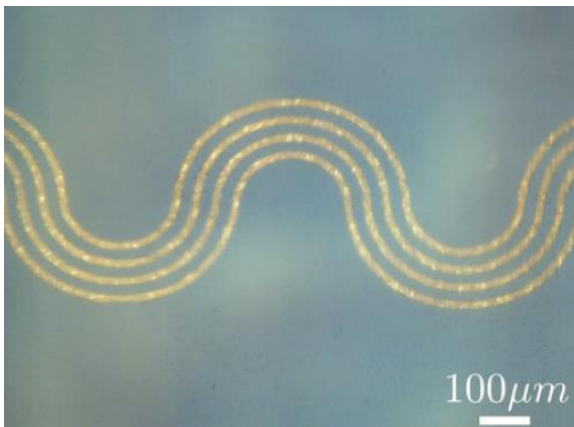
Figure 2-6 Optical microscope images of the fabricated multitrack meanders are shown. The hazy background is due to the tracks being embedded in PDMS [64]

The use of serpentine interconnects seems to be quite popular with multiple research groups [57], [65], [66].

One such group led by *Fan et al.* is looking at the use of fractals for the track shape. This allows the use of solid metals and other materials as conductors but complex manufacturing methods are required in order to produce these [65]. Increases in resistance due to extended length of self-similar serpentine wires are a problem which then requires duplication of connectors and reduces the current capacity of the interconnects. The chance of failure also increases to the creation of stress points within the materials during stretching. Due to the shapes used, it will not produce a true multi-axial stretchable solution.

One of the most interesting concepts that achieved multi-axial stretchable and flexible electronics is a concept developed by *Zhang et al*, using liquid metal interconnects with a bare silicon die [67], [68]. The metal used is a eutectic Indium-Gallium alloy, which has a melting temperature point of -19°C [69], which means that the device will remain stretchable and flexible over almost all conditions where a human would be able to function. This makes it perfect for biosensor applications as can be seen in Figure 2-7, in addition to the fact it is non-toxic, unlike mercury. This design creates flexible and stretchable electronics without the need to reinvent semiconductors, allowing a lower cost to manufacture. It also allows the integration of microfluidic lab on chips due to it being based on existing microfluidic technologies. The use of existing silicon components is very likely possible; however, this was not investigated in the paper and neither was the interaction between the Galinstan and the pads on the silicon die.
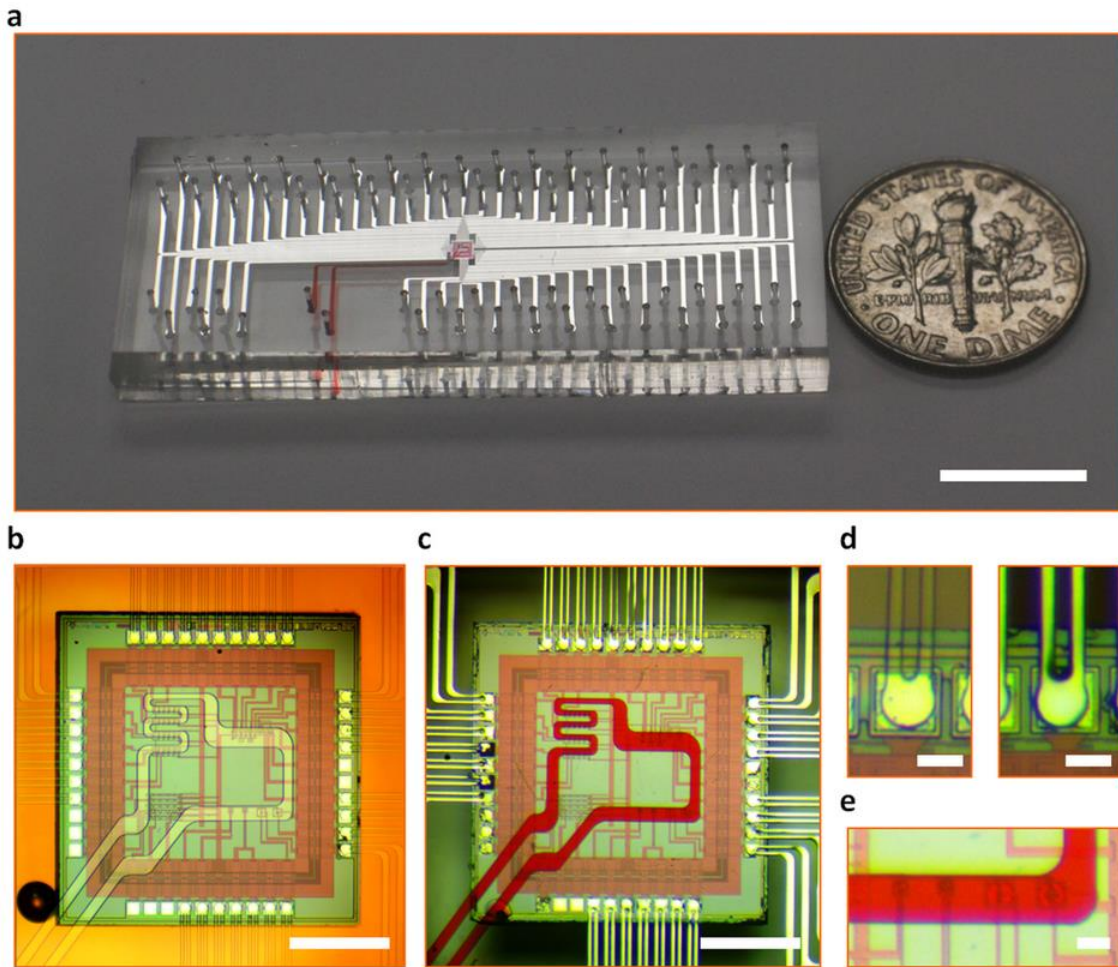
Figure 2-7 (a): Optical image of the packaged CMOS/microfluidic integrated system. (b) Optical micrograph showing the microfluidic channels are aligned with CMOS pads and sensors. (c) Optical micrograph showing the interconnect channels are filled with liquid metal and the microfluidic sample delivery channel is filled with red food dye. (d): Optical micrograph of an interconnect channel aligned with a CMOS contact pad before (left) and after (right) liquid metal is injected. (e): A microfluidic channel is accurately aligned with the sensor area. Scale bars: (a) 1 cm; (b) 500 μm; (c) 500 μm; (d) 50 μm; (e) 50 μm. [67]

2.5 Materials and Processes

The materials used to construct these systems are hugely important. They need to be selected in such a way that allows the system to be flexible and stretchable while maintaining durability. Additionally, because of the biomedical and athletic applications, any exposed materials must be biocompatible as well.

To contain all the systems, a suitable substrate is required, and the stringent requirements narrow the selection of available materials quite substantially. PDMS is an optically clear silicon based polymer [70] that has similar mechanical properties to human skin [51] and is both widely used in the electronics industry[56], [71]–[73] and biocompatible [64], [74], [75]. It also has the ability to be shaped with extremely high precision and is non-reactive making it useful for lab-on-chip and microfluidic applications [52], [67], [71], [76]. The optical clarity of PDMS also makes it suitable for optical applications, which can decrease the cost and overall size of lab-on-chip solutions [73], [76]–[78]. This makes it an excellent material choice. Other materials such as PMMA have similar properties, but unfortunately have a considerably higher Young's Modulus than PDMS and especially when compared to human skin [66], [79]–[81] making them unsuitable for on-body conformal electronics.

Hydrogels open up a new range of possibilities for substrates and device form factors. They are a network of hydrophilic polymer chains in which the dispersion medium is often water. They can be made of either natural or synthetic polymers allowing them to be biodegradable and even conductive for uses in ECG and EEG electrodes [82]. They are extremely absorbent, taking in as much as 95 wt% water [83].

Recent developments within the realm of tough hydrogels has enabled a research group within MIT to create a 'smart band-aid' which is capable of sensing temperature of a wound and based on this information dispense drugs which diffuse through the hydrogels [83]. In order to create the hydrogel substrate various

polymer networks were created within a range of dissipative polymer networks to form the hydrogel as can be seen in Table 2-1. Certain types of hydrogel have been shown to have fracture strengths of over 17MPa [84]. However, as tough as and pliable that hydrogel is, it has a single drawback that makes its use for electronics extremely challenging. Hydrogel is normally between 73wt% and 95wt% water, which means that any electronics or even interconnects must be completely encapsulated in order to prevent liquid ingress within components and short circuits from interconnect to interconnect in addition to shocking the wearer. Another issue is due to the porous nature of these hydrogels, liquid conductors cannot be used. This means any interconnect systems must utilise self-similar serpentine or fractal patterns to prevent breakage when stretched. A comparison between hydrogels, PDMS and PMMA can be seen in Table 2-2.

Table 2-1 Compositions of a set of tough hydrogels with elastic network and dissipative networks (Note that while the water concentration in hydrogels at as-prepared state ranges from 73 wt% to 85 wt%, it may increase up to 95 wt% after swelling in water.) [83]

		Dissipative polymer networks		
		Alginate	HA	Chitosan
Elastic polymer networks	PAAm	12 wt% AAm, 0.017 wt% MBAA, 2 wt% alginate, CaSO$_4$ (20 × 10^{-3} M concentration in gel)	18 wt% AAm, 0.026 wt% MBAA, 2 wt% HA, Iron (III) chloride (3 × 10^{-3} M concentration in gel)	24 wt% AAm, 0.034 wt% MBAA, 2 wt% chitosan, TPP (3 × 10^{-3} M concentration in gel)
	PEGDA	20 wt% PEGDA, 2.5 wt% alginate, CaSO$_4$ (20 × 10^{-3} M concentration in gel)	20 wt% PEGDA, 2 wt% HA, Iron (III) chloride (3 × 10^{-3} M concentration in gel)	20 wt% PEGDA, 2 wt% Chitosan, TPP (3 × 10^{-3} M concentration in gel)

Table 2-2 Comparison of substrate materials

Substrate Material	Advantages	Drawbacks
PDMS	Bio-Compatible	Thermosetting polymer making reforming after intimal cure impossible
	Similar Young's Modulus to that of human skin	

	Used extensively in microfluidics research	
	Optically Clear	
	Capable of feature sizes of <50nm [85]	
PMMA	Bio-Compatible	Much stiffer than human skin [79], [86]
	Used extensively in microfluidics research	
	Optically clear	
	Capable of feature sizes of <10μm [87]	
	Thermoplastic polymer allows for repeat reforming	
Hydrogels	Ability to support biological structures and cells for lab on chip applications	'Wet' Material which then requires all electronics to be coated with an insulator (PDMS) [83]
	Similar mechanical properties to skin	Untested biocompatibility but possible
	Fluids can diffuse through material for drug delivery	Cannot support liquid conductors due to diffusion

In order to carry an electrical current through the system, some sort of conductor is required. Metals are normally the primary candidates for this task, however, in order to become stretchable, complex geometries are required [21], [57], [62], [65] and even then, repeated deformation will quickly lead to fatigue and failure. Three possible alternatives exist. The first is the use of conductive polymers, which normally consist of conductive nanoparticles being suspended and blended into a non-conductive polymer with desirable mechanical properties or are chemically synthesised to be conductive. This will lead to the creation of an electrically conductive polymer, but the conductivity of the final material is normally relatively poor when compared to metals [44], [88]. The second method is the use of non-metallic structures such as carbon nanotubes or graphene [47]. The main barrier for these materials is their high cost and low yield during manufacturing. They are incredibly difficult to produce with any kind of reliability while maintaining the quality of the material [89], [90]. An alternative solution could possibly be to use metals while in their liquid state. One example is that of mercury which has a melting point of -38.9°C [91], it is however, highly toxic and harmful to the environment. Another option is an alloy called Galinstan, which melts at -19°C and is a much safer material [69]. Figure 2-8 shows Galinstan being handled by hand, which is within normal operating procedures for the material. Galinstan is a eutectic mixture of gallium, indium and tin, which allows it to stay molten at room temperature and much lower. This creates the opportunity to use a fluid as a conductor and allows for incredible flexibility and conformability for any systems that take advantage of this. Galinstan forms an oxide layer almost instantly [92], which allows the material to actually be controlled when filling micro channels using this oxide layer [93]. This material shows great promise [67], [94]; however, the one drawback is that it causes a phenomenon called liquid metal embrittlement [90] when exposed to other metals. For this reason, some investigation has been carried out looking into the effects on a range of other metals, and, why this embrittlement occurs [95], [96]. This research never looks at how the Galinstan or other metal is

affected when both are used as conductors. More research needs to be done in this area to ascertain the long-term viability and application as a conductor in the production of electronics.

Figure 2-8 Non-toxic Galinstan being handled without protection equipment [97]. **This handling has proven to be safe with the only effect being that it can dry out the skin.**

2.6 Sensors

It is important to be aware of the different types of sensors that are used to collect information about various medical conditions or vital signs for the human body. Each of these sensors operate in a different manner and require different interfaces to the body, thus substantial work needs to be carried out looking into the compatibility of each of the most widely used sensor types with the production processes and system architecture.

In order to collect data from the world around it a system must have some kind of input device, be it a button or something far more complex. An investigation of some relevant sensor technologies for monitoring vital signs is important. However, there

are thousands of kinds of sensors and metrics to monitor, with huge amounts of research on each. For this reason, only a select few kinds of sensors will be investigated here. Vital signs are defined as a humans' signs of life, specifically, the pulse rate, respiratory rate, body temperature and blood pressure [98]. There are different ways to monitor each of these metrics, but for this project, the measurement of all vital signs is the bear minimum. Photoplethysmography is capable of monitoring all of these signals, bar body temperature, but can also monitor oxygen saturation levels in the blood [99], [100]. This research is being carried out by a group of researchers at Loughborough University looking to perfect the PPG sensor so that it is capable of being resistant to motion artefacts and skin pigmentation through the use of a multi-spectral approach [101]. This technology is still in development but seems to be nearing a point where commercial integration is possible. PPG utilises the changes in the penetration and reflection of light as it passes through the skin, for which a diagram can be seen in Figure 2-9.
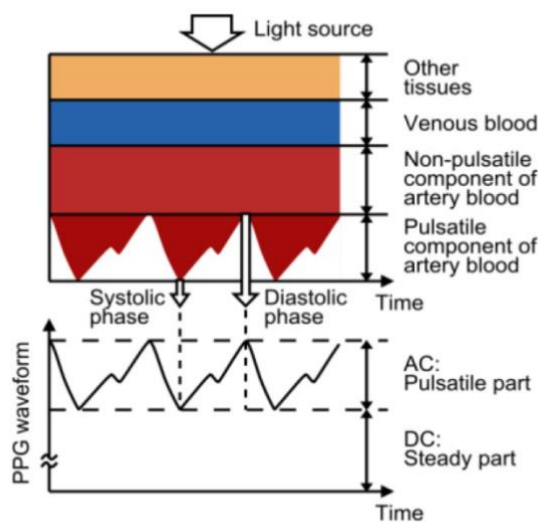
Figure 2-9 Diagram demonstrating penetration of light for the use of PPG sensors and how the waveform is produced [102]

An alternative to the use of PPG for pulse rate and respiration rate is by measuring electrical signals and properties of the body. The use of impedance pneumography can allow the monitoring of respiration rate that can be measured with as few as two contact electrodes, however, performance of the system can be improved by increasing this number to four [103]. Pulse rate can easily be measured with a two electrode ECG; work has been carried out on the use of liquid metal as the electrode contact. They are designed to improve the comfort, cost, and simplicity of standard electrodes.
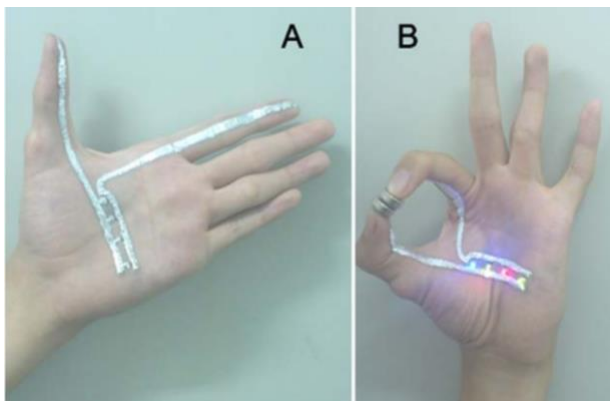
Figure 2-10 Circuit drawn onto skin using Galinstan. [104] **The above circuit includes simple LEDs as discrete components attached to the skin utilising the surface tension of Galinstan as an adhesive. Power is delivered through a battery being held in (B).**

The team succeeded in proving this [104]. However, not much is known about Galinstan as an allergen or if extended skin exposure could cause harm, which makes a system such as the one shown in Figure 2-10 improbable. Another important metric to monitor is that of glucose levels. However, this is more difficult as there have been no successful attempts at measuring glucose levels non-invasively. For this reason, researchers have turned towards some semi-invasive solutions which either use very fine needles that do not completely pierce the skin [105] or even ablation techniques that just monitor the interstitial fluid, which according to some research, is a more reliable and accurate measure of the body's actual glucose levels [106]. This research has barely scratched the surface of the various sensor

technologies that are available, let alone the ones that are currently in development. For this reason, it is hugely important that any system design is able to be flexible enough to accommodate whatever the best sensor packages available at the time.

2.7 Manufacturing Processes

Generally, electronics manufacture has been confined to a standardised set of production tools that are based off rigid substrates, or in some cases, Kapton based "Flex" substrates. This process involves etching of copper tracks in an acid bath, laminating multiple layers when required, drilling, then electroplating vias and finally coating the boards in a layer of solder resist or other kind of insulator. Components are then bonded to the boards by a solder paste that is normally screen printed before individual components are picked and placed, then the entire board is baked in order to melt the solder paste and actually create a firm bond [107]. An example of a conventional rigid flex PCB can be seen on the left in Figure 2-11, and a cross section of such a system can be seen on the right.
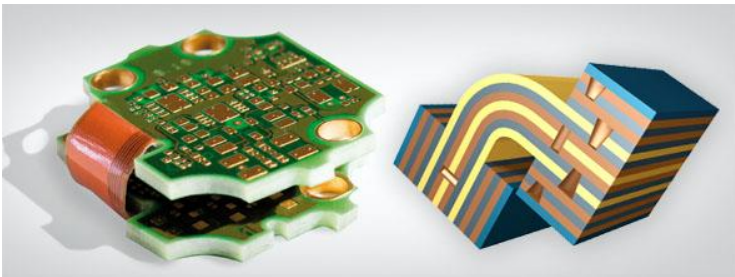
Figure 2-11 An example of a rigid flex PCB that combines both flexible and rigid substrates with the a diagram showing a cutaway of the internal structure. [108]

This process is not compatible with many other materials due to the processing steps that require the use of chemical reactions or high temperatures. It is also a batch process rather than a continuous one, which offers the opportunity to increase production output if electronics could be produced using continuous processes.

One example of a continuous process is Roll-to-Roll manufacturing which can be used to increase manufacturing output while simultaneously reducing cost. This process is not compatible with current PCB manufacture due to the use of rigid substrates. However, with investigations carried out on flexible substrates that use microfluidic or printed conductive traces, Roll-to-Roll processing presents an incredible opportunity to create a shift in how electronics are manufactured. To produce channels at the fine resolutions required for microfluidics, a process called Hot Embossing can be used, which has been shown to be capable of producing structures less than 1µm in size [109], [110]. An example of the equipment can be seen in Figure 2-12, where one roll contains a heated negative tool and the other is heated and supports the substrate.
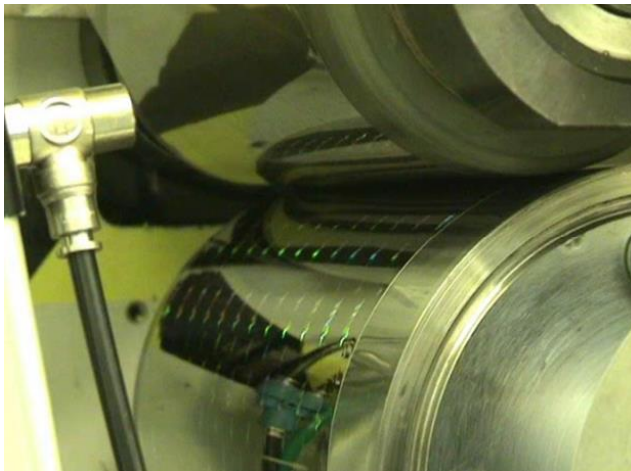
Figure 2-12 Roll-to-Roll Hot Embossing of refractive elements (Photo courtesy of VTT Finland)

The substrates used are normally thermoplastic polymers; work is being carried out using thermoset polymers [109], such as PDMS. Before this becomes a viable option, certain hurdles need to be overcome as the PDMS must be fed into the process as a resin and cured during forming, which vastly complicates the process. Roll-to-Roll processing can also be used to print conductive traces in a similar way to how newspapers are printed, taking advantage of techniques such as gravure or screen-

printing [50], [55], [111]. These techniques pose their own set of challenges. The inks that are currently available often suffer from poor conductivity or require baking at high temperatures. In addition to this, achieving the resolution required for interfacing with modern high density ICs has proven to be quite difficult due to edge quality becoming an issue at less than 100μm [111].   Other researchers have carried out work on developing CNC methods for laying down Galinstan, such as creating a CNC ballpoint style pen [112] and a CNC airbrush [113]. The main issue with these techniques is that they may not be capable of scaling while maintaining low cost due to their freeform nature and thus are more suitable for prototyping.

Once the channels have been created using some sort of embossing or casting process, they need to be filled with a conductive fluid in order to become useful. Due to the small scale, the behaviour of fluids greatly differs from 'macrofluidic' behaviour in that surface tension, fluidic resistance, and energy dissipation can dominate the system [114]. This means standard filling techniques may not be as effective as they would be at larger scales, thus requiring an alternative approach. One such approach is to create a negative pressure gradient above the surface of a submerged microfluidic part [115] (see Figure 2-13) . This technique is similar to that used for degassing polymer resins during processing and casting. This process is also capable of alleviating the issue of Galinstan's oxide layer due to the use of a vacuum during filling.
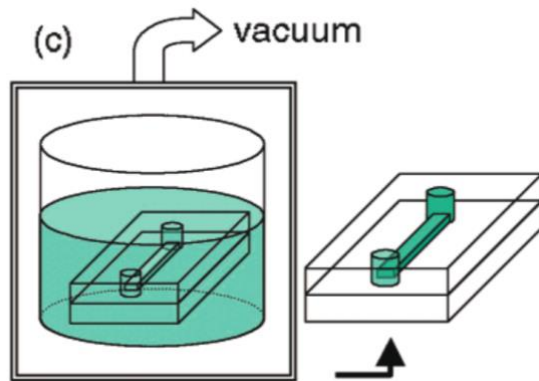
Figure 2-13 Atmospheric pressure reduction above a submerged device [115]

A research group at Harvard University have carried out work using the reverse of the process described above. Instead of using a vacuum, a positive pressure was used on the side where a gallium-indium alloy was present and essentially forced the fluid through the microfluidic chambers and channels. This was carried out at room temperature when a critical pressure, which depended on channel geometry, was reached. Something noted was that treatments carried out to prevent the EGaIn alloy wetting to the PDMS, such as plasma treatment, did not make a significant difference to the performance when filling the channels [116]. The filling tests were also performed with mercury as a comparison, which showed that the EGaIn alloy did not retreat from the channel when pressure was removed, unlike the mercury, which fully retreated from the channel. The team interestingly noted that EGaIn's rheological properties are almost completely dictated by its oxide skin, as when exposed to HCl (which has been shown to remove the oxide skin [52], [92], [93], [116], [117]) a loss in structural stability was observed. It was concluded that EGaIn behaves as an elastic material until the applied surface stress surpasses a critical value, which was found to be in the range of ~0.5N/m. Once this critical surface stress is reached, the material will readily flow as a liquid and return to an elastic solid once the stress is released [116]. An example of this flow behaviour can be seen in Figure 2-14.
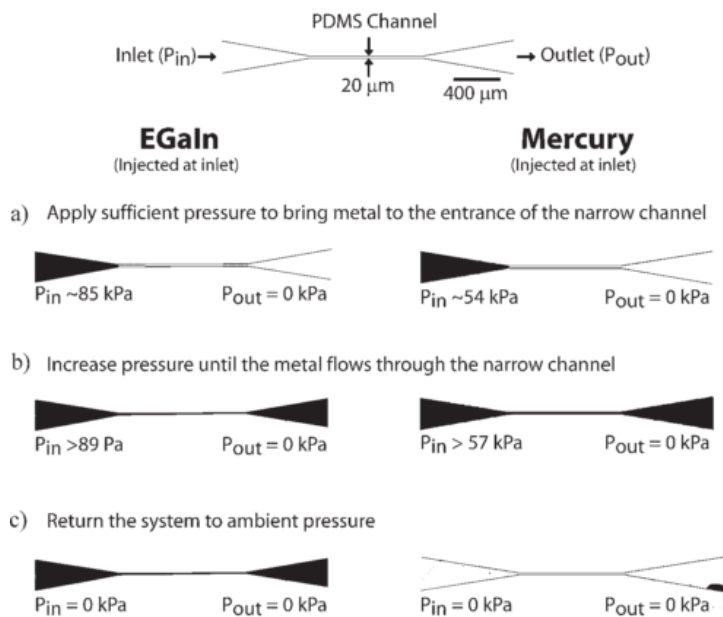
Figure 2-14 Examples of liquid metals in microchannels and their dependence on pressure. The dimensions of the channels fabricated from PDMS are labeled at the top of the figure. The remaining images are back-lit, top-down optical photographs of EGaIn (left column) and Hg (right column) in PDMS microfluidic channels. The PDMS is transparent, whereas the metals block the light and consequently appear dark. i) Both metals filled the channels until they reached the narrow portion of the channel. ii) When a critical pressure was exceeded, both metals rapidly (in<1 sec) filled the channels. iii) When the system was returned to ambient pressure, the EGaIn structure was stable, whereas the Hg instantaneously (<1 s) withdrew from the channel. All pressures are gauge pressures. [116]

At some point during Roll-to-Roll manufacturing, layers will need to be bonded together in order to create complex, multi-layer systems. PDMS is a strange material in that adhesives that are not made of PDMS tend to bond poorly to its surface, while two PDMS parts can be bonded without any other adhesives. Work being done by *Eddings et al*. has completed a comparison of different bonding techniques for PDMS. The results of which can be seen in Figure 2-15, where using uncured PDMS

as an adhesive formed the strongest bond. However, this method could lead to blocking of microfluidic channels when laying down the adhesive, partial curing, where the layers are bonded together before they have fully cured, shows the most promise due to the simplicity and lack of additional resin that could possibly block any channels after forming. If complete curing is required before bonding, Oxygen plasma and corona discharge are both options that are capable of being used in Roll-to-Roll processing. Both of these processes are essentially a surface treatment that will not affect the geometry of the part being created.
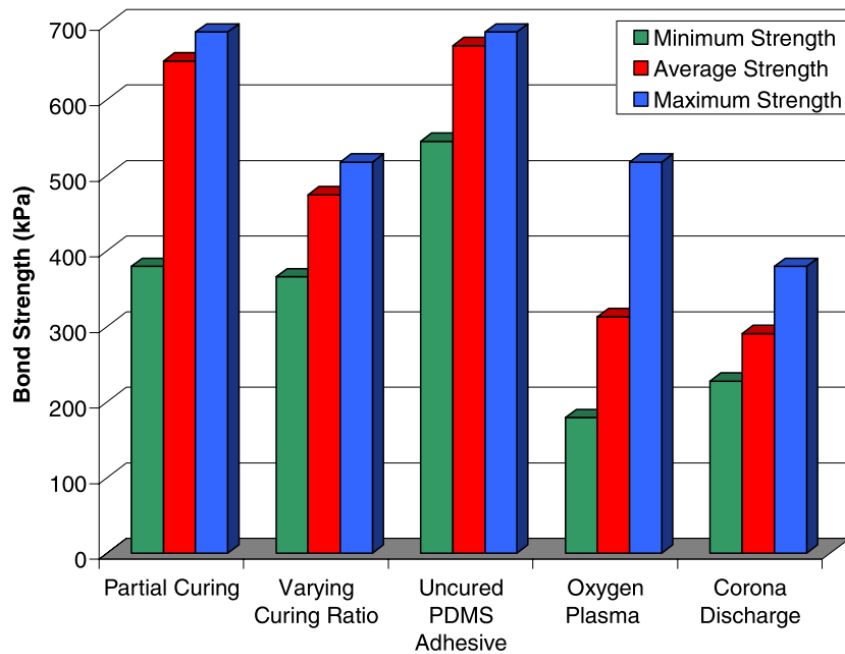
Figure 2-15 A comparison of five different bonding techniques at their optimal conditions at 60 ∘C. Partial curing experiment: 35 min precure, varying curing ratio experiments: PDMS base to cross-linking agent (15:1), uncured PDMS adhesive experiments: completely uncured PDMS layer stamped, oxygen plasma treatment: 700 mTorr chamber pressure, 20W RIE power, 30 second exposure time. Corona discharge: 15 kV output, 30 s exposure time. The minimum and maximum bond strength values are shown with the average bond strength to illustrate the range of values obtained during experimentation. [118]

2.8 Fabric Based Technologies

Smart textiles are deemed by many to be the next step for fashion, performance and medical garments. Allowing integration of sensors to monitor both the environment and the wearer and in some cases even reacting to this information would open up a world of possibilities.

There are currently two main ways of integrating interconnects into textiles; the first is to weave conductive strands into the fabric when it is being produced, the second is to add interconnects to the fabric afterwards using some kind of printing or attachment process.

Applications for conductive threads are not just limited to smart textiles, they have been used for years in certain niche applications: clean room garments, military apparel, medical application and electronics manufacture [119]. They can be used for a wide range of functions within these applications, for example protective clothing in explosive environments, infrared absorption and electromagnetic interference (EMI) shielding [120]–[122].

2.8.1 Woven Electronics

Woven electronics use some type of conductive fibre that is woven into the textile or garment to create interconnects. Systems that include this technology have already reached the consumer market. An example of this technology is the Smart Sock and Fitness T-Shirt from Sensoria [123]. Sensoria have used conductive fibres that are woven into a sock to create both interconnects and pressure sensors. It is unknown which technology these socks use. One possible technology is an e-textile sensor described by *Enokibori et al* who measure the change in capacitance. Hollow conductive fibres are included within the weave of the textile which, when compressed, display a change in capacitance. This change in capacitance can then be converted into a pressure reading [124].

This technique yields flexible fabrics that, depending on the weave used, can actually stretch. Due to the conductive fibre being made of metal which cannot be deformed elastically [119], must be integrated into the fabric in such a way as to include slack so that as the fabric is stretched the conductive fibre straightens rather than being deformed elastically. An example of this can be seen in Figure 2-16.
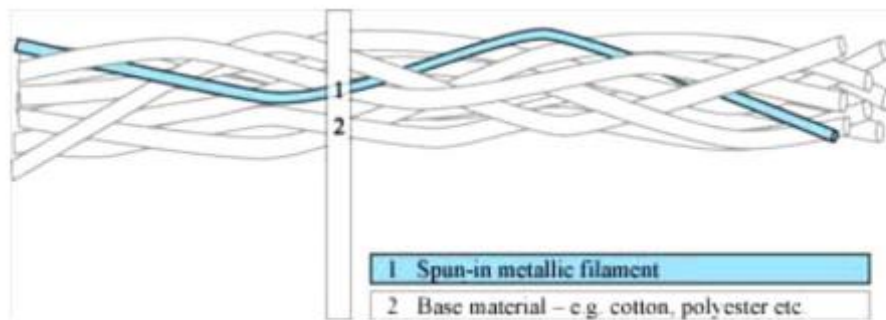
Figure 2-16 Schematic of conductive fibre twisted in with the normal fibres [119]

This same methodology can be used with embroidery, which creates similar results but allows more control in the design and positioning of the conductive threads [119], in addition to allowing any fabric to be used at the base if certain properties are required.

An alternative to weaving in conductive fibres is treating the existing materials in order to make them conductive to create an electrically conductive textile. Common processes to perform this are evaporative deposition, electroless plating, sputtering and coating the materials with a conductive polymer [125]. Due to the ability to vary the coating composition on strands of the weave, it is possible to create textile transistors. The crossing yarns act as the gate and drain coated with PEDOT:PSS, with the contact point having an added electrolyte. A diagram demonstrating this configuration can be seen in Figure 2-17. The resulting transistor, when operated at 1.5V had an on-off current ration of over 1000 [126].
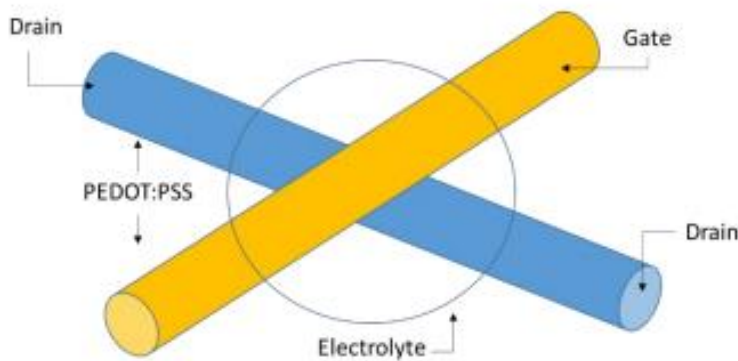
Figure 2-17 Two yarns coated with PEDOT:PSS, one serves as the gate contact for the transistor while the second serves as drain and source contact. At the crossing of the two yarns, an electrolyte is placed. A redox process at the interface between electrolyte and PEDOT:PSS turns the transistor on and off [119], [126]

Work carried out by Loughborough University and Nottingham Trent University have successfully created transmission lines using embroidery techniques. The research used the DC resistance as an initial indicator of RF performance, which was found to be suitable. However, the results indicated that the current had a preference to flow down a single thread rather than traverse between threads [127]. This aligns with other research that found embroidered or woven conductors are not the most efficient design for wireless transmission lines or antennae due to large losses, thus reducing the usable frequency range in addition to the power efficiency of the device [128]. This can be attributed to limitations in conductor size of the threads (<1.5mm) or in the case of plated conductive fabrics, which was found to be restricted to manometer scales [128]–[130].

2.8.2 Printed Textile Electronics

Electronic textiles can also be produced using various printing techniques that leverage various conductive inks. These inks always contain a metallic precursor such as Ag, Au or Cu, which are highly conductive suspended within a carrier fluid [119]. This allows the inks to be printed using a wide range of commercial

techniques. This includes both screen-printing and inkjet printing. Printing methods allow for easier integration of electronics into textiles due to the textile acting only as a substrate when compared to weaving interconnects directly into the fabrics. Inkjet fabrication offers a digital production method that requires no masks or stencils to be made making it suited for low volume production. It is capable of a resolution of approximately 50μm features and a throughput of 100m²/h. Due to the nozzle size, difficulties are encountered when using high viscosity materials and dispersed particle inks that can cause clogging. For this reason it is preferable to use organic semiconductors as inks [119].

One of the drawbacks of inkjet printing is that many of the inks require some form of baking after deposition. The reason for this is that the metallic particles suspended within the carrier fluid do not create a continuous electrical connection. By baking the ink and substrate, the carrier fluid is evaporated and the metallic particles are sintered together to form a continuous electrical connection [119]. This means that possible substrates must be capable of withstanding temperatures in excess of 180°C, which is the sintering temperature for Silver Nano-Particle (15-20nm in diameter) inks [119], [131], [132].

Using combinations of different inks and print geometries, sensors can be created or assembled. Work is currently being done by the National Textile Centre at North Carolina State University who are investigating printed electronic circuits on non-woven fabrics. The project goal is to create garments that are able to monitor a variety of physiological parameters including heart rate through ECG, as well as respiration and temperature. Research is being carried out in partnership with some conductive ink manufactures in order to vary the properties of the ink. This partnership has enabled the successful production of antennae on non-woven textile structures using various print processes [119].

In order to make these systems both flexible and stretchable, two techniques are available. The first is polymer or organic based inks that can be elastically deformed

without breaking. However, these inks normally exhibit poorer conductive properties than their metallic counterparts do [104], [132]–[134]. The second is the use of complex geometries for use with conductive metallic based inks. It has been found that the most effective design is that of three-dimensional self-similar serpentine conductors. These designs allow reductions in the stress imposed on the conductors and contain additional material to take the loads of the stretching fabric. An example can be seen in Figure 2-18, where a layered self-similar interconnect laminated onto fabric is deformed in both FEA simulations and experimentally, which can be seen in Figure 2-18. However, the use of serpentine interconnects does not completely solve the issues that plague non-elastic materials as the repetitive deformation and fatigue eventually weakens the material, causing cracking and thus degradation of signal quality [37], [42], [135] due to the effects of work hardening and plastic deformation..
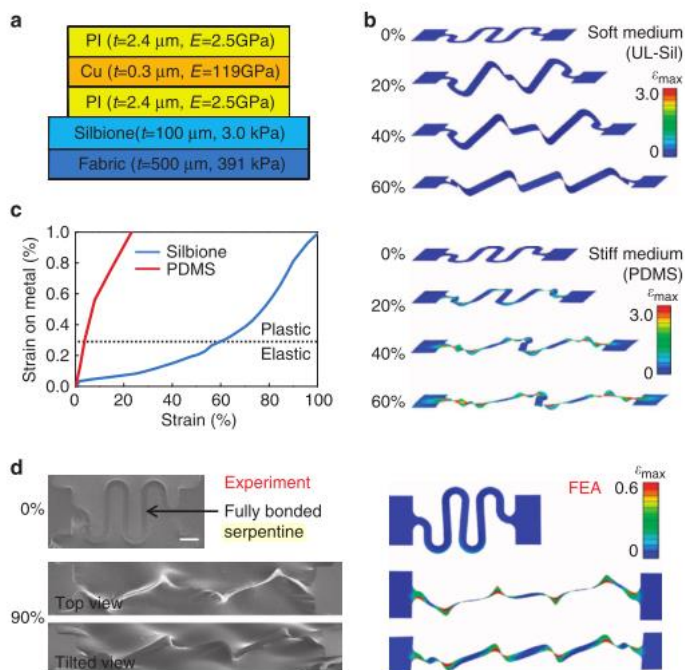
Figure 2-18 Mechanics of materials and structures for stretchable electronics. (a) Cross-sectional illustration of representative layers in a stretchable electronic system. (b) Deformations of a FS trace and distributions of maximum principal strains in the

metal computed by FEA for a system consisting of electronics/UL-Sil(3.0 kPa)/fabric and electronics/PDMS (B1–2MPa)/fabric. (c) The computed maximum principal strains in the metal as a function of the strain applied to the entire system show enhanced stretchability with the UL-Sil material compared with PDMS. (d) Scanning electron micrographs (scale bar, 200mm) and corresponding FEA results of undeformed and uniaxially stretched (90%) configurations of an FS trace bonded to a UL-Sil/fabric substrate [61].

2.9 Summary

Currently a huge array of both competing and complementary technologies exists to create flexible, stretchable electronics. Each of these technologies has its own set of strengths and its own set of drawbacks that either prevents it from coming to market or limits its application. In many cases, the production methods used for these technologies are either very new and have problems that need to be solved before they can scale, or they are slow and labour intensive, drastically raising the price of the finished products.

In order to successfully create a device that is flexible, stretchable and suitable for mass production, a multitude of existing technologies that have not previously been integrated together will have to be partnered with each other using both novel technologies researched during this project as well as production methods to manufacture them.

One major drawback of many of these technologies is that of inaccessibility. The consumer electronics industry has years of experience using certain tools and technologies that have been developed over the last 60 years. Any new technology should leverage this experience and knowledge rather than attempting to replace it or start again. In addition to this, world leading corporations such as Intel, IBM and Taiwan Semiconductor Manufacturing Company have invested billions of dollars [136] into existing fabrication technologies and currently produce incredibly

advanced systems that could not be replaced by any of the technologies detailed above. Therefore, in order to both lower the barrier to entry for the technology and engineers alike, any production methods or technologies developed should leverage existing silicon IC production methods and embedded electronics systems knowledge.

The current array of technologies available all seem to show some promise and will play a vital part in bringing 'invisibles' to life. Important aspects such as interconnect designs, novel material development and manufacturing processes all play a role in the enablement of such devices and shaping the research presented here. The current state of technologies all exist independently of each other and require further investigation into their integration. In order for this to occur a set of requirements would need to be developed for future devices. These parameters of usefulness would then be able to guide technology selection and thus the direction of this research.

3 PARAMETERS OF USEFULNESS

3.1 Introduction

The parameters of usefulness are a set of guidelines and rules that have been synthesised for the possible applications of conformal electronics and systems. They have been assembled using the available data detailed in the background research in Chapter 2. The parameters set out to define what goals the technology must achieve to allow the creation of useful products and the processes to manufacture them.

The final product will help to set the parameters for production, even though developing the sensor itself is outside of the scope of the project, proof of concept items will need to be created in order to demonstrate the viability of the research when applied and the suitability of the production processes that are utilised. It is hoped these parameters could be used by commercial or research institutions to manufacture products and systems that could utilise the production processes researched and specified below.

3.2 Parameters of Usefulness

Below are a set of initial guidelines and constraints that need to be met for the researched technologies to be viable within a commercial environment. From these guidelines, appropriate experimentation and testing can be planned to ensure that the materials and technologies can meet these goals and not result in an over or under engineered system.

3.2.1 Assumptions – Constraints – Standards

In order for this technology to be successful in a marketplace, especially across a wide variety of applications, costs must be scalable based on environmental requirement and functionality. A few examples of currently available integrated sensor systems are detailed in Table 3-1. All of these systems are poised to target a different level of consumer. The American Football helmet targets large teams rather than individuals, the heart rate monitor targets the general part time athlete and the hockey goal keeper armour looks to a niche market of individuals within a chosen sport.

Table 3-1 Example applications and the costs the technologies must reach in order to be commercially viable

Application	Currently Available Technology or Item Cost	Total retail cost for system using Flexible Stretchable Technologies
American Football Helmet	Riddell Revolution Speed Flex Helmet - $399.99 [137] Riddell InSite - $150 [138], [139] Total system Cost - $549.99	1. Best $400-450 2. Ideal $450-$500 3. Acceptable $500-$550 4. Unacceptable $550+
Heart Rate Monitor	Polar H7 Bluetooth Smart Heart Rate Sensor - $70 [140]	1. Best $5-20 2. Ideal $20-$40 3. Acceptable $40-$70 4. Unacceptable $70+

Hockey Goalie Body Armour	Gryphon Goalkeeping Bodyguard (No integrated sensing technology) - $200 [141]	1. Best $200-$220 2. Ideal $220-$240 3. Acceptable $240-$300 4. Unacceptable $300+

All the technologies integrated into the system must be currently in mass production. In order to create a low-cost system, technologies that are not able to be used in production or that require large amounts of research until they are ready to be integrated should be avoided where possible as this would drastically increase both system costs and time to market. Where possible, systems should not be classed as a medical device so as to avoid excessive testing and regulation. This means that all materials that come into direct contact with the user must be biocompatible and the device must be non-invasive. The product should only be used initially in a non-medical consumer/research setting where there is no risk of injury or loss of life in case of failure. Any product developed using the technologies researched must endeavour to meet at least the following standards in order to ensure the safety of not only the consumer, but the environment during the product's entire lifecycle;

- Information Technology Equipment Safety Standards (IEC 60950-1, IEC 62368-1)
- Batteries if used (IEC 62133)
- EMC Standards for markets where the device would be used (Various EN standards for Europe and FCC standards for the US)
- Specific Absorption Rate for Electromagnetic radiation (EN 62311)
- Privacy and information security – All communication between the device and base station would need to be encrypted and secured.
- Chemical makeup – The device should be RoHS compliant
- Environment and Sustainability (UL 2887)

- All materials that come into direct contact with the user must be biocompatible (ISO 10993)

- NEMA enclosure rating of IP65

- Relevant IPC and J-Standards that govern the design, manufacture and testing of electronics. However, many of these standards would not apply due to the unique makeup and construction of the intended systems.

The standards mentioned above are not an exhaustive list but are intended to be a guide for both research and manufacture. As standards such as these are continually updated, it would be up to the engineer designing such a product to ensure that all the relevant standards are complied with.

3.2.2 Architecture and System Design

If any processing or data analysis is carried out on the device, it should be kept to a minimum in order to improve power efficiency. The device would only process the input data to the point where it can be sent to the base station or smartphone. These devices have a larger, more capable CPU and data storage system, which allows more detailed analysis to be carried out. Any wireless communication systems used should comply with industry standards and be as low power as possible (ANT or Bluetooth Low Energy are two possible solutions that are currently available). The sampling rate of the system should be variable in order to be adjusted based on activity or research requirements. This would allow improved battery life and enhanced sensor operation. Any system designed with these technologies should have an ingress protection rating of IP68 to a depth of 3m or more, which will allow the sensor to be worn during any activity or sport that does not involve submersion in very deep water. Additionally, this would prevent sweat, moisture or dirt causing any issues with the internal electronics as well as protecting the user from any possible harm. If bare die ICs are used within the system, they will need to be protected with a UV resistant coating, be it within the substrate or over the entire device.

3.3 Application Based Specifications

3.3.1 General Overview and Design Guidelines

In order for the technologies researched to be applicable in mass production, certain things need to be taken into account when investigating materials and various processes. Production methods, where possible, should be continuous in order to increase output and reduce costs. An example of this is the Roll-to-Roll manufacturing method. All processes and methods used should be flexible, allowing for modification based on the needs of the design. The aim is to mirror the design flexibility that conventional PCB assembly and manufacture allows. This reduces the barrier to entry as well as easing the transition into utilising this new process and giving designers freedom to create new and innovative products. Where possible the process should produce items that match the relevant standards from conventional PCB manufacturing processes, meeting IPC-A-600 would cover conditions for which PCBs can be accepted and rejected during the quality assurance stage of manufacture. IPC-6012 specifies the required performance of PCB module mounting, interconnecting structures and HDI boards or layers. IPC specifications being an industry standard, should be referenced when developing new processes to make sure any lessons learned from conventional electronics production are incorporated into these new technologies.

The processes used should be easily customisable to accommodate any number of layers allowing for increased complexity. At minimum, it must be able to produce a device with two electrical layers and one component layer. An ideal system would be capable of having up to 16 electrical layers and 4 component layers. All processes must be capable of the precision required for manufacturing antennae as an integrated part of the manufacturing process. Any and all assembly should be component agnostic in the same way that conventional pick-and-place methods allow almost any component to be used as part of a PCB. Finally, the entire process

should aim to be completely automated, with as little human intervention as possible.

3.3.2 Application Dependant Design Guidelines

To create an application agnostic design methodology, and to create flexible and stretchable systems, the application must be kept in mind at all times. For example, the requirements for a system to be integrated into a snowboard to perform performance measurements would be vastly different to those of an on-body sensor patch that could be worn every day.

Clarification in these requirements can be separated into four main classifications that, in theory, should cover almost any possible application. The requirements for each level increase with the classification class. These four classification classes are as follows;

1. Soft Matter Consumer Electronics

   These devices could utilise flexible stretchable electronics to improve the density of current electronic systems, to enable new user experiences or embed systems into locations that would ordinarily be incompatible with existing technologies. Examples of this could be utilised widely in the IoT domain, such as in smart bedding, sports equipment or folding devices

2. On-body Sensor Applications

   These devices would utilise their conformal nature to allow long term end users to comfortably wear these devices, enabling the unobtrusive monitoring of biometrics. These systems could be heavily utilised within medical, health and sports applications. Examples of these sensors are low profile, lightweight ECG systems, activity monitors and skin galvanometers. Some of these systems could be safety critical and would require high reliability and redundancies in their designs.

3. <u>Protective Equipment Monitoring Systems</u>

   Protective equipment is used in a huge variety of applications, examples of which are the defence, industrial and sporting sectors. Many of these systems would likely be safety critical, while being placed under far larger environmental stresses than a typical consumer device. Examples of these devices are smart body armours and helmets.

4. <u>High Performance Monitoring Applications</u>

   These systems would be used in scientific, industrial and other demanding applications that require high reliability and precision. Structural health monitoring systems are an example of an integrated system that would benefit from a highly conformal measurement system to enable high precision measurements without affecting results or the design of the device under test.

4 RESEARCH APPROACH

After completing the above literature review, it is possible to begin research on forward looking designs and concepts. By overviewing existing standards and processes, further work can take advantage of multiple technologies and techniques that would not ordinarily be combined; allowing the creation of a novel product and manufacturing method to create a low-cost system. Such a product will need to include solutions for the following components:

- Flexible and stretchable substrate
- Flexible stretchable interconnects
- Passive components capable of withstanding deformation
- Ability to support certain rigid components such as integrated circuits
- Flexible stretchable antennae
- User interaction components capable of withstanding deformation

These components can be seen as blocks that will need to interact with each other to create a functioning device. They will also need to be compatible with an efficient manufacturing process, so component and technology selection should always keep this in mind. The way these interact can be seen in Figure 4-1, whereby the overall design of a device can directly influence the capability of the system. For the process diagram shown in Figure 4-1b, the order of these blocks would likely move around based on the chosen design of a final system in addition to the specific components selected for a particular application. An example would be the use of a trace antenna instead of a chip antenna [142] which could lead to some blocks being split up or being duplicated. This chapter will attempt to systematically decide on an

appropriate set of experiments that are required to aid in the realisation of truly flexible and stretchable electronics.
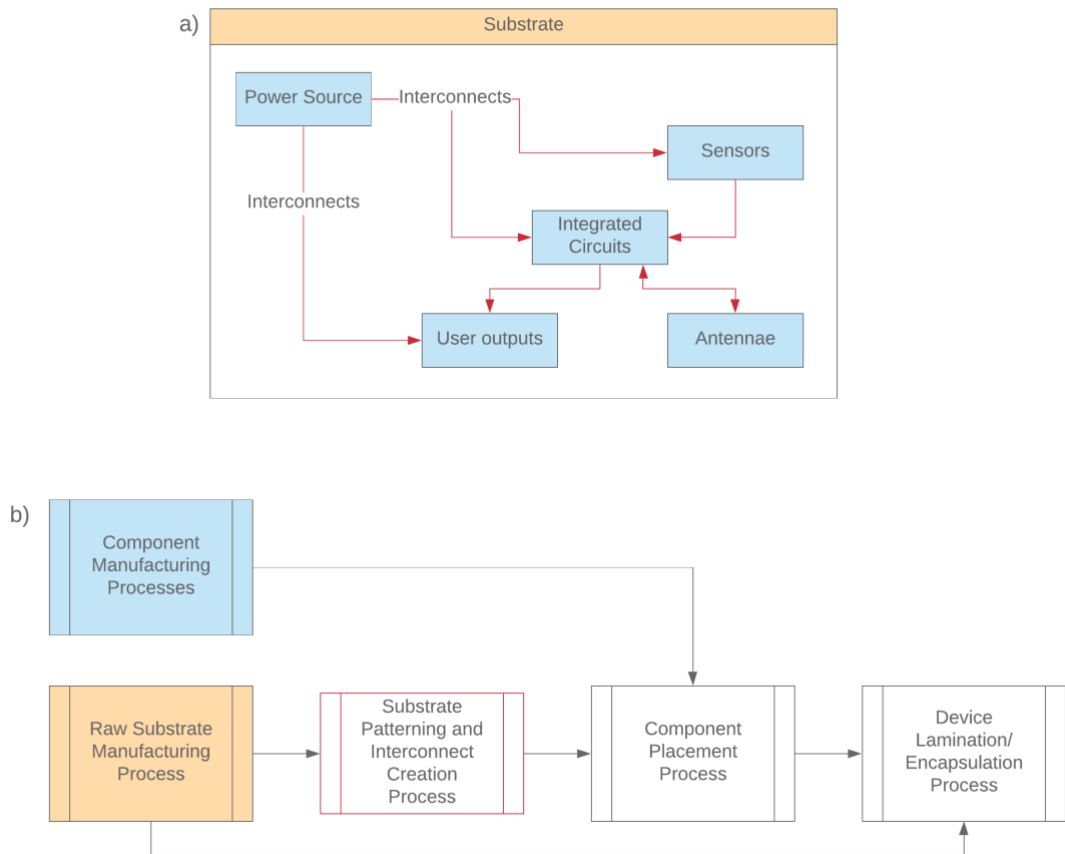
Figure 4-1 Colours in two diagrams are to connect relevant components in the system block diagram (a) to the high level process diagram (b).

4.1 Substrate Selection and Substrate Manufacture

In order to create flexible and stretchable electronics a suitable substrate would need to be chosen, due to the main goal involving long term contact with the skin and biological applications. It would need to be biocompatible and non-reactive. PDMS and PMMA are both possible fits for this application, however with its superior mechanical properties which are remarkably similar to that of human skin, PDMS is a superior candidate. Additionally, wide use within both the medical and

semiconductor industry for various purposes means that there is a lot of expertise when working with it and a large amount of literature regarding its mechanical properties [68], [134], [143]–[146] and biocompatibility [74], [147]. Fabric based technologies have major limitations with regard to interconnects, as they either need to be woven in or able to be attached to the fabric in some way. This completely rules out the use of liquid conductors and any microfluidic technologies unless combined with one of the other processes or technologies detailed above.

In order to take advantage of PDMS as a substrate material, it needs to be proven that it can be easily processed utilising mass manufacturing methods and rapid digital manufacturing methods. As PDMS is often used in the semiconductor industry for the creation of lithography stamps and masks [68], [78], [148], [149] a significant amount of knowledge already exists around its manufacture and handling. There is however more limited understanding of rapid manufacturing processes surrounding the material. A study will be required to observe and analyse the use of laser machining on PDMS and investigate the link between process parameters and finished channel geometry.

4.2 Electrical Components

Components for such devices include power sources, sensors, user outputs, antennae and integrated circuits. All of these need to be selected carefully in order to comply with the environment that will occur within a system when being used in situ. However, their selection and behaviour are not only heavily application specific, but the selection of available components is far too wide to test. Therefore it is important to classify some of the possible mechanical conditions these components could undergo and understand how these forces could be transferred onto the components during deformation.

4.3 Interconnects

In order to achieve conformal electronics, maintaining a good electrical connection between components throughout any and all deformations that may occur during use. Material selection is a large part of this, of which the one chosen must exhibit certain mechanical properties in addition to being electrically conductive. Due to the expectation that these products will likely undergo repeated deformation in the same location, it is important that any material chosen is able to resist work hardening, which over time could induce cracks. This will especially be an issue for designs that utilise self-similar serpentine interconnects, which are often made of gold. By using a metallic compound that is liquid at expected operational conditions, it is possible to remove any and all concerns regarding cracking and breaking. Additionally, this has the added advantage of enabling self-healing if any of the interconnects do break. The two materials that are generally available and both fluid at room temperature are Mercury and Eutectic Gallium-Indium alloys. Mercury is not a viable material due to its toxicity [150] to living organisms and would therefore be an inappropriate choice for a wearable device. However, Gallium-Indium alloys while non-toxic [151] can embrittle other metals [152], [153], for which overcoming this issue is an important goal.

4.4 Design Concept

The sections above detail the various components required to create a conformal system and the possible gaps in knowledge that need to be filled in order to realise such a device. A diagram of a possible design can be seen below in Figure 4-2, of which will be used for the development of possible manufacturing processes.
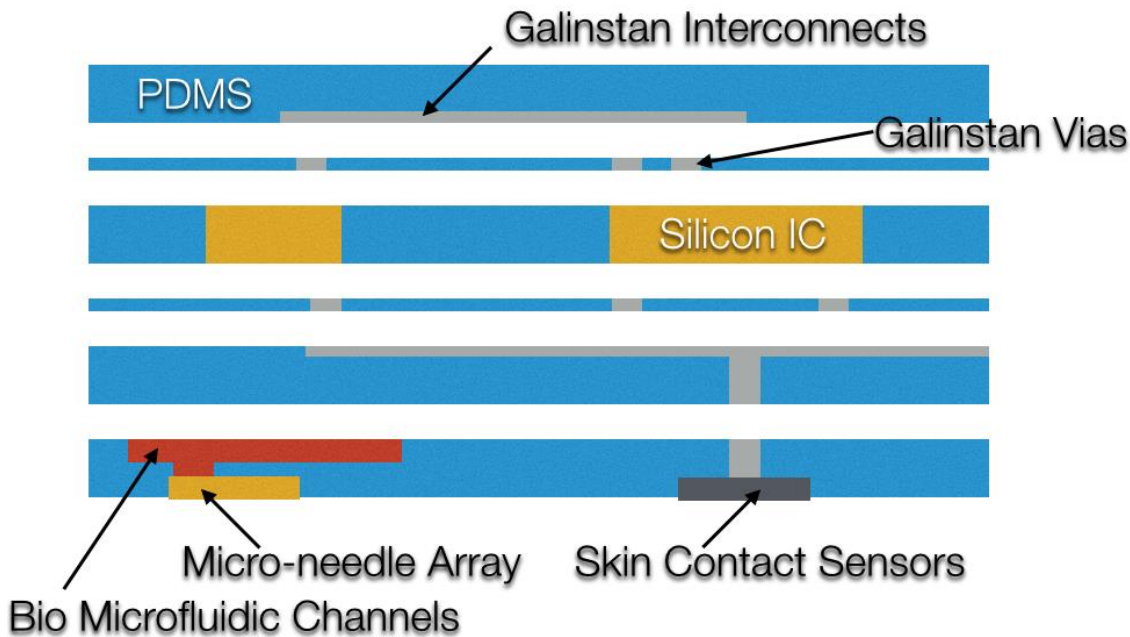
Figure 4-2 Proposed layer stack up for Galinstan-microfluidic hybrid circuits

By using PDMS as a substrate, it gives a surface on which very high-resolution structures can be created. This allows the construction of extremely fine pitch fluidic channels. By filling these channels with Galinstan, flexible and stretchable interconnects will be created that are also self-healing [48] as long as the substrate and channel encapsulation remain intact. The suggested layer stack up can be seen in Figure 4-2. This design has been developed in such a way that would allow it to be produced using only Roll-to-Roll production methods, thus greatly reducing the cost of manufacture. It also allows the conventional multilayer design methodologies that are currently used in PCB design to be used with very little modification. This system design also allows the integration of microfluidic lab-on-chip systems due to the crossover in design methodologies and manufacturing processes also being fully capable of fabrication lab-on-chip systems. This creates the opportunity to integrate lab-on-chip systems, electronics and optics [78] for a fully hybridised system and a manufacturing process that allows the creation of incredibly dense, low cost systems.

Another concept that was investigated was the use of printed traces instead of using more complex microfluidic traces. A major issue with printed traces is their poor mechanical properties, which would lead to poor stretchability of the system, unless serpentine geometry was used, which is not ideal as it exacerbates the problem of relatively poor conductivity in these materials nor provides uniaxial stretching.

Figure 4-2 shows a proposed layer stack up that would enable the integration of various components that can currently be purchased in commercial production quantities and some that are not yet available. The proposed method uses Galinstan contained within microfluidic channels to create flexible stretchable interconnects between components and sensors. Due to the liquid state of Galinstan, it would allow the creation of interconnects that are both self-healing and totally conformal. Investigation needs to be carried out as to its effect on other metals and its electrical properties. These channels could also be used for the transport of biological substances to Lab-on-Chip devices to allow for further diagnostics as long as they are paired with the relevant collection methods such as micro needle arrays. These channels would be manufactured using Roll-to-Roll hot embossing that would allow the creation of incredibly high-resolution channels in order to allow the direct connection to modern fine pitch bare die IC components. In order to create vias or sections that penetrate more than one layer, lasers would be required to cut through the material, as hot embossing does not possess this capability. The layers would be produced in groups with thin 'capping' layers, which could then be easily filled without risking damage to the sensitive IC components. The layers would then be bonded together in a stack and the individual devices diced. By placing the sensitive silicon devices within the PDMS substrate instead of placing them on top allows the device to stay as close to the neutral axis as possible reducing the stresses on the device while creating a sealed unit that has the possibility to be waterproof.

4.5 Manufacturing Processes

The selection of the correct manufacturing process is just as important as the design of the system itself. The processes that will be investigated in this thesis will be based around the design detailed in §4.4. In order to manufacture such a system, a few crucial steps would need to be developed. The creation of thin PDMS films is a process that already exists and is currently being worked on by multiple teams all over the world [52], [71], [76], [110], [154], Some of these process are able to pattern microfluidic channels during the thin sheet manufacturing process, however, most of these processes rely on roll-to-roll moulds or chemical etching. These processes are costly and unsuitable for rapid prototyping. The lack of a rapid prototyping method for the manufacture of systems can drastically hinder the adoption rate of new technologies. This is an important field to venture into and will be the topic of Chapter 5.

Once the PDMS sheets have been patterned, they will need to be laminated together. There are multiple options for creating a bond between two layers of PDMS, however, selecting the correct bonding process is crucial to creating a reliable system, especially when this bond is required to contain liquid metal conductors. This bond needs to maintain homogenous mechanical properties across the device under load or risk creating stress raisers that cause delamination. Additionally the available bonding processes take a range of time to take effect, and should therefore be selected carefully to keep manufacturing costs low when moving into mass production. The optimal way to investigate this is to simulate a system undergoing various deformations using finite element analysis and investigate the required bond strength. This avenue of study is the main body of work in §6, where investigations into the required bond strength of laminations will be carried out using finite element analysis.

5 LASER MACHINING OF PDMS TO CREATE PREDICTABLE MICROFLUIDIC CHANNELS USING A CONTINUOUS WAVE CO$_2$ LASER

5.1 Introduction

The research in this chapter was published at the Electronic Components and Technology Conference (ECTC) in 2016 by the IEEE [155]. The full paper can be seen in Appendix I.

In order to achieve digital manufacturing of conformal electronics, various challenges and bottlenecks need to be overcome with regard to both their design and manufacture [156]. To solve this problem this study proposes the use of a CO$_2$ laser in order to create channels in PDMS for liquid metallic interconnects, which can be deformed without inducing fatigue and cracking [92].

For the channels to be useful in electronic system design, the manufacturing method must be capable of varying channel geometry across the length of the channel. An additional challenge that requires a solution is to include vertical vias that are able to form a three dimensional electronic interconnect structure or circuit design

[157]. Conventional methods that are used to create these channels for Lab on Chip applications normally involve the use of complex lithography, moulding or embossing techniques [158], which can introduce problems when creating holes directly through the substrate in order to enable vertical interconnects. One of these issues is requiring sacrificial layers in order to create a single component, which when scaled can lead to increased costs [159].

In this work, several laser based manufacturing methods for creating the channels have been investigated for the direct fabrication of microfluidic channels within a Polydimethylsiloxane (PDMS) substrate. The use of lasers as a processing tool allows the creation of varied channel sizes in addition to drilling and cutting directly through the material all as a digital process that requires little to no tooling.

This study aims to identify the optimal laser cutting parameters using a continuous wave Carbon Dioxide laser for the cutting and engraving of a PDMS substrate. The use of a CW CO_2 laser allows the low cost, continuous manufacture of PDMS based microfluidic devices with few if any restrictions on channel geometry, while being capable of small-scales and high precision. Various laser parameters such as power levels, trace speed and repetitions were tested to narrow down the optimal combination in order to create a uniform high-quality cut and surface finish. This has led to a data set that was produced to enable the correct selection of parameters when machining PDMS with a CW CO_2 laser. An evaluation of the quality of the obtained channels was subsequently carried out using various metrology tools to provide a clear understanding of the effects of laser processing parameters on the surface finish, depth and geometry of the machined channel in the PDMS substrate. It is envisaged that the use of low-cost CW CO_2 lasers in both the small-scale prototyping and mass manufacture of microfluidic channels on PDMS substrates will be viable for scalable three-dimensional manufacturing of wearable electronics.

5.2 Aims and Objectives

PDMS is a material that is often used in the waterproofing and production of various electronic devices [78], [160]. As such, the properties of the material are well documented, however, its integration with a laser is not. The aim of this experiment is to research the behaviour of PDMS sheet when machined with a continuous wave CO_2 laser and gain the ability to predict the channel size, shape and finish based upon the configuration options chosen for the laser. This study seeks to find a correlation between the finished channel and various laser parameters, as due to the wide range of applications in which this could be used, there is not an optimum depth that should be targeted, but the ability to select a depth and thus calculate the required parameters to achieve it.

5.3 Methodology

5.3.1 Sample Preparation

The chosen material was a derivative of PDMS from Dow Corning, specifically Sylgard 184. This was chosen for its fast cure time and availability in large quantities. Sylgard 184 is shipped as a two-part resin, which must be then mixed at a recommended ratio of 10:1 (resin to hardener). Mixing was carried out by hand for approximately 3 minutes per 100g of resin. After mixing, it was then placed into a vacuum chamber for approximately 15 minutes to degas the mixture, allowing the creation of uniform, homogeneous test samples. Next, 200mm by 200mm float glass plates were pre-coated with a soap and water solution and allowed to air dry. This created a thin film allowing for the easy removal of the PDMS sheets after curing. The mixed resin was then poured carefully on to the glass plate and a second glass plate was placed on top with 2mm thick spacers between and allowed to cure at 22°C for 48 hours. The plates were then separated with the assistance of compressed air and the sheet of cured PDMS was peeled carefully away from the glass.

5.3.2 Laser Machining

The laser used for the patterning of test geometry on the PDMS sheets was a 100W Synrad CO_2 Marking Laser with an FH Flyer Marking head, also manufactured by Synrad. The laser was configured with a focal point of 300μm and had a characteristic wavelength of 10.6μm. A CO_2 laser was chosen due to its ability to easily cut the polymer substrate. Other types such as Nd:YAG and Excimer lasers were tested but neither were able to cut the polymer due to incompatible emission and absorption spectra or, in the case of the excimer, were too slow to be used in a viable continuous production process. The laser is a continuous wave unit that uses Pulse Width Modulation to adjust the output power of the laser. The configuration settings exposed to the user include the power output, as a percentage of 100W and trace speed, up to a maximum value of 990mm/s. The movement of the laser is controlled by the movement of a small mirror mounted in a fixed position above the workpiece. This allows for high trace speeds and excellent levels of precision; however, this setup does limit the viable workpiece size. Additionally, the beam contacting the workpiece will change its angle of incidence depending on the focal position rather than being fixed in a perpendicular orientation , as would be the case with a bed mounted on a Cartesian plotter head.

5.3.3 Metrology Techniques

To quantify the effect of the laser configuration on channel geometry and quality, a range of parameters were tested. These include three power settings (60W, 80W 100W) in combination with nine speed settings between 250mm/s and 50mm/s in 25mm/s intervals for comparison and evaluation. These configuration values are summarized in Table 5-1. Each combination of parameters was tested three times in order to identify the repeatability of the process. Eighty-one lines, 20mm in length and with 10mm spacing between each line were marked onto the pre-prepared PDMS substrate. Once all cuts were made, the samples were diced into groups of three lines and washed with isopropyl alcohol, then dried with clean air

blasts. During initial testing, it was found that imaging and measuring the PDMS samples was not possible due to the material's high clarity in the visible spectrum. To overcome this issue, it was found that a surface coating of a Gold-Palladium Alloy was required. This coating was applied using sputtering, allowing the creation of a 12nm Au-Pd layer to facilitate imaging and surface profiling, which was thin enough not to cause any significant changes in measurements. An example of the images produced both before and after the coating was applied can be seen in Figure 5-1. The coating allowed increased resolution and reduced the number of zones with missing information within the machined channel. However, due to the reflectiveness of the coating, it did create large sections that became over exposed on the surface, for which data could not be collected, this was not an issue as it was not an area for concern within this investigation.

Table 5-1 Experimental laser power configurations used

Laser Power Levels	Focal Diameter	Trace Speed	Energy Output per m²
100W	0.3mm	250 mm/s	1333.33
		225 mm/s	1481.48
		200 mm/s	1666.67
		175 mm/s	1904.76
		150 mm/s	2222.22
		125 mm/s	2666.67
		100 mm/s	3333.33
		75 mm/s	4444.44
		50 mm/s	6666.67
80W		250 mm/s	1066.67
		225 mm/s	1185.19

Laser Power Levels	Focal Diameter	Trace Speed	Energy Output per m²
		200 mm/s	1333.33
		175 mm/s	1523.81
		150 mm/s	1777.78
		125 mm/s	2133.33
		100 mm/s	2666.67
		75 mm/s	3555.56
		50 mm/s	5333.33
		250 mm/s	800.00
		225 mm/s	888.89
		200 mm/s	1000.00
		175 mm/s	1142.86
60W		150 mm/s	1333.33
		125 mm/s	1600.00
		100 mm/s	2000.00
		75 mm/s	2666.67
		50 mm/s	4000.00

Figure 5-1 A) Example image captured of a sample before coating B) Image of the same sample after applying a 12nm Au-Pd coating.

Each of the diced segments were imaged using an Alicona InfiniteFocus with a 10x magnification lens, however, the lines cut at 100W 50mm/s-100mm/s were imaged with 5x magnification due to their size. The system was configured to acquire a lateral resolution of 3μm and a vertical resolution of 750nm. Once the data was acquired it was imported into MountainsMap7.2 Premium Surface Imaging & Metrology Software (Digital Surf, France). Processing was carried out within the software to perform interpolation in order to fill any missing gaps within the acquired data and create a three-dimensional depth map of the surface. An example of this interpolation can be seen in Figure 5-2, with b) being an interpolated three-dimensional model of the surface.
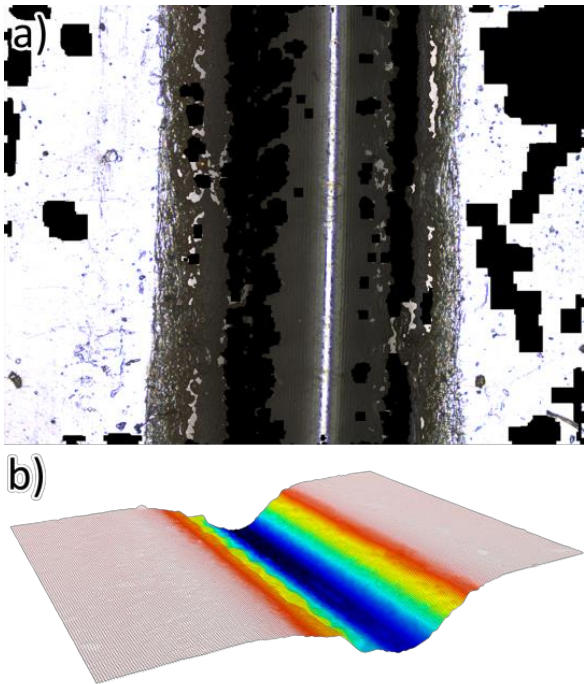
Figure 5-2 a) Channel Texture bitmap and b) depth map after gap-fill interpolation (Sample 1 - 80W at 100mm/s)

Field Emission Gun Scanning Electron Microscope (FEGSEM) images were taken of a selection of a cross section from some samples in order to observe any changes to the material structure and any re-deposition that may have occurred. These cross sections also allowed observation of some of the surface qualities of the channels as well as any kind of thermal fracture that may have occurred. A selection of these images can be seen in Figure 5-3. These images include a close up of the entire channel as well as some of the artefacts that could be seen occurring around the channel itself like in Figure 5-3(b) and Figure 5-3(d).
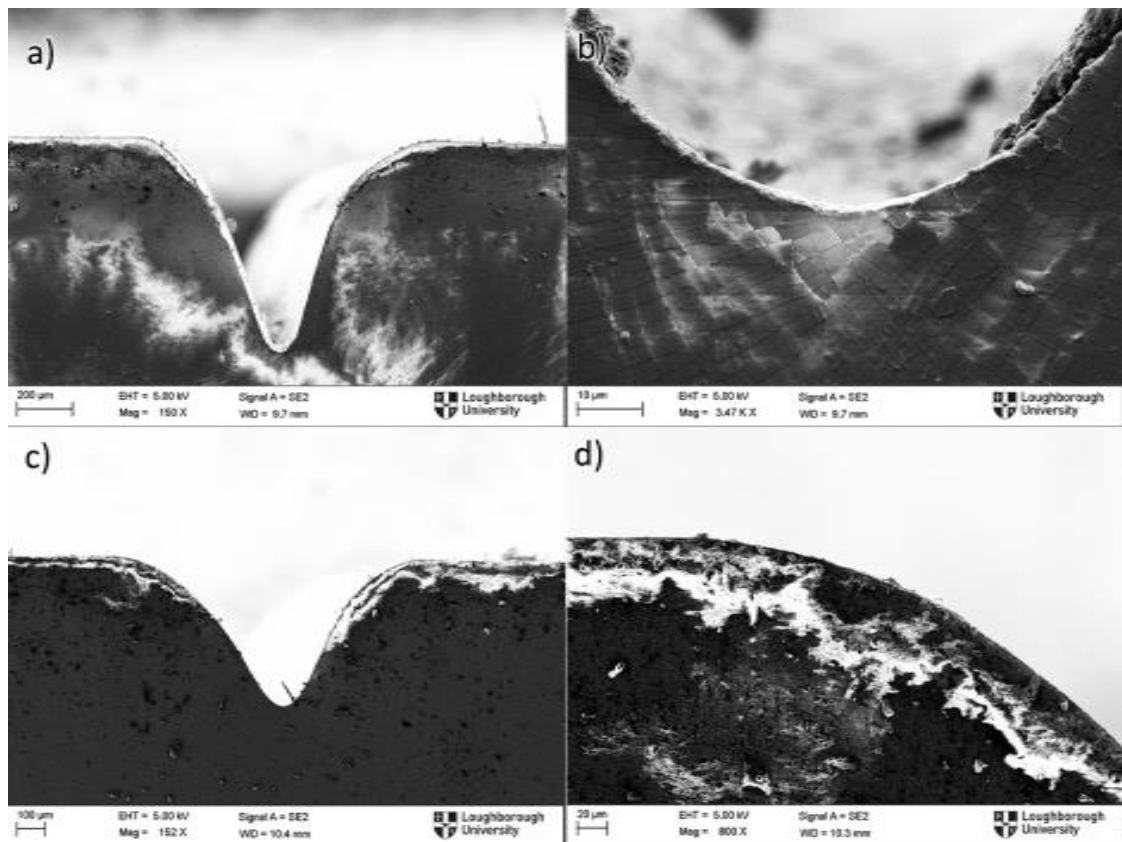
Figure 5-3 FEGSEM Images of two samples, which demonstrate some of the artefacts that were left around the channel after processing. Images a) and b) are from a 100W exposure at 50mm/s and demonstrate what appears to be thermal induced fracture of the material. Images c) and d) are from a 100W exposure at 75mm/s and clearly show re-deposition along the edges of the groove.

5.3.4 Analytical Techniques

Depth profile maps were imported into Digital Surf MountainsMap Premium 7.2, where the imported data had an interpolation step and then a report generated to create a set of graphs and tables that allowed analysis to be completed on the data. Channel depth was measured using two methods: i) by calculating the maximum depth using every profile across the 1.4mm imaged sample, ii) by using the "Valley Depth Tool" which intelligently identifies the bottom of the valley and averages only

those points. The latter was preferable to the profile tool, as the deepest part of the channel may not always be vertically aligned. Channel quality was evaluated using the upper and lower envelopes of all the profiles (Figure 5-4) and a difference calculated at each point as can be seen in Figure 5-5.

The channel edge shape was identified qualitatively as either having a smooth or blunt transition. An example of smooth transitions can be seen in Figure 5-2 and Figure 5-3. A blunt transition is a sharper transition that has a ridge; edges of this type were quite uncommon.
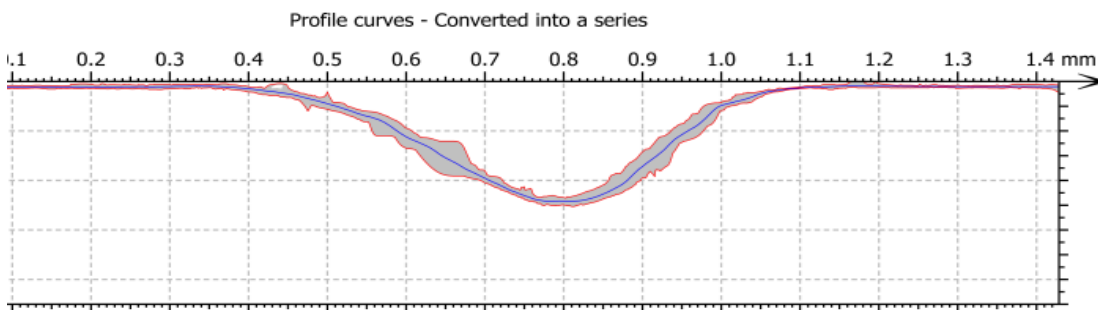
Figure 5-4 Profile curve stack (grey) showing upper and lower envelopes (red) and mean (blue) for Sample 1 - 80W at 100mm/s

Parameters	Step 1	Unit
Maximum height	144	µm
Mean height	37.3	µm
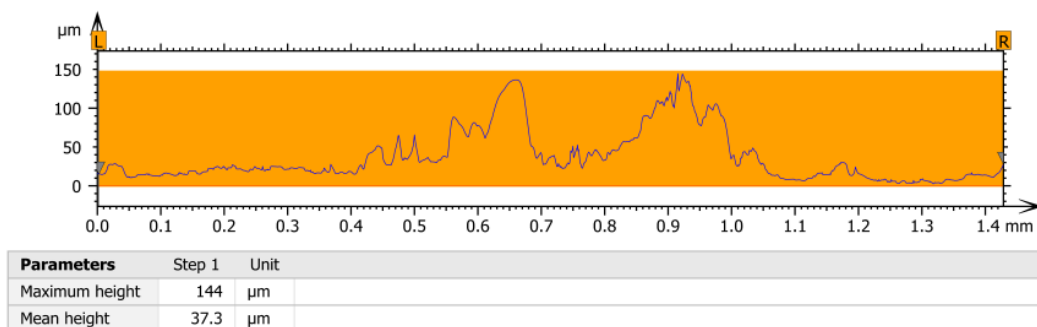
Figure 5-5 Profile curve range calculated as the difference between upper and lower envelopes as seen in Figure 5-4.

Statistical analysis methods employed to characterise included taking the mean, range and standard deviation of each sample repetition. Initially the data was

investigated for outliers and erroneous values, these were classified as any value that was 50% greater than the mean of the other two values, therefore the data presented is complete. These were then plotted onto various graphs seen in §5.4, for critical relationships such as depth vs speed. Attempts were made to fit a curve utilising an exponential curve fit to identify correlation between various laser parameters and the properties of the machined groove. Additional statistical data was able to be generated for each three-dimensional model from within the MountainsMap software, which allowed analysis of the surface quality and texture. This enabled the calculation of the following datapoints;

- The mean peak height (Rc) as defined by Equation (5-1 where n= number of samples and Zt= height between valley and proceeding peak.

$$\mathbf{Rc} = \frac{1}{n} \sum_{j=1}^{n} \mathbf{Zt}_j \qquad (5\text{-}1)$$

- Arithmetical mean deviation of the mean height, which is a measure of the arithmetical average value of the departure of the profile above and below the centre line throughout the sample (Ra) as defined by Equation (5-2. Where n = number of samples and y=deviation from the centre line.

$$\mathbf{Ra} = \frac{1}{n} \sum_{i=1}^{n} |\mathbf{y}_i| \qquad (5\text{-}2)$$

- Number of peaks per mm (RPc) are the number of peaks that extend above a predetermined centre line.

5.4 Results and Discussion

The results can be divided into two categories, channel profile shape and surface finish. Profile shape covers the channel geometry such as channel depth, channel

quality, slope angle and edge transition type. Surface finish covers the waviness and surface roughness of the channel.
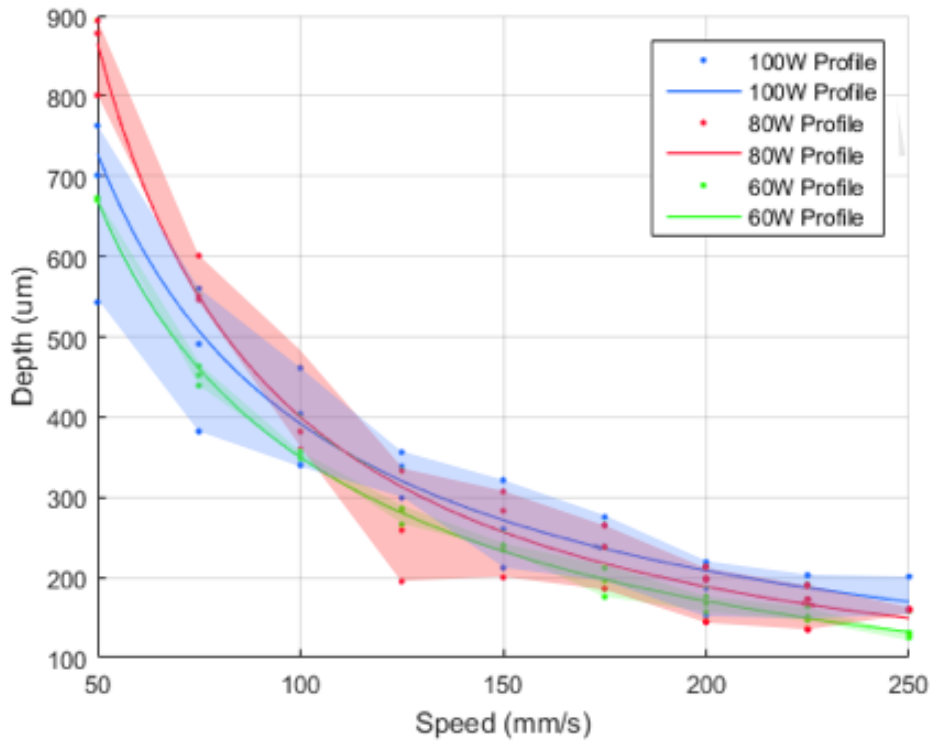
Figure 5-6 Depth vs Speed at the mean maximum profile depth. Coloured bands represent variance in measurement across samples, solid line represents fitted average
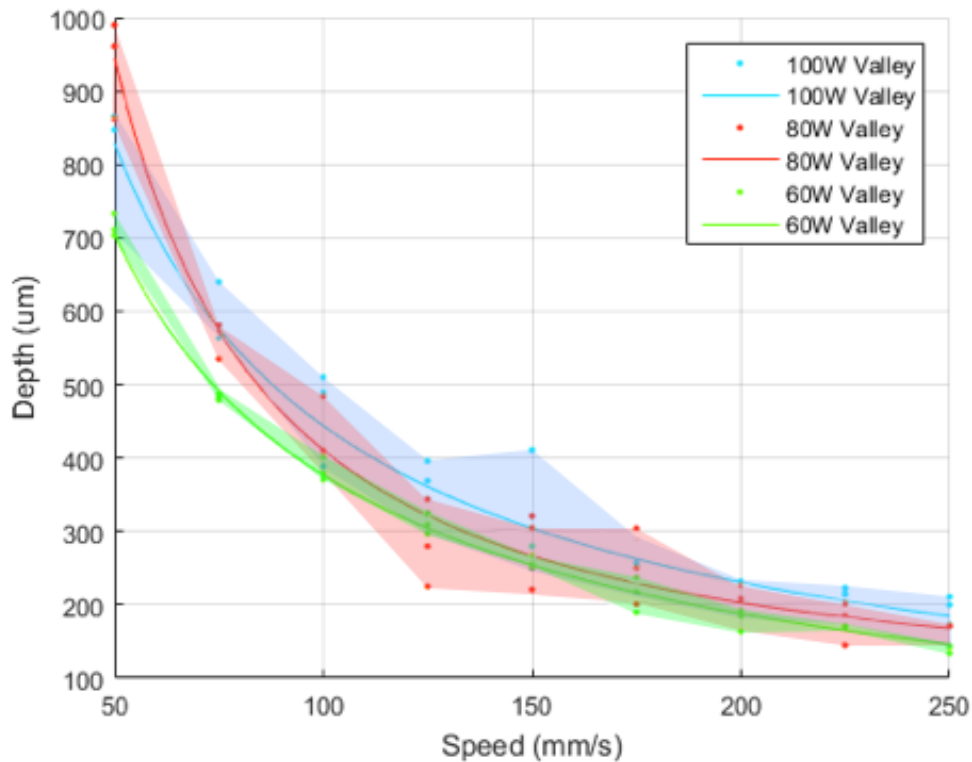
Figure 5-7 Depth vs Speed using Valley Depth Tool. Coloured bands represent variance in measurement across samples, solid line represents fitted average

5.4.1 Channel Profile

Data for the channel depth displayed in Figure 5-6 and Figure 5-7. It can be seen that when the cut was made using 100W power at speeds below 125mm/s the depth did not increase as expected. The expected result was that as the power level increases the channel depth increases and as the trace speed decreases, the channel depth increases as well. This therefore means that the 100W channels traced at 50mm/s should be the deepest channels. It was seen in the depth maps that the shape of the groove no longer followed the Gaussian profile as all the other lines did in addition to being much wider. This can possibly be attributed to the increased energy, a higher energy input concentration and longer exposure time, thus creating a larger heat affected zone which may possibly be recasting the burnt, ejected mass.

Another possibility is when the material is burnt, boiled or vaporized, due to the high energy levels involved, there is a possibility the ejected mass is obstructing the beam and absorbing a significant portion of the energy from the laser. During the experimentation and the cutting of the channels, large amounts of burnt material were observed being ejected from the material and being blown around the containment vessel of the laser. Figure 5-8 shows schematically the process which material goes through as it is being exposed to a laser beam.
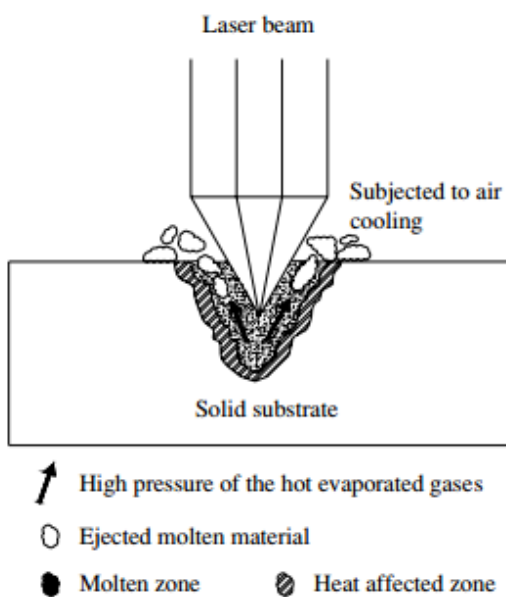
Figure 5-8 The schematic model of the formation of bulges and the material ejection process during polymer machining by laser [161]

The material is ejected by the rapid expansion of high temperature vaporized and molten material. This caused the material to be recast along the edges, which is visible Figure 5-3(d). This would also explain why the repeatability and quality of the channel is drastically reduced. These hypotheses will need to be investigated, further incorporating SEM imagery and high-speed imaging of the process itself. Investigation of the material structure within the groove can then be carried out in addition to observing the behaviour of ejected mass. The observed behaviour however, does indicate a loss of control of the process at higher energy levels. A loss

of control is evident when the dramatic increase in maximum variance with respect to the channel depth, as seen in Figure 5-9, was investigated in addition to energy level. The ribbon plots in Figure 5-6 and Figure 5-7 demonstrate that as laser power increases the variation in depth increases as repeatability decreases, regardless of trace speed or overall cut depth.

Besides this observation, the data had R^2 values of between 0.926 and 0.997 indicating an extremely strong correlation between trace speed and channel depth.

The channel quality can be quantified using the variance graph produced for each sample as seen in Figure 5-4. These values were then plotted in Figure 5-9. It can be seen that above 125mm/s there is no major relationship between speed, power and channel quality. However, as the amount of energy input into the material increases and the exposure time is extended, the channel quality is further reduced evidenced by Figure 5-9. It shows a strong negative correlation between both trace speed and variance. Some of this increase can be attributed to the increased channel depth, however, the same trend still exists when running this comparison with the variance as a percentage of the channel depth.

Due to the configuration of the laser, the slope angles produced are largely dependent on the incidence of the beam. The laser used a scanning head configuration, which uses an articulated mirror to redirect the beam. This means that the incidence angle between the beam and material surface changes as the beam follows its programmed cutting paths [162]. This angle is, at its maximum will be approximately 10° away from vertical. This angle is not enough to cause any noticeable effect to the depth as seen in the relatively consistent depths achieved across multiple samples. It will however affect the slope angle of the grooves. The advantage of using a scanning head such as this is the ability to achieve much higher trace speeds than a conventional Cartesian bed laser. In addition to higher trace speeds, scanning heads are less affected by speed ramping due to the much lower

mass and thus the inertial effects generated during acceleration and deceleration of the laser when compared to an equivalent Cartesian bed system.

Two types of edge transition exist within the scope of this experiment, smooth and blunt. A blunt transition is defined as having a sharp drop-off from the surface to the bottom of the channel. This drop off will have a width that is narrower than the overall depth of the channel. A smooth transition is one that is wider than the depth. It was found that there was no correlation between transition type and either power or speed. The link between the power and transition produced a spearman coefficient of 0.068, and for the speed and transition link a value of -0.582. This shows there is a modest correlation between speed and the likelihood of a specific transition occurring, however it is far from a strong link. The transition depth is more likely affected by the angle of incidence, for which the laser interacts with the material; this was not a controlled variable for this experiment. This is due to the way a scanning head operates.
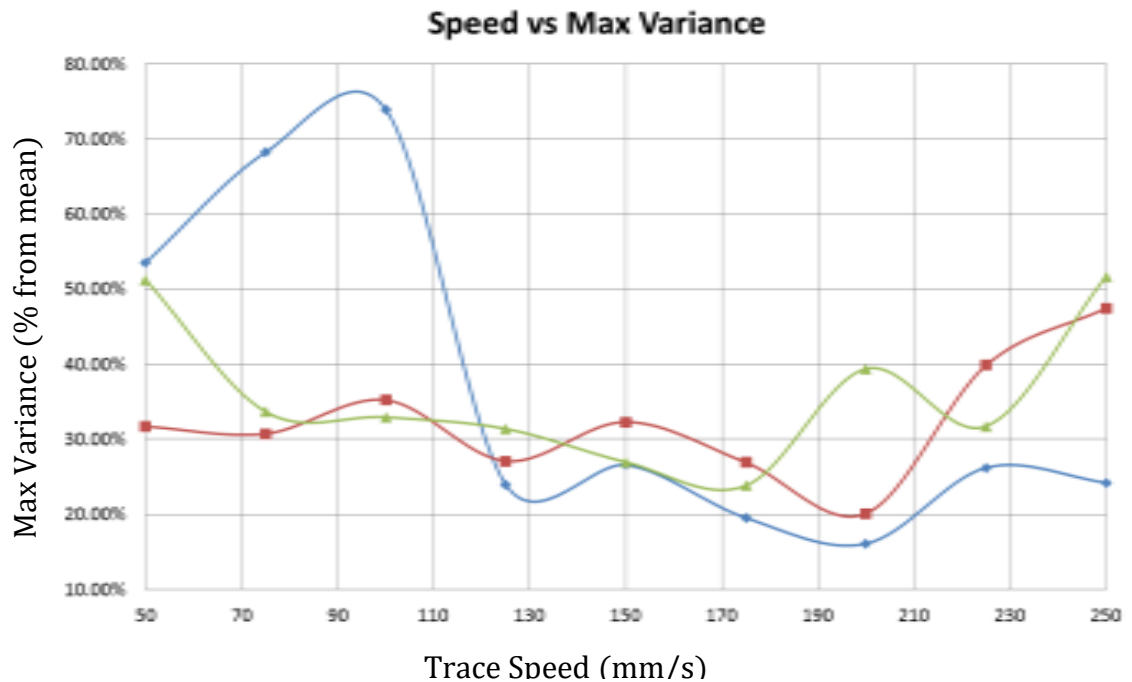
Figure 5-9 Speed vs Max Variance of the channel. Key: Blue = 100W, Red = 80W, Green = 60W.

5.4.2 Material Integrity

It can be seen in Figure 5-3(b) that cracking has occurred at the bottom of the channel likely due to the high thermal stresses induced within the material. These stresses are caused by the extremely rapid temperature rise and steep thermal gradient between the areas of material exposed to the laser and the immediate surrounding areas, both on the surface and below the penetration depth of the beam. As of yet it is unknown if this structure of cracks which are less than 200nm in width will have an effect on the surface wettability with Galinstan or more importantly absorb the fluid and allow penetration of the fluid into the material. This cracking only occurred at higher levels or relative energy deposition that occurred at over $5000J/m^2$. This result matches the hypothesis of these fissures being caused by high thermal stresses and possibly rapid thermal expansion as material is vaporised and ejected from the groove. Further exploration into this phenomenon could be carried

out by investigating if crack presence is directly corelated to the density of the energy deposited and its rate. An investigation into this behaviour could be performed by varying focus size, power and trace speed.

5.4.3 Surface Finish

Surface texture is a significant part of overall surface finish and can be quantified using various metrics that are defined by various standards, specifically BS EN ISO 4287 [163]. From this standard, a specific set of metrics can quantifiably allow the comparison of a set of surfaces. These indicators are Mean Peak Height (Rc), Arithmetical Mean Deviation (Ra) and the number of peaks per millimetre (RPc). The use of these metrics defines the height and frequency of peaks and troughs on the surface as well as defining their deviation from the maximum value. A typical report generated by Mountains Map from each depth map as seen in Figure 5-10, can be created and plots of these values from the samples can be seen in Figure 10. The only drawback to using these values is that they can only be generated for a single profile extracted from the three-dimensional depth maps. Each profile was selected from the deepest part of the channel.
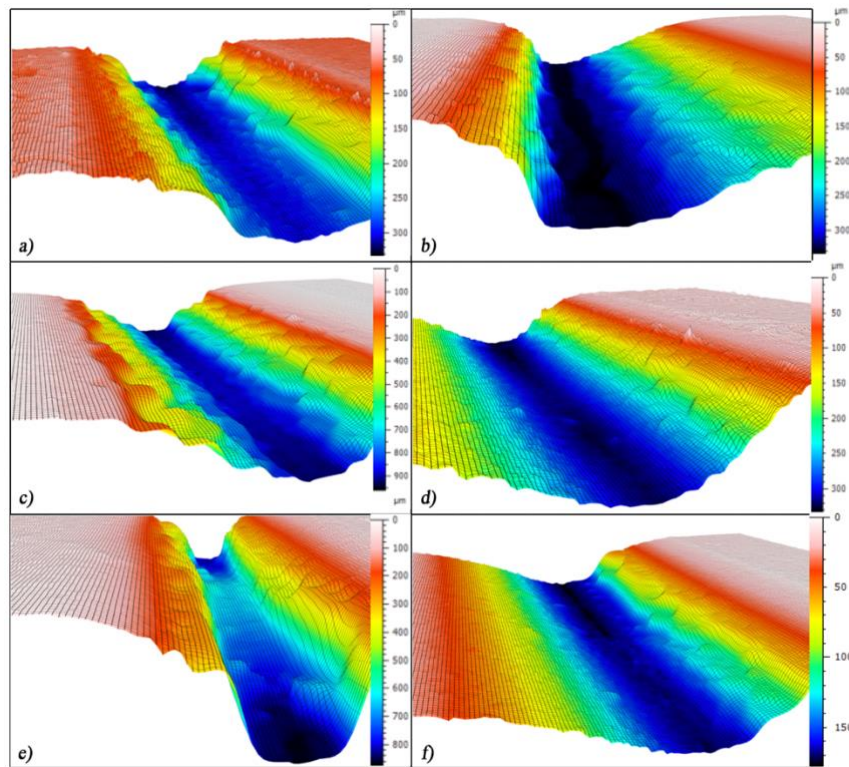
Figure 5-10 Surface maps of samples used to investigate surface finish a) 60W at 50mm/s b) 60W at 250mm/s c) 80W at 50mm/s d) 80W at 250mm/s e) 100W at 50mm/s f) 100W at 250mm/s (All scales are in μm)

It can be seen from Figure 5-11(a) that Mean Peak height appears to be affected by the amount of power input into the material but not by the trace speed. However, the 80W power output appeared to generate the smoothest channels with the lowest overall mean peak heights. However when this value is paired with the mean deviation shown in Figure 5-11(b), this relationship becomes far less significant as there is a discernible relationship between power and the deviation of peak height. There is however, a correlation between the deviation and trace speed ($R^2 = -0.581$), with higher trace speeds producing a more even and nominal channel surface. This is likely due to shorter exposure times to the laser and thus reducing the thermal stresses on the material and resulting in less thermal fracture and additional burning, where the material does not have the required energy to be

ejected from the exposed zone. As for the number of peaks that appear over the measured length, there is no correlation to trace speed or power, which is apparent when the R2 values of -0.011 and -0.116 are examined. This can clearly be seen in the chaotic nature of Figure 5-11(c). This is very likely due to the chaotic and violent nature of the burning and vaporization process that occurs within the laser's focal point on the surface.

Based on the results obtained in this experiment, it can be seen that between 125mm/s and 175mm/s would seem to be an optimum trace speed, balancing both surface finish and repeatability across all power levels tested. This is likely due to providing material sufficient energy to be ejected from the groove cleanly. Depth adjustment should therefore be carried out by varying laser power rather than trace speed.

a

b

c)
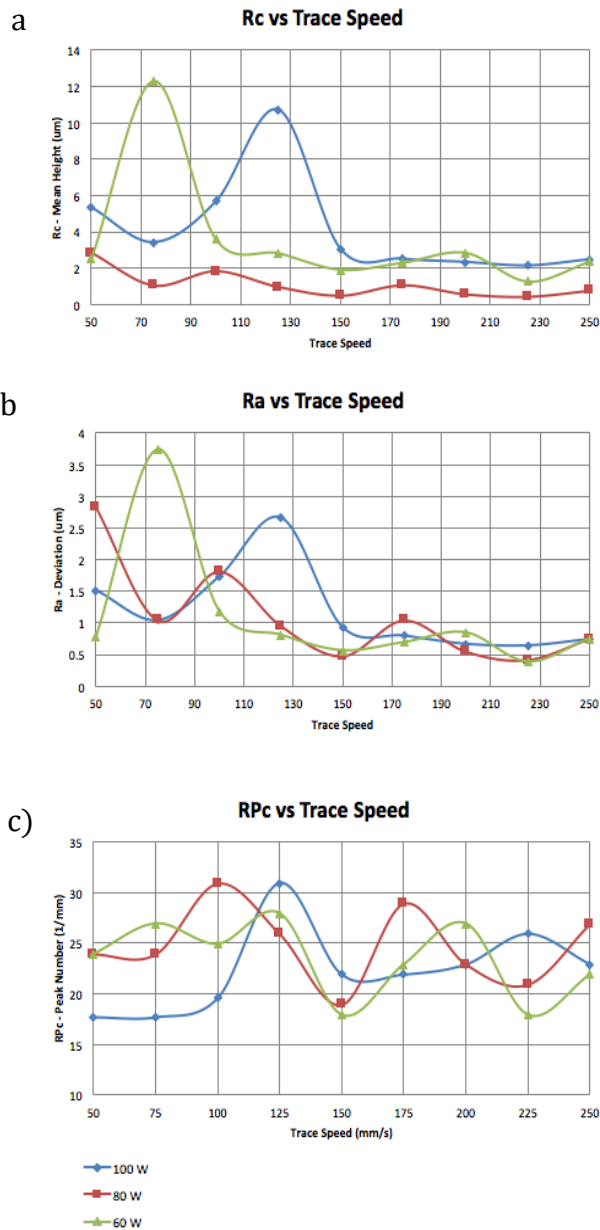
Figure 5-11 Data extracted from each sample surface profile report presented above.
a) Mean peak height (Rc) vs trace speed. b) Arithmetical mean deviation of the mean
height (Ra) vs trace speed. c) Average number of peaks per mm (RPc) vs trace speed.

5.5 Conclusion

From the results obtained, it can be seen there is a strong correlation among laser power, trace speed and channel depth. However, increases in power can negatively affect the channel quality and consistency of geometry. Therefore the channels created are less repeatable and have increased variability across their length; making higher laser powers unsuitable for the manufacture of Galinstan carrying channels as it could create current bottlenecks by increasing the electrical resistance in localised regions. An example of this inconsistent channel width can be seen in Figure 5-10(e), where inconsistent geometries tended to be more prevalent at higher energy deposition rates, such as when speeds were below 100mm/s and above 80W In addition to higher power levels alone negatively affecting channel quality, lower trace speeds also had this effect, therefore this can be directly correlated to power density.

Based on the results obtained in this study, there are limitations on channel dimensions as, in order to create deeper channels, repeatability and channel quality would need to be sacrificed. Additionally a limitation of the laser process used resulted in asymmetric channel geometries as seen in Figure 5-10(b) in some cases due to the changing angle of incidence of the beam. This caused changes in the amount of light absorbed and reflected by the material which resulted in an asymmetric cross section, and could negatively affect interconnects and lamination during deformation of a device. This could create pressure concentrations and could lead to delamination and leaks of liquid metal under bending and compression.

An ideal channel for use in flexible electronics would be to have sharp edges to allow for a good bond when laminating layers of PDMS together. The processes investigated within this study were not able to achieve this reliably, and thus would not be suitable for production of flexible, stretchable systems. They may however still be viable for small scale prototyping though. A possible solution to this problem would be to add a temporary sacrificial laminate to the top surface of the film,

allowing the channel to be truncated and thus achieve the required geometry. This would require further investigation into the required thickness of the sacrificial laminate in conjunction with required laser parameters.

This study was unable to quantify the absorption spectra when plotted against angle of incidence of the material over a range of temperatures. This greatly effects the final channel geometry due to the changes in the amount of power the material is able to absorb. This is an important phenomenon that will need to be included in any models that are able to predict both channel geometry and surface finish.

Further testing of the channel surface, with respect to its interaction with the fluid Galinstan, is required in order to investigate how the material flows through and wets to the machined channel wall surface. It is highly likely a cleaning process will be required to remove debris left over from the laser patterning in order to improve wettability of the surface as this will greatly affect the filling processes and pressures required.

6 SIMULATING THE DEFORMATION OF GALINSTAN BASED INTERCONNECTS WITH PDMS SUBSTRATES

6.1 Introduction

Within this chapter, an investigation into the viability of a laminate-based design for flexible, stretchable electronics is carried out. By using a laminated design process, manufacturability of the system is drastically improved over other processes; however, it does introduce a unique set of problems. The first of these is the required bond strength between layers; lamination methods have various techniques to bond the PDMS films, each with their own distinct advantages and disadvantages. Knowledge of the required bond strength allows the selection of the correct bonding process. The second issue concerns the continuity of fluid within a laminated structure during deformation. The use of Galinstan as an interconnect material allows the flexing and stretching of the substrate material without the fear of a permanent break in a trace, as long as the substrate can withstand the deformation. Once the force on the material is released and thus the deformation is removed, the fluid should refill its original space. However, understanding the fluid behaviour within the trace and at what point the trace continuity will fail, is an important aspect of being able to create a viable system, even if this failure is

temporary. The use of FEA allows for detailed investigation of the forces applied to the internal lamination bonds within the system assisting in the selection of the correct bonding technique. FE modelling of experimental models allows for fast iteration and insight into mechanical behaviours during deformation that would not be possible with physical experimentation. The process of developing and solving an FE model can be broken down into a selection of discrete tasks which can be seen in Figure 6-1 which can be used to guide the research carried out in this chapter.
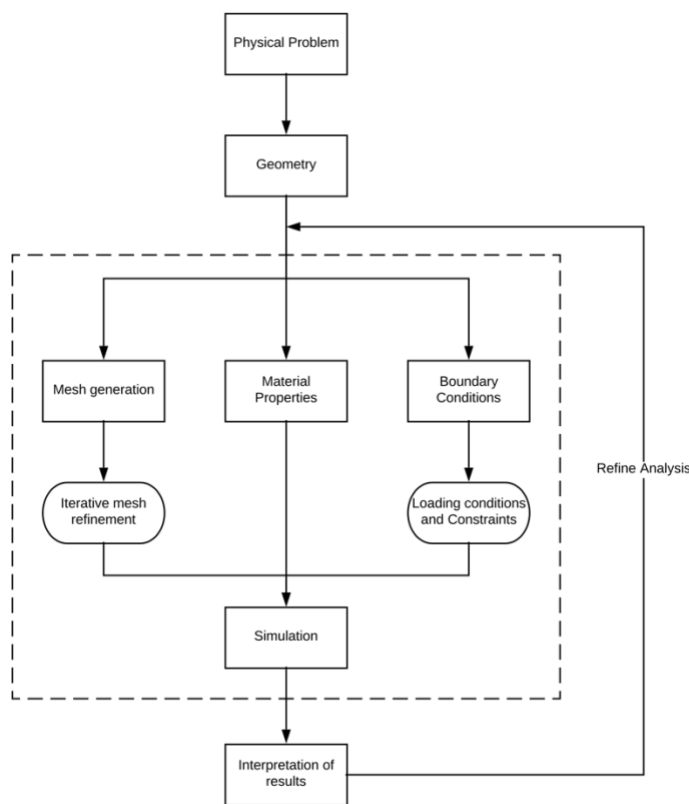
Figure 6-1 Finite Element Analysis Systems Diagram of FE components

6.2 Aims and Objectives

The overarching aim of this study is to identify the optimum bonding technique for laminating layers of PDMS that could be used as part of a conformal electronic system in addition to verifying that an embedded silicon IC would not fracture under

potential deformation. In order to achieve these aims, the following objectives will need to be accomplished.

1. Construct simulation models for a PDMS-Galinstan laminate assembly
2. Quantify the various bond strengths required within the lamination stack and select a suitable bond process
3. Develop an understanding of the forces experienced by an embedded silicon die within a laminated structure.

In order to evaluate the plausibility of the overall system design two conditions would need to be met. The first is that an embedded silicon die would not fracture during a range of possible deformations, which would require the measured Von-Mises stress to remain below the ultimate yield stress of silicon. A major limitation of this evaluation criteria is that it will not identify any failures of etched components or traces on the die itself. Due to the unique design of various dies, it is not plausible to attempt to model them and investigate this failure mode and would have to be validated experimentally.

6.3 Modelling Parameters

In order to solve complex three-dimensional deformation problems, the use of finite element analysis software is required. Of the options available, Ansys Workbench 19.2 (Ansys Inc., Canonsburg, Pennsylvania, USA) was chosen due to its flexibility, ease of use and powerful analysis capabilities. The real world is complex and intricate, requiring infinite computation power to solve perfectly, therefore certain simplifications were made. These simplifications and assumptions were chosen to reduce the required compute power, to reduce experimental complexity, distilling the problem to its fundamental components.

6.3.1 Selection of Solver Methods

Finite Element modelling techniques have been used extensively to model the behaviour of both rigid and flexible systems [146], [164], [165]. It allows the fast

iteration of designs to be "manufactured" and tested digitally at low cost, enabling researchers to target their efforts towards an optimal design for physical experimentation and validation. The software selected for this purpose was Ansys Workbench 19.2 (Ansys Inc., Canonsburg, Pennsylvania, USA) due to its powerful processing and analysis capability and its use by researchers investigating soft polymer deformations [164], [166]. Ansys Workbench is separated into a set of distinct modules. The most appropriate module to solve the problems detailed above is Ansys Mechanical which is designed to solve various structural analysis problems. Within Ansys Mechanical, structural problems can be computed using a range of solving methods which are as follows:

- Static Structural
- Transient Structural
- Explicit Dynamics
- Rigid Dynamics
- Modal

Each of these solvers have been designed for a specific set of problem types and have various strengths and weaknesses that must be balanced to optimise accuracy against the required compute time for each problem. Of the solvers listed, the static structural, transient structural and explicit dynamics solvers will be investigated further as they are applicable in solving the presented problem. The rigid dynamics solver is normally applied to problems that do not account for any kind of soft body and is designed to solve for behaviours in mechanical systems. The modal solver is used to identify modal vibration frequencies within a constrained model, which is outside the scope of this research.

6.3.1.1 Static Structural

A static structural analysis calculates the stresses, strains, and forces involved within structures induced by a load that does not induce any significant inertia or damping effects. Some conditions are required such as a steady state load and

response. The static structural solver is capable of the following types of loading [167]:

- Externally applied forces and pressures
- Steady-state inertial forces (such as gravity or rotational velocity)
- Imposed (non-zero) displacements
- Temperatures (for thermal strain)

Static Structural models the deformation as a set of static equilibrium equations that need to be solved at every increment before it can move on to the next step. When presented with a non-linear problem, Ansys Static Structural uses Newton-Raphson equations to approximate and determine a solution incrementally. Ansys Static Structural however, is not ideal for computing complex time dependant responses, such as impact and dynamic contact mechanics. These problems normally induce non-linear material behaviour, large element deformation which require the number of iterations required to solve the problem to increase drastically [168]. For Ansys to solve all the conditions within the problem, it must iterate through every node and check they are satisfied. The problems being investigated utilise slow moving forces and relatively low strain rates, so therefore fall within the confines of static structural solvers. However, if Ansys is unable to satisfy every node, convergence will not occur, which will result in the simulation returning no results and defining the problem as impossible to solve [169]. This could therefore result in limitations to the amount of deformation that can be applied to the PDMS substrate.

6.3.1.2 Transient Structural

By definition, transient analysis involves loads that are a function of time. A transient analysis can be performed on rigid assemblies and flexible structures.

Transient structural analyses use the ANSYS Mechanical APDL solver, which can calculate the dynamic response of the structure under test and any general time-dependent load. It can be used to determine strains, stresses, and forces as well as

time-varying displacements in an assembly or structure during response to transient loads. Loading time scales are such that inertia and damping effects are considered during calculations. If inertia and damping effects are not important, it may be possible to perform a static analysis instead. Due to the way in which simulations will be setup, inertial and damping effects are negligible and thus not important to creating an accurate model.

The solver is designed for long duration problems, whereby they are broken into multiple steady state problems, which are then added together to calculate displacement, stress, strain and forces over time [167]. It therefore functions almost identically to Static Structural, however it does come at the expense of a longer compute time due to the additional problems that require solving. This would still fail to converge on large element distortions and thus limiting the rate and amount of deformation that can be applied to the PDMS.

6.3.1.3 Explicit Dynamics

The Explicit Dynamics solver is a transient explicit dynamics module that can perform a variety of engineering simulations, including the modelling of nonlinear dynamic behaviour of solids, fluids, gases and their interaction [167]. Ansys Explicit Dynamics solver utilises wave propagation theory, allowing the use of deformable bodies in conjunction with rigid models. Resolution of the equilibrium equations at each step, as required by Ansys' Transient and Static Structure solvers is not necessary when using the explicit solver. The stiffness matrix is modified using geometry and material changes at the end of each step by advancing the kinematic state from the previous step without any iteration. Accelerations and velocities are assumed to be constant during each discrete time step and are used to solve the next increment in the sequence. This makes it especially useful for problems involving high speed impacts and applications of forces, which are not applicable to the problem presented here as loads are to be applied slowly to avoid the rate dependant properties of the materials and simplify the problem.

The Explicit solver may use more calculations to carry out this analysis; however, each calculation is relatively inexpensive computationally. In order for explicit analysis to be accurate, a large number of increments, of a sufficiently small size need to be used; however, if there are too many increments the time taken to solve them could be excessive. Explicit solutions are not always stable, as they need to meet certain conditions, such as the stable time increment, which is defined, as "the minimum time required that a dilatational wave takes to move across any element in the mesh" [170]. This often leads to simulations being more computationally intensive overall, as the reduction in expense for a single calculation is outweighed by the overall increase in calculations required when compared to static or transient structural solvers.

6.3.1.4 Solver Selection

By weighing up the strengths and weaknesses of each solver method, it was decided that the Static Structural would be best suited to solve the problems encountered within the scope of this paper. However, when adding internal fluid elements to the simulations, the Static Structural solver would not be able to take the additional fluid pressure changes over time into account. For this reason, any simulation that required the use of an internal fluid would be solved using the transient analysis method. Both the static and transient methods use the same underlying solver, but applied slightly differently to accomplish their goals, however when compared to the Explicit solver, compute times were shown to take less than ten percent of the time as can be seen in Figure 6-2. These values were generated by creating a simple representative model and running this same model through each solver.
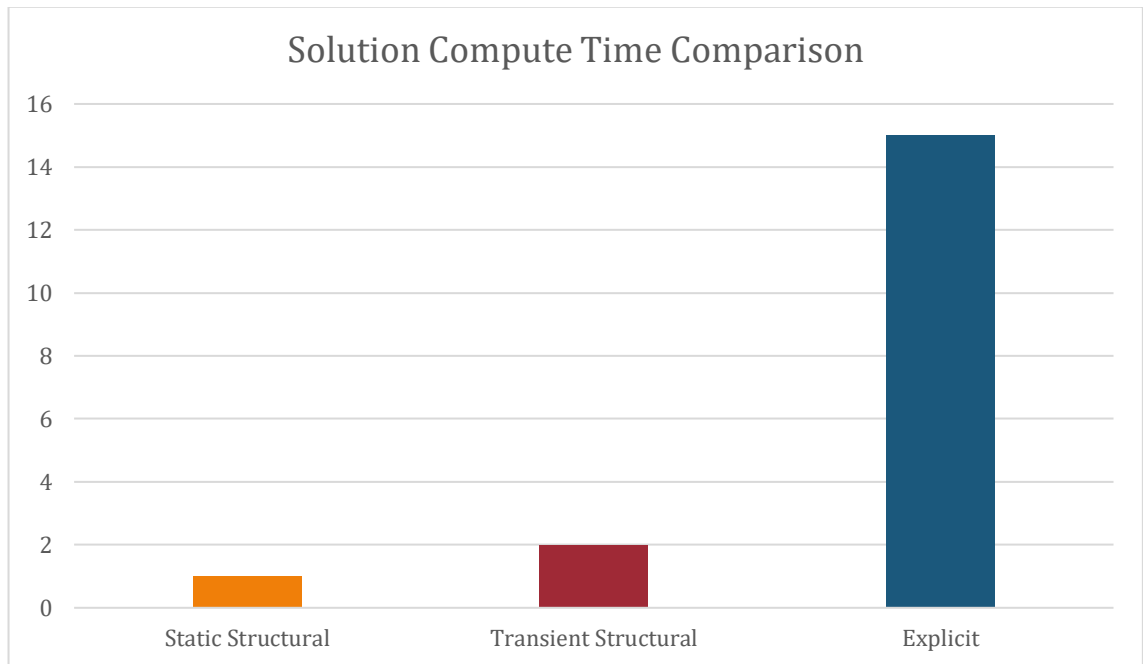
Figure 6-2 Mean time taken to compute a solution for various problem types using the viable solver methods. All values are presented as a multiple of the time taken to solve the problem using the static structural solver. A shorter bar is representative of a faster mean solve time.

6.3.2 Geometries and Meshing

When designing the geometry to be simulated, it must be kept in mind that physical verification of these digital models can be quite challenging. In order to overcome this issue, the geometries chosen need to be larger than would be used in mass manufacture. This improves the ease at which the results of the simulations can be verified.

The overall geometry chosen was to use a square block with rounded corners as seen in Figure 6-3. The use of a large block was chosen to allow it to be gripped by various rigs during verification stages. Internally it is able to contain various channel structures in varying positions to allow accentuated testing of the channels at an increased scale. This larger scale creates the opportunity for easier optical

monitoring of the deformation of the system in addition to improved manufacturability. A length of 150mm was chosen as it allowed ample space for the model to be gripped or clamped during validation, without affecting the test area towards the middle of the piece. This large geometry was chosen due to limitations of the materials characterisation tools. When validation of models is carried out, load cells that are immediately available within the department can be used in testing.
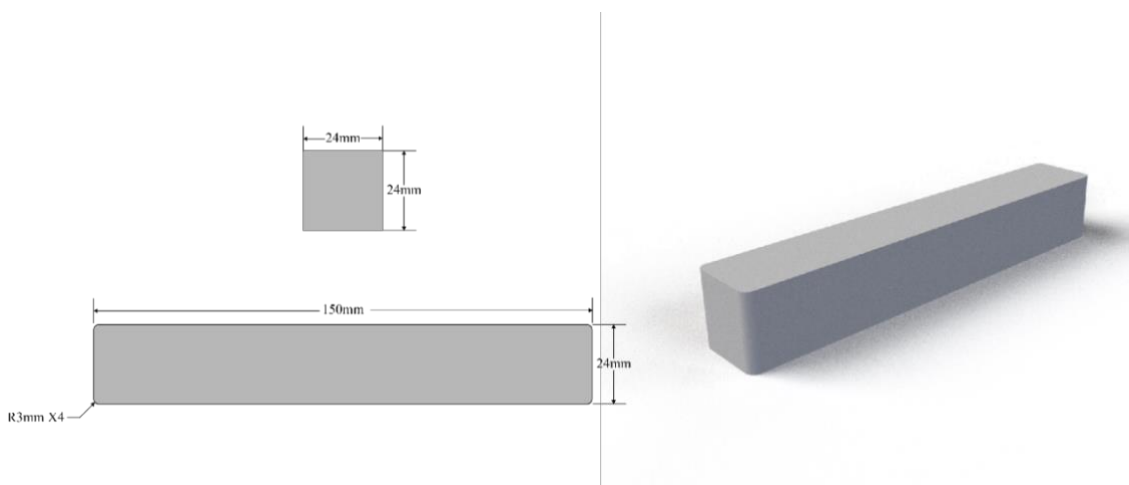
Figure 6-3 Test sample geometry

When creating models within most finite element packages, the geometry must be subdivided into a mesh. This mesh is a polyhedral approximation of the part which enables mathematical modelling to be carried out on the part. Where possible, it was attempted to keep meshes orthogonal to the part and maintain hex element types allowing for a more uniform mesh. However, due to some of the complexities of the geometry, sections of the model used tetrahedral elements.

In order to properly mesh the components, a variety of meshing methods and refinements were used. Most sections utilised edge meshing with a fixed number of divisions per edge. This combined with the use of face meshing allowed for the creation of an even hexahedral mesh across all samples. Rigid body surfaces solely

utilised face meshing in order to achieve an even mesh. An example of how these edge divisions were used can be seen in Figure 6-4.
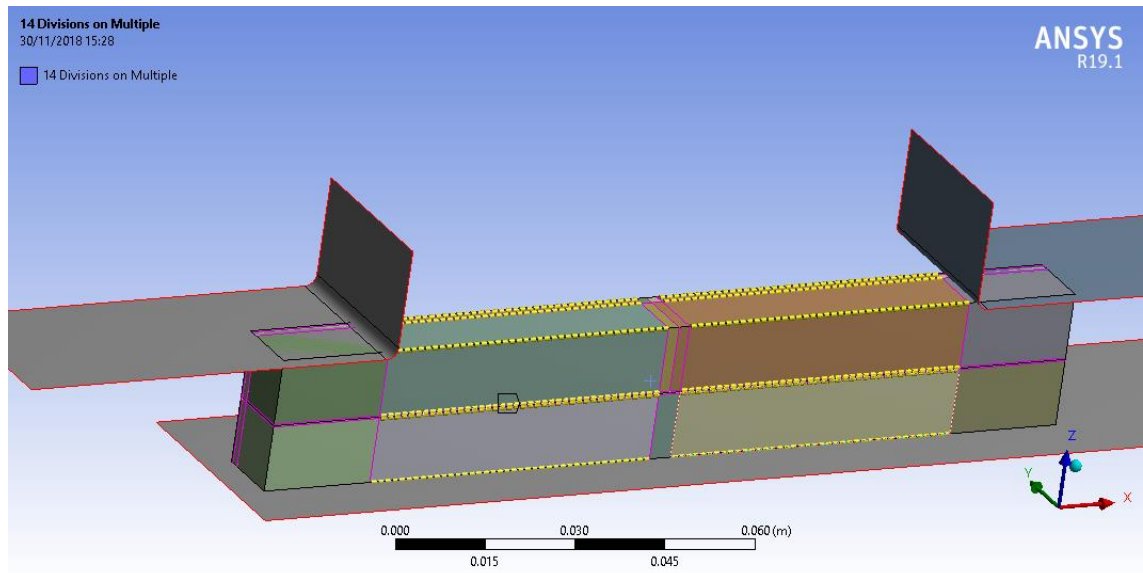
Figure 6-4 Edge divisions used to create a precise and even mesh

Care must be taken when meshing the model to prevent various instabilities within the simulations. One such instability can often occur during large deformations if the chosen mesh is not dense enough. Hourglassing is an instability within the mesh that can cause inaccuracies throughout result outputs and can be seen in Figure 6-5. It occurs when the strain or position changes are not applied to a single integration point, deforming an element into a trapezoid shape. This effect can be alleviated with the use of a denser mesh by having at least four elements through the thickness of the section. An example of this four-element solution can be seen in Figure 6-5.
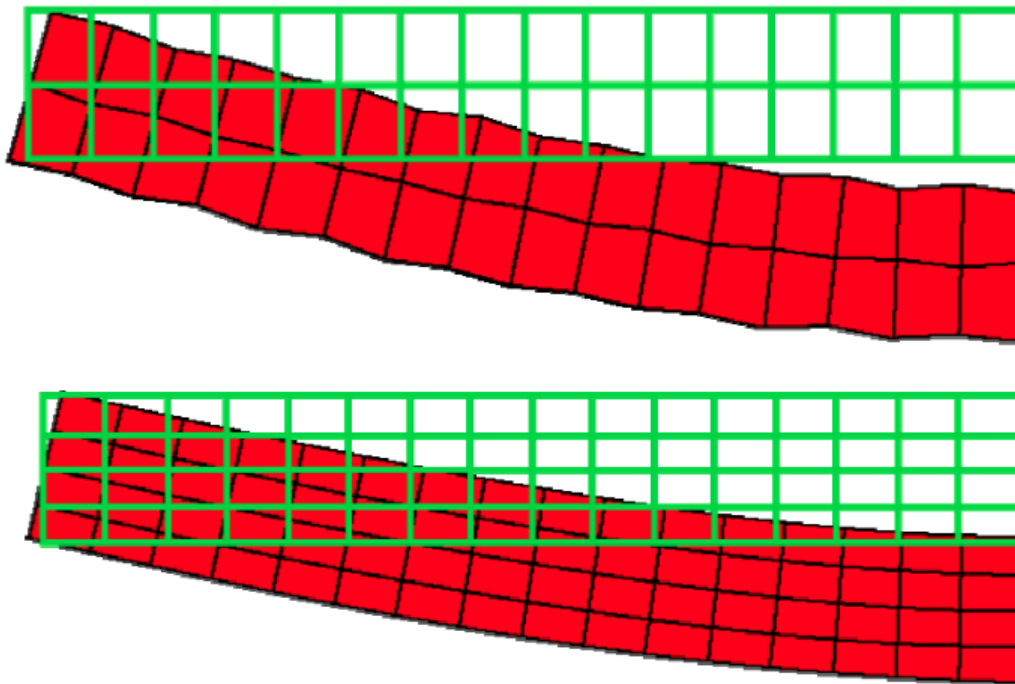
Figure 6-5 (Top) Demonstration of hourglassing effect when compared to a denser mesh with no instability (Bottom). Both models were subject to the same constraints and deformations [171]

Ansys has over 160 element types to enable accurate and efficient simulation of a variety of problems. They can be separated into two-dimensional and three-dimensional elements and then within that, they are grouped into sets that each have specific use cases and advantages. However, increases in accuracy normally come at the cost of increased compute time. Looking at the type of problem and the geometry to be simulated indicates that the best element type would be solid elements for the PDMS and silicon components. In order to simulate the contained Galinstan fluid, some kind of fluid element would need to be used, which grants the choice of either standard fluid or hydrostatic fluid elements, depending on how the problem is to be modelled and the available compute time.

Each element within this mesh must then be assigned a type. Ansys has a wide range of element types that each solve a different set of problems. Every element will be associated with a 'Family'. This allows mathematical differentiation between shells, membranes, rigid and other problem types. In order to do this, elements will also have different numbers of nodes and have a different element shape with one of two geometric orders, linear or quadratic approximation. The way FE simulation works can lead to compounded errors along the model, especially if the solution for the parameters is sufficiently smooth. A higher order approximation can improve this and is preferable to a linear geometric order.

Ansys has an integrated recommendation algorithm that will select an element type that it suggests will be optimal for the problem being solved. It is possible to override the selection that Ansys makes using an ADPL Command, however, in all cases used, Ansys selected the desired element type automatically.

For the PDMS components, Ansys automated recommendation engine selected the SOLID187 element type, which is well suited to non-linear, hyperplastic materials, unless they are fully incompressible, which is applicable to the applications and material types being used here.
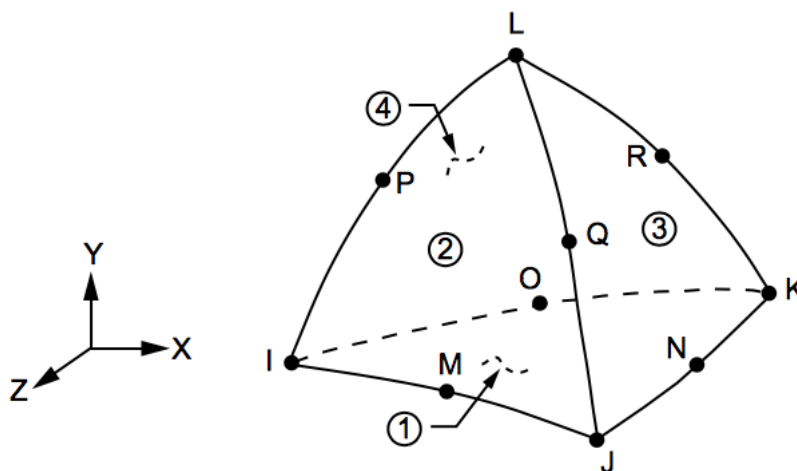
Figure 6-6 SOLID187 Element Geometry [172]

The element types that were selected for use by using Ansys' recommendation engine for the anisotropic silicon components were SOLID186 elements. These are 3-D 20-Node Structural Solid elements, with an option to interchange between a homogeneous and layered type by toggling KEYOPT(3). This option was disabled in order to simulate a homogeneous solid material. The diagram of this element type can be seen in Figure 6-7.
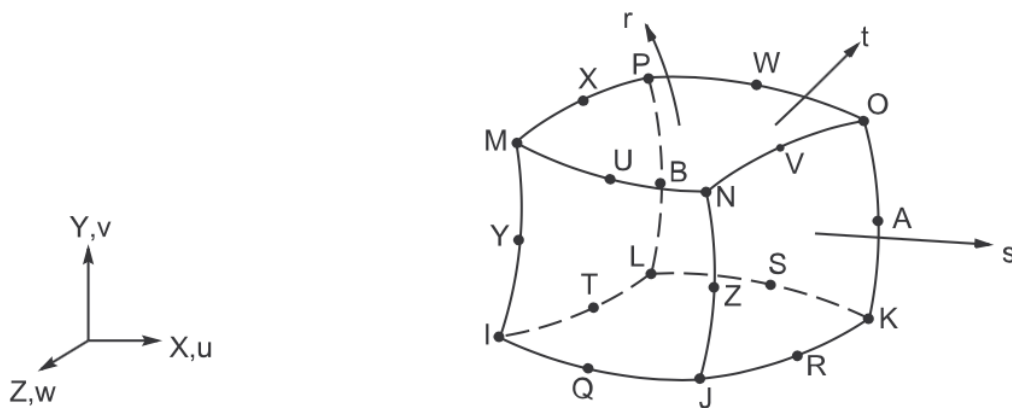
Figure 6-7 SOLID186 - 3-D 20-Node Homogeneous Structural Solid Geometry [173]

Given that PDMS is a rubber material with a near incompressible response, the use of reduced integration was employed to help reduce volume and shear locking issues. Volume locking may occur where the requirement for an element to have no change in volume causes an over-constraint on the displacement field. This can result in the mesh artificially becoming far stiffer than it should [174]. Shear locking is seen in elements that are exposed to bending, where integration points can be subject to nonphysical shear strains because the element undergoes shear rather than bending due to the element composition, also creating an artificially stiff mesh [175].

In order to simulate the internal Galinstan filled components, it was decided that the combination of Ansys Computational Fluid Dynamics modules to solve the internal fluid problems was not required due to the increased complexity that comes with

combining multiple problem types, which drastically increases the compute power required to solve the problems. Due to the way the problem is defined, a set of assumptions can be made to drastically simplify the way the fluid is modelled. Instead of modelling the Galinstan as a discrete fluid encapsulated within the PDMS structure, it could be modelled as a contained hydrostatic fluid. The downfall of this method is that it would not display any leaks or be able to display any air that could possibly enter the channel during failure, however it does allow for a large reduction in the required compute time to solve the problem. The process required to create a 3D hydrostatic, contained fluid within a solid mesh required the use of Ansys' ADPL Commands which can be seen in Figure 9-1. This command lined the specified faces with a set of secondary surfaces which were then assigned the HSFLD242 element type, as seen in Figure 6-8, which is specifically designed for the simulation of three-dimensional hydrostatic fluids. This element type is well suited for the calculation of fluid volume and pressure especially for coupled problems involving solid-fluid interaction. Fluid pressure within the volume is assumed to be uniform throughout and is therefore unable to apply pressure gradients, which in turn, is unable to simulate sloshing effects. Both temperature and compressibility effects may be included but were not utilised in this case and fluid viscosity cannot be applied to this element type.
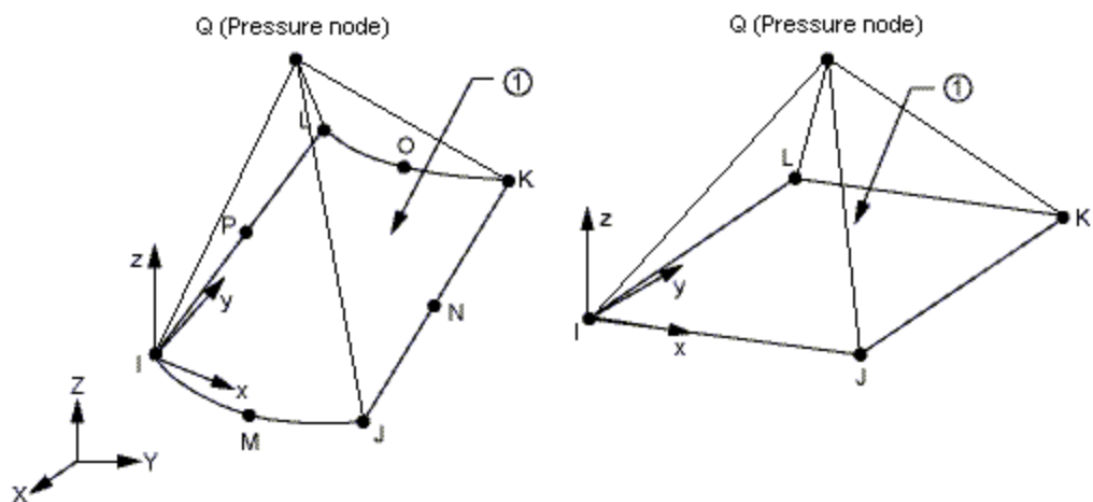
Figure 6-8 HSFLD242 - 3-D Hydrostatic Fluid Element Geometry [176]

An example of the mesh used to model the problems can be seen in Figure 6-9. Limitations on a mesh density were artificial in nature, being applied by ANSYS licenses rather than a technical requirement [177]. Thus, the number of elements for the PDMS block was set at approximately 21,000 elements, allowing room for meshing of other objects within the simulation.
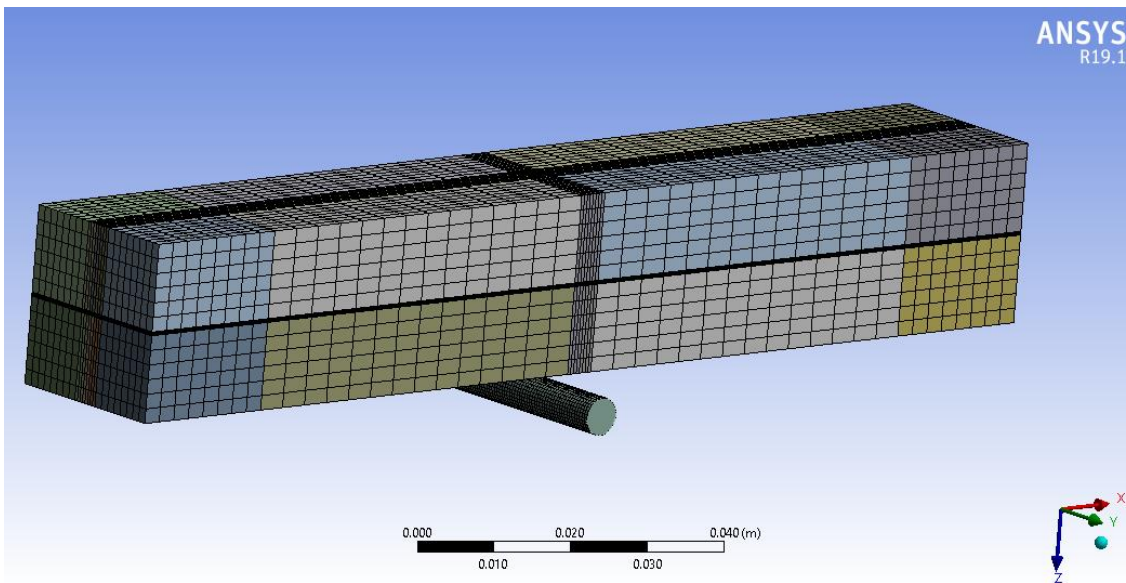
Figure 6-9 Example of meshing on three-point bend test model

6.3.3 Material Models

The mechanical behaviour of objects within finite element analysis are described mathematically using various material modelling techniques. PDMS would normally be modelled as a hyperelastic or viscoelastic material due to its nonlinear response. The Mooney-Rivlin, Neo-Hookean and Ogden models were evaluated and compared with a standard elastic model. In all cased below, W = strain-energy function per unit undeformed volume.

Mooney-Rivlin:

$$W = c_{10}(\bar{I}_1 - 3) + c_{01}(\bar{I}_2 - 3)$$
$$+ c_{11}(\bar{I}_1 - 3)(\bar{I}_2 - 3) + \frac{1}{d}(J - 1)^2$$

(6-1)

Where $\boldsymbol{c_{10}, c_{01}}$ *and* $\boldsymbol{c_{11}}$ are empirically determined material constants, $d =$ material incompressibility parameter, I_1, and I_2, = invariants of components of the right Cauchy-Green deformation tensor and J is the ratio of the deformed elastic volume over the reference (undeformed) volume of materials.

Neo-Hooke:

$$W = \frac{\mu}{2}(\bar{I}_1 - 3) + \frac{1}{d}(J - 1)^2$$

(6-2)

Where μ = initial shear modulus of material.

Ogden:

$$W = \sum_{i=1}^{N} \frac{\mu_i}{\alpha_i}\left(\bar{\lambda}_1^{\alpha_i} + \bar{\lambda}_2^{\alpha_i} + \bar{\lambda}_3^{\alpha_i} - 3\right)$$
$$+ \sum_{k=1}^{N} \frac{1}{d_k}(J - 1)^{2k}$$

(6-3)

In the Ogden model W expressed in terms of the principal stretches $\lambda_j =$ stretches of the left Cauchy-Green tensor. Where N, μ_i, α_i, d_k are all material constants. Where J = determinant of the elastic deformation gradient

The material values for the hyperelastic model were sourced from research carried out by Payne [178] and used a material model that was developed to represent human skin. Due to the intended applications for devices utilising the technologies researched here, it was logical to ensure materials would be able to conform to the deformations of human skin. The material properties used for the purely elastic model of PDMS can be seen below in Table 6-1. This simplification is possible due to the low rate of strain and thus reducing the hyperelastic effects to negligible levels.

Table 6-1 Parameters used to model PDMS material models using a purely elastic response [178]

Variable	Value
Density	$965 \; {}^{kg}/_{m^3}$
Young's Modulus	$1.32 \times 10^7 Pa$
Poisson's Ratio	0.499

For situations where Galinstan was present, the use of a three-dimensional fluid hydrostatic element type meant that the only required property for Galinstan was density, the value used was $6440 \; kg/m^3$. This greatly simplifies the material model required, as it is not possible to assign viscosity to the HSFLD242 element type.

The material used within the models was one that was required to represent discrete components that are normally manufactured on silicon substrates. Due to the complex nature of these parts and their small-scale manufacture, they were modelled as a 5mm x 5mm x 1mm block and is assumed to be a bare silicon wafer material. The molecular structure of crystalline silicon means that it cannot be modelled as an isotropic material and must be modelled as an anisotropic material instead. Therefore, Miller indices must be considered to model the material properties of the cubic crystal structure, an example of the notation and structure can be seen in Figure 6-10. The material properties used to generate this model can be seen in Table 6-2, Table 6-3 and Table 6-4.
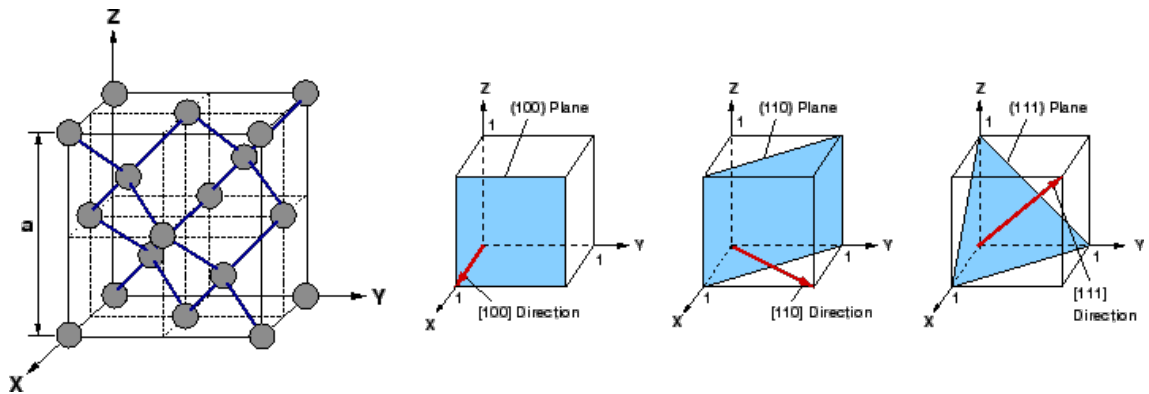
Figure 6-10 Illustration of the silicon structure and Miller Index notation [179]

Ansys comes with an integrated material library from Granta Design [180]. This includes an anisotropic silicon material model with the following properties. By using these integrated material libraries, the time taken to develop the model was drastically reduced.

Table 6-2 Material properties used for anisotropic model of silicon [180]

Property	Value
Density	$2330 \, kg/m^3$
Isotropic Secant Coefficient of Thermal Expansion	Tabular – See Table 6-3
Zero Thermal Strain Relief Temperature	$22°C$
Anisotropic Elasticity	Tabular – See Table 6-4
Isotropic Thermal Conductivity	$124 \, W/m \, C$
Specific Heat C_ρ	$702 \, J/kg \, C$

Table 6-3 Coefficient of Thermal Expansion for Anisotropic Silicon [180]

Temperature (ºC)	Coefficient of Thermal Expansion ($^\circ C^{-1}$)
20	2.46×10^{-6}
250	3.61×10^{-6}
500	4.15×10^{-6}
1000	4.44×10^{-6}
1500	4.44×10^{-6}

Table 6-4 Anisotropic Elasticity of Silicon Material Model [180]

	D[*,1] (MPa)	D[*,2] (MPa)	D[*,3] (MPa)	D[*,4] (MPa)	D[*,5] (MPa)	D[*,6] (MPa)
1	1.66×10^5					
2	64,000	1.66×10^5				
3	64,000	64,000	1.66×10^5			
4	0	0	0	80,000		
5	0	0	0	0	80,000	
6	0	0	0	0	0	80,000

The final material used was structural steel which was again included in Ansys' material models from Granta Design. This material was only used for tools used to apply forces during certain tests. For this reason, the properties themselves are not vastly important, only that it is significantly harder and stiffer than the PDMS it is applying a deformation to. The properties for structural steel can be seen in Table 6-5.

Table 6-5 Overview of crucial material properties for Structural Steel [180]

Property	Value
Density	$7850 \, kg/m^3$
Young's Modulus	$2 \times 10^{11} Pa$
Poisson's Ratio	0.3
Bulk Modulus	$1.6667 \times 10^{11} Pa$
Shear Modulus	$7.6293 \times 10^{10} Pa$

6.3.4 Boundary Conditions

Each simulation requires a different selection of boundary conditions and will be discussed within the following simulation sections. A common thread throughout all simulations was the rate of load. Each application of force or displacement occurred at rate of 1mm/s to 3mm/s leading to each time step being allocated between 10 seconds and 15 seconds. This low rate was chosen to enable the simplification of material models, reducing the effects of hyper elasticity to negligible levels and enabling the use of purely elastic material models for all components.

6.3.4.1 Contact Boundary Conditions

For each of the models, some versions contained additional internal components to simulate the inclusion of large silicon dies, which in turn required contact conditions

to interact with the PDMS. The relationship between the two surfaces was defined as being a bonded interaction. This means that the parts cannot separate or incur a gap during deformation, nor can they slide against each other. This allows the simulation of a perfect bond, which the reaction force required to maintain the bond can be measured and to then select the correct bonding technique during manufacturing.

For the laminated versions of the models, again the relationship between the two surfaces was defined as a bonded interaction. This allowed the force between the two surfaces to be measured during the applied deformation to the workpiece and the required bond strength to be calculated using both a pressure measurement and force probe of the surface. Based on research carried out by *Kersey, Ebacher et al* [181] the bond strength between PDMS and Silicon, if properly prepared without a primer, is capable of withstanding approximately 468kPa ($\pm$ 128 kPa), so therefore applied pressures must not exceed this value to prevent delamination between the PDMS and silicon die.

Contacts between clamping surfaces and the device under test are all modelled as frictionless. With good experimental design this can get close to realistic values through the use of lubrication, thus reducing frictional effects to negligible levels; having little effect on the final result.

6.3.4.2 Hydrostatic Fluid Containment Conditions

In order to simulate the presence of Galinstan within the channels in the model, an assumption was made that there would be no fluid flow within the channel, therefore, the Galinstan fluid could be modelled as a hydrostatic fluid. By making this assumption, it was not necessary to create a hybrid fluid-solid model, that although modern packages such as ANSYS are able to do, places an incredibly large computational requirement on the problem. Therefore, it was decided to use a combination of hydrostatic elements and an initial hydrostatic pressure. The hydrostatic body parameters that were used can be seen below in . Due to the low

stresses and forces involved, it was acceptable to model the Galinstan fluid as incompressible. The limitations of modelling the fluid in this way meant that no fluid movement would occur within the channels, thus possibly reducing the peak pressures that could occur as the fluid would ordinarily move to one end of the channel.

Table 6-6 Hydrostatic Fluid element parameters

Property	Value
Density	$6440\,kg/m^3$
Fluid Mass	Volume of the fluid element
Fluid Material Model	Incompressible
Coefficient of thermal Expansion	$6.1 \times 10^{-5}\,°C^{-1}$

6.4 Simulations

The constraints chosen when building a finite element model are crucial to producing a model that can be validated. Therefore, the use of simulated end clamps was employed to ease difficulties when validation was attempted in the lab. For each set of conditions, a slightly different set of constraints was chosen. Each of the tests were carried out using fixed displacements or rotations rather than using force, which in turn allowed for easier verification of the models.

It was decided to carry each test out separately to better understand the behaviour of the sample in one axis at a time. It is thought that a system such as this would undergo multi-axis deformation, however, this would be unpredictable and random. Therefore it would be advisable to break the simulation down into manageable tasks.

All models used very similar analysis settings to apply to the solver. Two load steps were applied when required, the first to apply the clamping force and the second to

apply the force under test. The only exception to this was the compression model which only required a single step. Each step was five seconds long in order to allow the load to be applied slowly, allowing the problem to be modelled as a steady state one, and thus simplifying the level of detail required in material models. Many silicon rubbers have properties which can change with regard to the strain rate applied [182], by slowing the rate at which the load is applied, these effects become negligible. The large deflection option was enabled to allow the simulation of the soft polymers. This option allows ANSYS to adjust the stiffness of the component based on the changes in its geometry during deformation. For silicone rubbers, this is required to accurately portray their behaviour within the simulation.

6.4.1 Uniaxial Extension

In order to create a model that can be validated, a method of gripping the sample must be included, therefore, the last 20mm of material at each end was clamped.

The lower surface was modelled as a rigid plane and affixed with an encastre boundary condition. The PDMS block was then placed onto this surface and attached with a frictionless boundary condition, in order to allow the block to slide during deformation and prevent artificially raising the stress in the polymer by being unrealistically fixed to the work surface. Frictionless contact was chosen in order to simplify the model rather than attempt to model the frictional forces that would occur as they would likely be negligible with good experimental design.

Two curved clamping plates were then placed onto the block. These were modelled as rigid surfaces utilising a frictionless contact relationship with the PDMS block. These two surfaces were then constrained using joints in order to restrict their movements to a single translational axis for compression or in the case of the extension side two translational axes. All joints were applied as "body-ground" in order to define their position as absolute within space.

In order to speed up simulation times, the model was cross sectioned down the length and a symmetry constraint applied. This allows the simulation to reduce the node count of the model by 50% without reducing the mesh density. This is carried out by only constraining displacements and forces normal to the symmetry plane and assuming anything parallel to the symmetry plane will be identical on both sides. For the systems being modelled within, this assumption is entirely acceptable. This model setup can be seen in Figure 6-11. This screenshot does not show the frictionless boundary conditions nor the joint conditions.

To hold the block in place on the rigid surface, three faces that were in contact with the ground plane were assigned an encastre boundary condition. This was applied in order to correctly constrain the workpiece in a way that would not negatively affect the strain force that will be applied. The setup for the simulation boundary conditions can be seen in Figure 6-12.
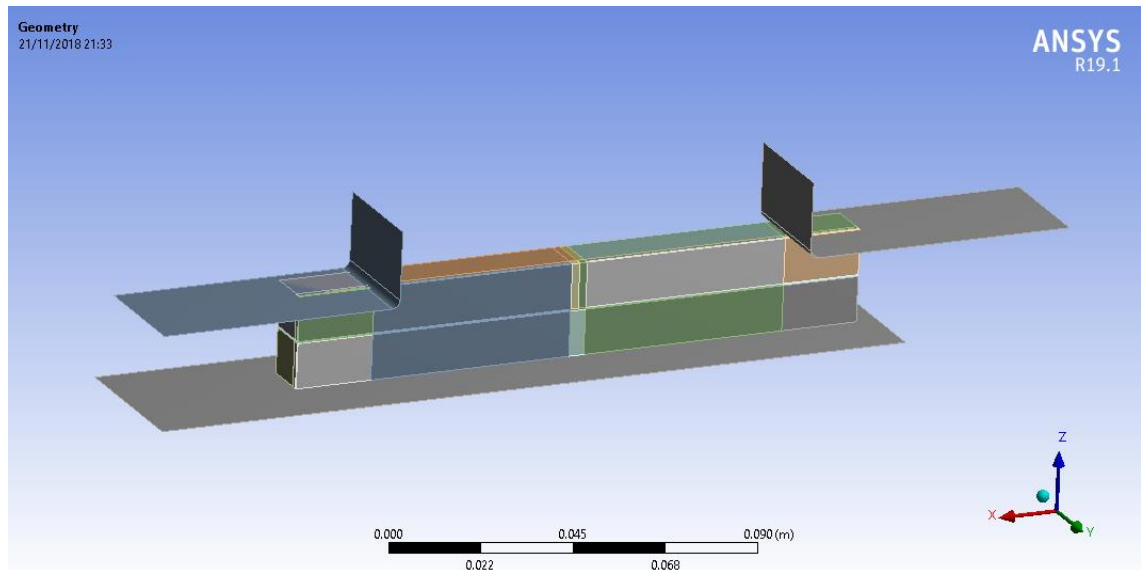
Figure 6-11 Model design for uniaxial strain test showing ground plane and clamping surfaces
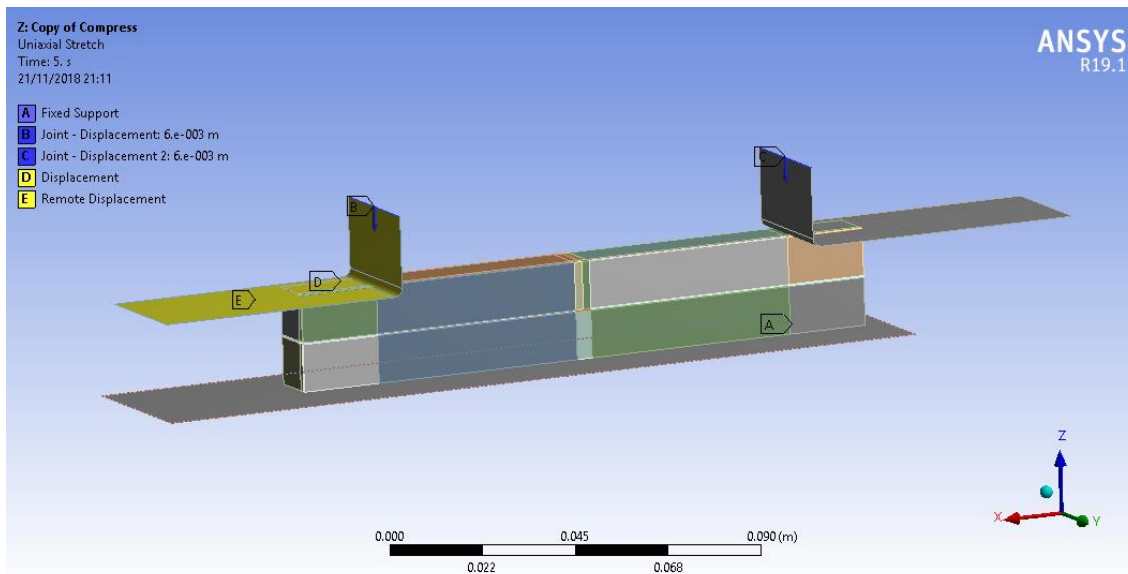
Figure 6-12 Boundary condition assignment for uniaxial strain model

The extension was then applied to the clamp surface on the side that was not encastre bound. This end then had a displacement applied of 25mm in the X axis and 0mm in the Y and Z axes to make sure the displacement occurred in a straight line. The applied displacement was an extension of 16% when compared to the original length of the sample, this extension value was obtained through anecdotal testing of the ability for the block to extend when being clamped in a vice and stretched, without causing fracture or tearing of the workpiece.

6.4.2 Axial Twist

A method of gripping the sample was once again included in this model, whereby the last 20mm of material at one end was clamped, with the lower surface being fixed in all axes, modelling an encastre boundary condition. The top surface then had a displacement of 12mm applied to it in order to simulate the gripping method of a standard vice clamp. This deformation was applied as its own discrete step as to create a baseline for further deformation and stresses applied to the sample. A 90º remote displacement was then applied to all four sides of the last 20mm of the opposite end of the sample. This deformation was chosen based upon anecdotal

experimentation that would enable the reliable twisting of the block without tearing the outer corners and artificially inducing failure in the workpiece. The use of a remote displacement allows access to additional axes, thus being able to introduce a rotational displacement. These faces were also fixed in the X, Y and Z directions to prevent any additional displacement. The applied boundary conditions can be seen in Figure 6-13. This test did not utilise either rigid surfaces for compression or as a ground plane due to a fixed bond or friction required to prevent the surface slipping, thus allowing a rotational force to be applied. This model also did not use symmetry due to the applied forces having to cross the would-be plane of symmetry.
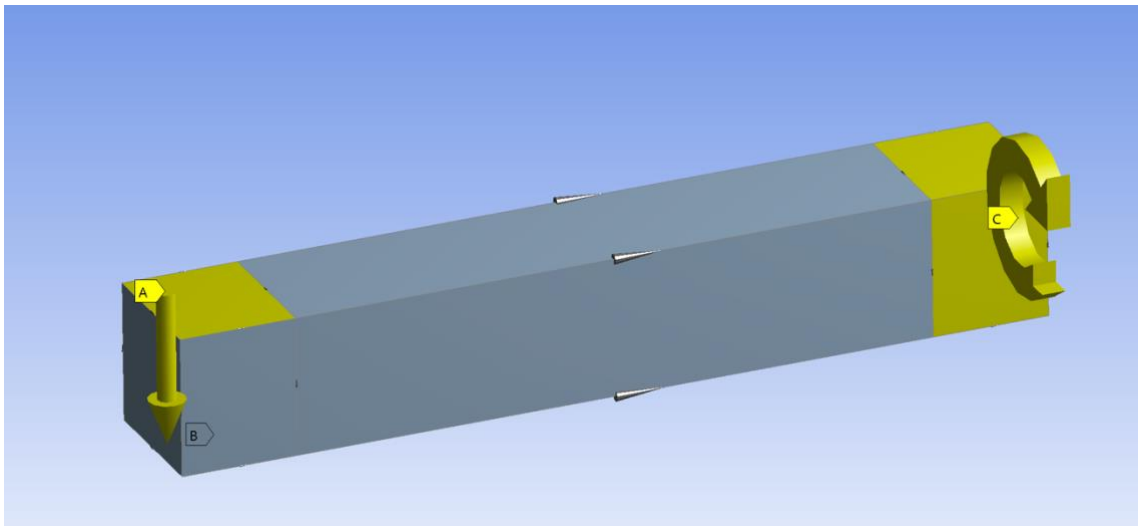
Figure 6-13 Axial Twist Applied Constraints (A) Clamp force (B) Encastre boundary condition (C) Remote Displacement used to apply a rotational displacement

6.4.3 Three Point Bend Test

The following set of conditions are not designed to mimic an ideal three-point bend test as it was deemed that during applications, the device would be applied to the skin, which during deformation, exhibits both bending and strain. Therefore, both ends of the sample were clamped using a base with encastre boundary conditions and a clamp force from above. The bend test force was then applied by a 5mm diameter rod that was moved upwards into the sample using a unidirectional

displacement. The contact conditions between the rod and sample were chosen to be frictionless to greatly simplify modelling and simulation. This could be carried out during verification through the use of lubrication between the rod and the sample. The applied boundary conditions can be seen in Figure 6-14.
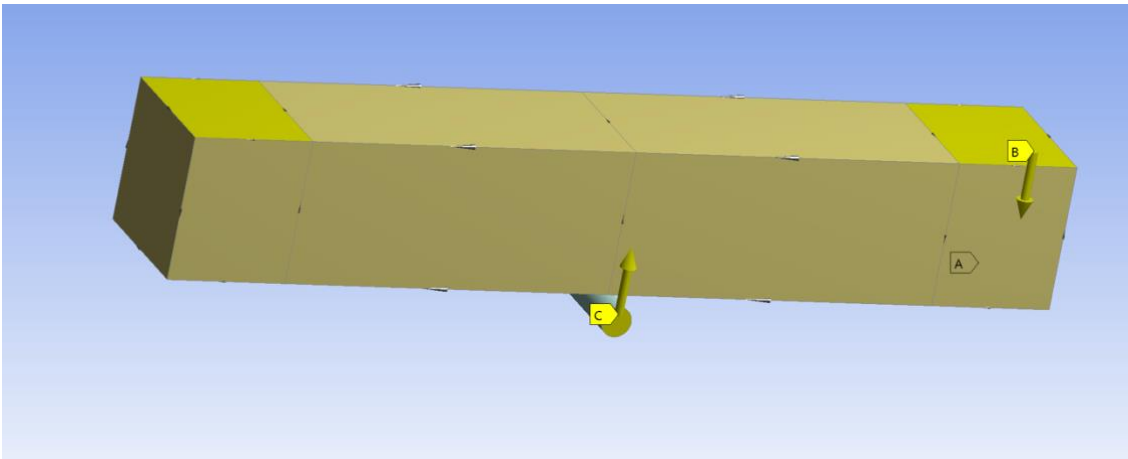
Figure 6-14 Three-Point Bend Test Applied Constraints (A) Encastre boundary condition (B) Clamp Force (C) Applied Vertical Displacement

6.4.4 Asymmetric Compression

The boundary conditions required to apply an asymmetric compression force to the sample are slightly different to the conditions used with the other kinds of tests, whereby a clamp would not be required for testing. This meant that an encastre boundary condition was applied to a small section of the sample base and the lower surface in order to anchor them. A frictionless contact condition was applied between the PDMS sample and the lower surface as well as between the PDMS sample and the compressive surface. A remote joint displacement was then applied to the top surface in the negative Z axis as can be seen in Figure 6-15. This was chosen to simulate the action of compressing the device by hand on the skin which would result in uneven compressive forces across the device.
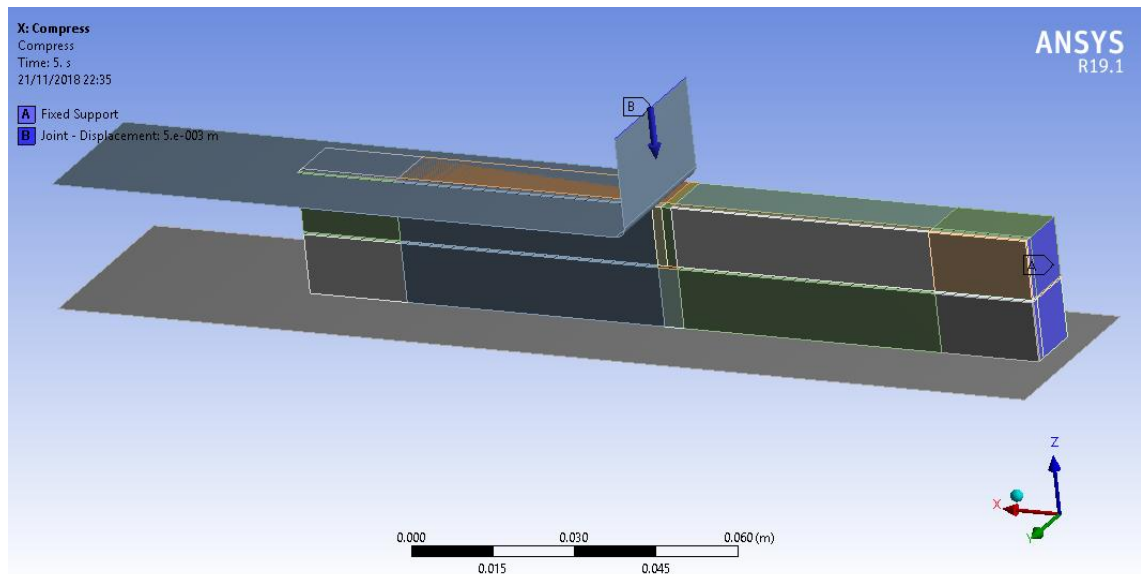
Figure 6-15 Asymmetric Compression Boundary Conditions (A) Encastre Boundary Condition (B) Compressive displacement through the use of a joint – Not shown, Ground-Body Fixed joint applied to lower surface

6.4.5 Analysis Methodology

In order to investigate the stresses that the components underwent, various solution views were created, which are designed to render element values for chosen outputs across the element and mesh surface. These values can then be probed, looking for maximum and minimum values, in addition to some statistical analysis such as standard deviations and means. The output values that are most useful for the performed analysis are the Von-Mises stress, principle stress and sheer stress. The Von-Mises Stress output is used to determine if a material will yield or fracture when deformed but relies on the material being ductile [183], silicon while brittle exhibits ductile behaviour before failing [184]–[188] so can therefore be analysed in this way. The principle stress corresponds to the maximum eigenvalue of the stress tensor, compared to the Von-Mises which is a metric of the stress tensor. Therefore principle stress is a real stress that can be measured during experimentations and thus correlation with real world models can be built. Shear

stresses of the components were also investigated as this would be the likely failure mode of any bonds or laminations within the system.

6.5 Results

6.5.1 Integrated Silicon Die Analysis

During deformation it is important that the delicate silicon IC is protected from large deformations and stresses by the PDMS material around it. The main stresses on the silicon die were seen to be present at the corners, in addition to a shear force across the top and bottom surfaces. These high stress regions can be seen at the corners of the IC in all but the twisting Von-Mises equivalent stress plots in Figure 6-16 below. This response is to be expected due to the deformation of the PDMS around the rigid component. The Von-Mises pattern that can be seen for the axial twist can be accounted to a group of circumstances.
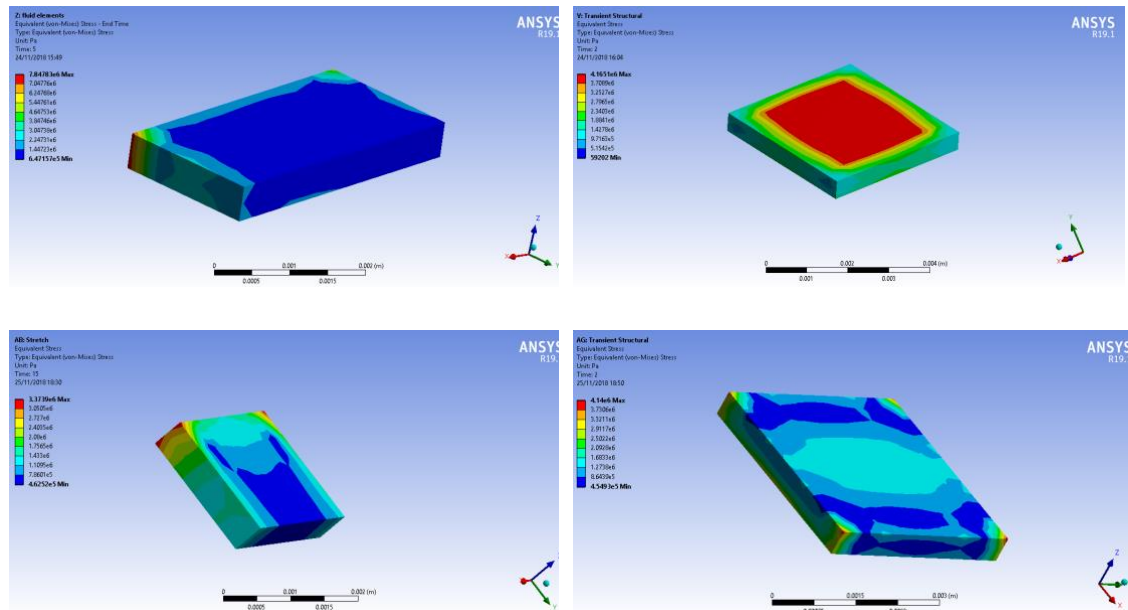
Figure 6-16 Von-Mises equivalent stress for each of the various conditions (Assymmetric Compression - Top Left, Axial twist - Top Right, Unixial tensile test – Bottom Left, Three Point Bend Test – Bottom Right)

Within the axial twist model, it can be seen in the maximal principle stress plot in Figure 6-17 showing opposing stresses on opposite sides of the component, then by combining this with the shear stress across the face of the part (Figure 6-18) and a relatively course mesh for this component, the resultant Von-Mises plot results in large stresses on the top and bottom faces of the component. Throughout all tests the stress applied to the die never exceeded 7.8 MPa, which did not get close to exceeding the fracture stress of a die of this size, which is in the range of 400 MPa [187], [189]. This however does not take into account any circuits that have been designed onto the die and would likely require detailed empirical testing of individual integrated circuits to gain more information on the failure rates of these components when undergoing mechanical deformation.
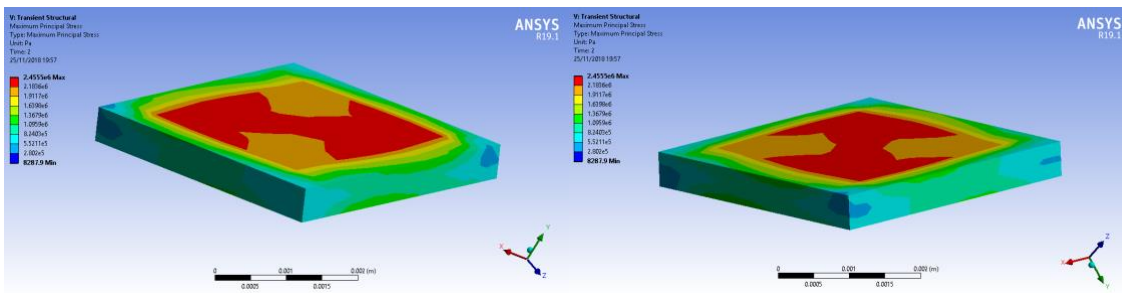
Figure 6-17 Maximum principle stress for axial twist conditions
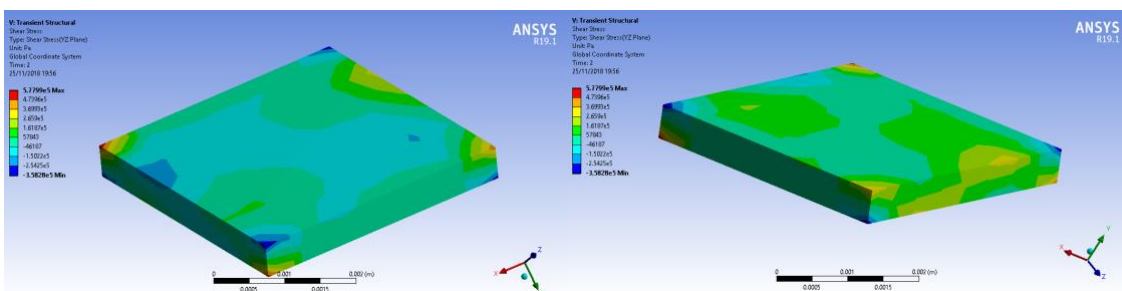
Figure 6-18 Shear stress of silicon die in axial twist conditions

A small but relevant stress was also applied at the interface of the fluid channel to the silicone die. The pressure applied to the face of the die is directly proportional to the deformation of the fluid channel. Due to the fluid being incompressible, any and all stress applied to the liquid through the deformation of the channel is transferred to an applied pressure evenly across all sides of the channel, including the locations of contact with the die. Silicon has a Young's modulus of at least 165GPa whereas PDMS has a Young's modulus of 13.2MPa, therefore the silicone will be essentially rigid throughout the channel deformation while the PDMS will deform to maintain the volume of the channel. It is most likely the failure mode for excess channel pressure will be that of the bond between the silicon die and PDMS substrate, which within these simulations experienced a maximum separation pressure of 160kPa (Figure 6-19) during the asymmetric compression condition.
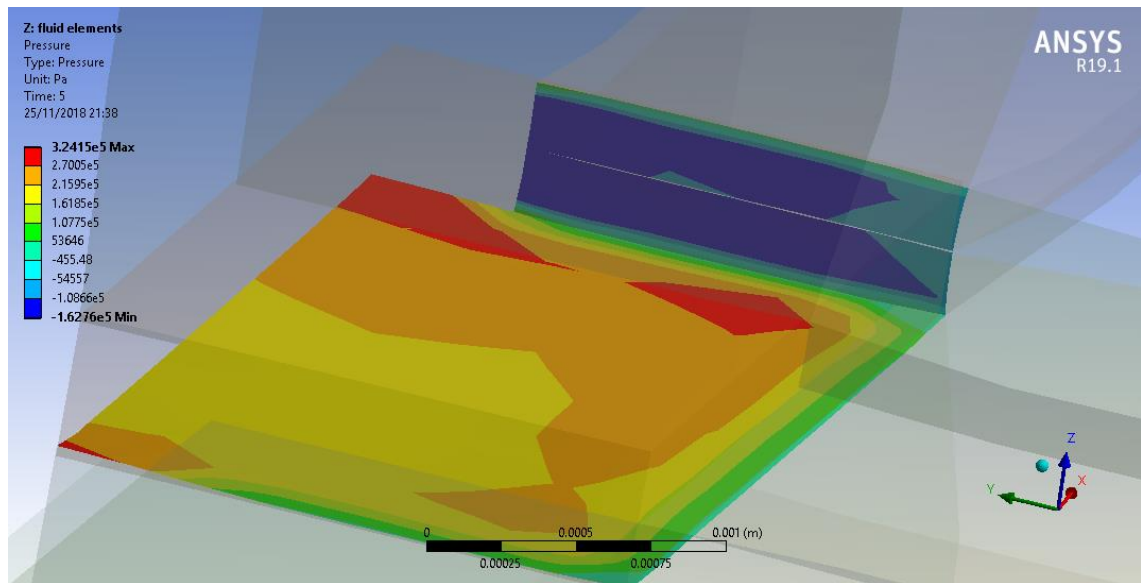
Figure 6-19 Pressure plot of silicon-PDMS contact region from asymmetric compression condition

6.5.2 Bond Strength Analysis

It can be seen that the largest frictional stress experienced within the PDMS was 159.2 kPa during the axial twist condition, as seen in . This occurs at the edge of the laminated sections in line with the edge of the embedded silicone component and can be contributed to the sudden change in stiffness of what is otherwise an almost homogenous cross section to something that is much stiffer. This additional stiffness better resists the applied forces, thus imposing the required deformation onto the softer and more conformal PDMS and its laminated bond.
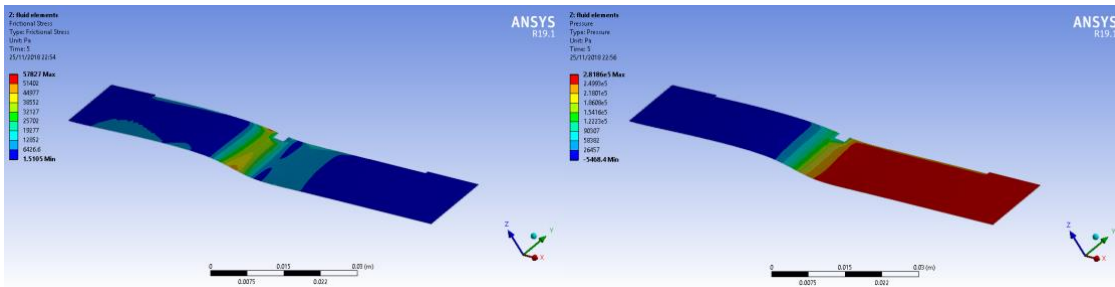
Figure 6-20 Frictional stress (Left) and pressure plot (Right) for asymmetric compression condition at PDMS to PDMS contact region
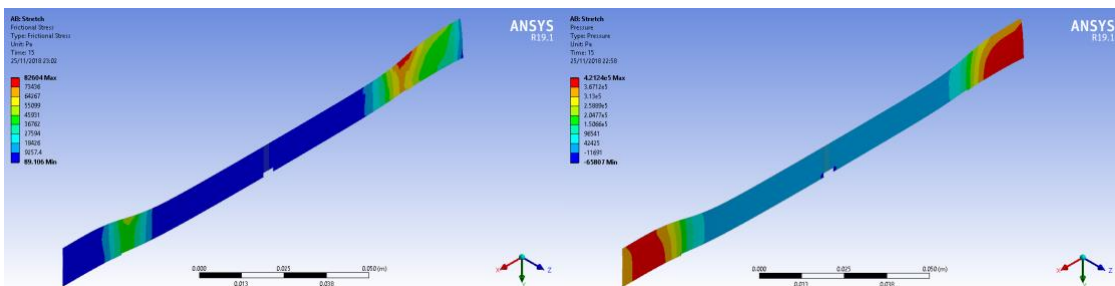
Figure 6-21 Frictional stress (Left) and pressure plot (Right) for tensile loading condition at PDMS to PDMS contact region
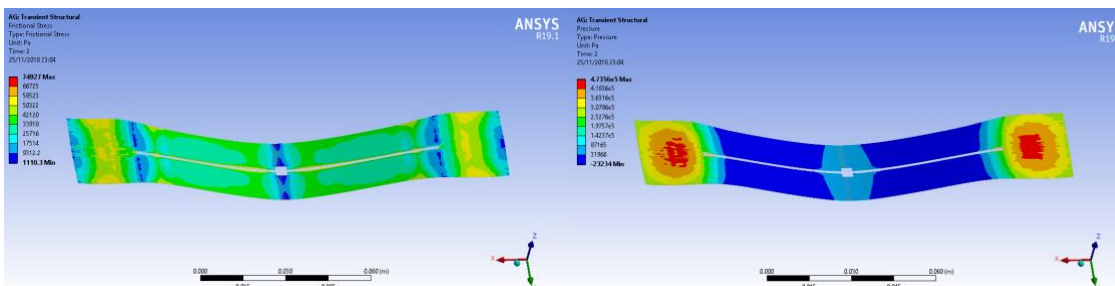
Figure 6-22 Frictional stress (Left) and pressure plot (Right) for three-point bend condition at PDMS to PDMS contact region
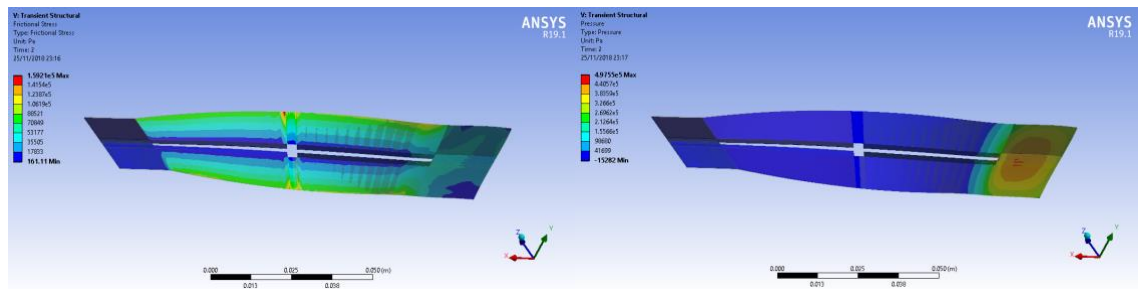
Figure 6-23 Frictional stress (Left) and pressure plot (Right) for axial twist condition at PDMS to PDMS contact region

6.6 Discussion

6.6.1 Silicon Die Structural Integrity

Throughout all of the conditions tested, the Von-Mises stress on the silicon die reached a maximum of $7.8 \times 10^6\ Pa$ which, when compared to its yield strength of $6.9 \times 10^9\ Pa$ [190] is well within a comfortable safety margin to survive the stresses that would likely be experienced within a device utilising this manufacturing technology. This survivability however, relies upon a good bond with the PDMS substrate to allow a continuous load transfer across the entire surface of the silicon die. It does not account for the fracture of any sensitive electronics that would be present on the die, as due to their unique and microscopic nature, would require an exponentially higher compute power as the node size would be required to be on the sub micrometre scale.

6.6.2 PDMS Bond Strength Requirements

In order to manufacture a device that utilises liquid metal channels, under most conditions, it would require manufacture of the substrates in layers in a similar way to existing printed circuit boards. However, PDMS poses a greater challenge when laminating layers, as if the bond were to have a Young's Modulus, Poisson's ratio or coefficient of thermal expansion that differed from the PDMS used for the substrate layers, this could create large stresses during use and deformation of the product,

likely leading to its early failure. Therefore, it is important to understand the bonding requirements in order to select the correct process and materials to carry out these joins. Additional care should be taken to optimise the bond type for manufacturing speed as this will reduce the time required to manufacture devices that utilise PDMS substrates. As mentioned prior, the research carried out by *Eddings et al* [118], bond strength can vary significantly as can the repeatability of the bond strength based on the specific process used. It is important for mass manufacture to select a process that will enable the highest yield possible, therefore, the lowest value produced within the error bounds of the process should still exceed the maximum bond strength requirement.

For each of the tests carried out negative pressures and shear forces were of concern as these are most likely to induce delamination. The frictional stress and applied pressure act perpendicular to each other, however, when investigating bond strength, the tensile strength of the bond is always weaker in tension than it is in shear [191], [192].

The applied pressure on the bond can be directly compared to the tensile and pressure tests that have been carried out by *Eddings et al*, wherein two PDMS components were bonded together using various techniques and the pressure required to sever the bond between them was measured [118]. The results collected included both positive and negative pressures, of which the former was acting to bring the two components together and the latter to tear them apart. The simulations carried out within the scope of this research peaked at 497.6 kPa in the positive direction and -65.8 kPa in the negative during the axial twist condition and uniaxial tensile test respectively. This relatively low delamination pressure is likely due to the thick blocks of PDMS used for modelling that would require delamination stresses to overcome a significant amount of material attempting to maintain its shape, in addition to the bond strength between the two components. When comparing these results to the bond strengths measured by *Eddings et al*, it can be

seen that any of their tested bonding techniques would suitably maintain the bond between the two PDMS components during testing, however, not all of these techniques would be suitable to bonding with other substrates such as silicon, and metals, in addition to having relatively poor repeatability. It is for this reason when developing these technologies for mass production, it is recommended to use partial curing of one of the substrates as the bonding technique allows a relatively fast adhesion process and does not require the use of plasmas which could damage sensitive integrated circuits.

6.7 Conclusion

Overall, the simulations carried out within demonstrate both the feasibility and viability of a laminated multilayer PDMS structure, utilising liquid metal filled microfluidic channels. The work identified that excess loading leading to the cracking of silicon integrated circuits is an unlikely failure mode; the maximum observable stresses were over 8000 times less than the empirical yield strength [189]. Rather, the forces that could possibly cause delamination while the system is in use are more likely according to the study presented above, where the maximum observed pressure was approximately 4 times less than the average PDMS-PDMS partial cure bond strength observed by *Eddings et al* [118]. It must be noted that at the time of writing there was no empirical data on the bond strength between silicon and PDMS. This could potentially be a cause for concern when applying a factor of safety and should be studied further. Long-term studies of work induced fatigue of the lamination bond strength should be carried out as these failure modes are usually considered to be a critical defect when they occur in modern printed circuits. It can be assumed that devices built in the way detailed above could have poor impact tolerance as the energy absorption is entirely limited by the amount of mass of the PDMS encapsulating the silicon dies (and any other components that may be used.) This however was outside of the scope of this project and should be studied

in detail if this technology is to be brought to the sports market; where impacts are a common occurrence.

The deformation and stresses experienced by the substrate itself were not investigated within the confines of this study due to the increased thickness that was chosen for these models; they would demonstrate significantly different performance when compared to sub-millimetre thick films of PDMS. Due to beam bending theorem, the strain experienced by the PDMS material would be far greater than that of a thin film due to the increase in the area moment of inertia and distance from the neutral axis.

7 DISCUSSIONS, CONCLUSIONS AND RECOMMENDATIONS FOR FURTHER WORK

7.1 Chapter Overview

The overall aim of this research was to identify and determine the feasibility of manufacturing flexible, stretchable electronics, utilising technologies and techniques that could be scaled for mass production. This research approached some components of this goal which are discussed here along with their limitations, in addition to suggesting a direction research on this topic could take in the future.

7.2 Discussion

Research into developing soft matter electronics has been relatively broad, with researchers approaching these problems from an array of angles that cover smart woven textiles [62], [126], [193] to electronic temporary tattoos [20] and many others in between. Recently more research has been carried out with respect to defining an approach to bring such wearable devices to market and identifying the relevant parameters and requirements that would need to be met in order to create a device that is useful and would make a positive impact on society. This research has not changed the outlook on the research carried out within this paper, and in some cases supported the work carried out within. Some research groups have been

investigating the use of liquid metal interconnects and processes to manufacture these systems en masse further validating the work carried out here [60], [66], [81].

The parameters of usefulness defined in Chapter 3 begin to investigate ways these technologies may be used, and through this investigation, begin to guide the selection and development of technologies to achieve these goals. These initial requirements were developed not for this investigation in particular, but as a way to assist in guiding the development of architectures and manufacturing processes. This line of questioning gave birth to an initial architecture concept that would guide further experimentation and study within this paper, forming the basis for material and process selection.

In order to begin research on a new technology within the modern climate of agile development cycles and fast paced iteration, it is important to be able to prototype systems at low cost utilising digital manufacturing techniques quickly and efficiently at low cost. The chosen approach that was investigated to solve this problem was to use lasers to manufacture channelled substrates without the overhead of expensive tooling, in addition to analysing the use of this process within a production environment. Based on the testing and analysis carried out, low cost, continuous wave CO_2 lasers could be used to provide prototype facilities for both engraving channels and cutting vias into PDMS sheet. This provides a good alternative to costly Roll-to-Roll fabrication centres in order to prototype a device at low quantity. However, it can be said the biggest issue that was discovered during the experimentation was the challenge of cleaning the workpiece thoroughly if a laser is to be integrated into a continuous manufacturing process such as Roll-to-Roll production.

As part of the development cycle of new production methods, it is important to build knowledge and understanding of the behaviour of components, and utilising this understanding to select the correct adhesives, processes and order of operations when producing a product. By modelling these interactions within an FEA package

it was possible to learn about how components may respond to the various deformations they may experience during their lifetime within possible products. This knowledge will allow engineers to better optimise designs for improved reliability and select the correct components. Even more importantly the knowledge gained within can assist an engineer in selecting the correct bonding process, which will in turn enable a reliable and compact product.

7.3 Conclusions

The main research aim, originally set out at the start of this project was "to identify a group of materials and techniques that are capable of producing flexible, stretchable electronics at commercial scales and at low cost." Initial work was carried out to identify the requirements and parameters of usefulness, to define and quantify what the materials and techniques had to be capable of in order to be successful. These requirements were then leveraged to conceptualise a device architecture that could operate within them and formed the foundation for the selection of possible materials and manufacturing techniques. The outcome was a multilayer laminate structure that was capable of supporting three-dimensional channel routing and integrating both leaded and bare die components. But, this would also require a radical rethinking of printed circuit board manufacture to enable a device to be manufactured at scale while keeping cost low.

Initial investigation began into manufacturing processes that could achieve both small scale prototyping without tooling in addition to being able to easily be integrated into a large production operation, thus the use of scanning mirror lasers were employed. Laser machining was investigated, covering a variety of possible wavelengths and beam generation technologies. Anecdotal experimentation exhibited superior absorption wavelengths within the confines of a CO_2 based system. This allowed cutting and engraving of the optically clear PDMS material whereas other laser systems failed to mark the PDMS substrate at all.

Performance of the CO_2 laser system was further investigated, looking at the process occurring within the material and utilising this knowledge to optimise the cutting and machining processes to produce more precise and repeatable patterns into the PDMS. Various output powers and trace speed combinations were investigated resulting in the discovery of an upper-limit power density; where any increase caused poor surface finish and inconsistent channel geometries. The study may not have determined an optimal parameter set, however, it did generate a collection of useful data, which could be used to optimise the process and define a starting point for greater understanding of the occurring phenomenon.

Finite element analysis was then employed to investigate how Galinstan filled channels would react to deformation as part of a laminated stack up. These simulations would enable the selection of an appropriate bonding technique for production, which resulted in an array of lamination techniques that could be supported in various situations, dependant on application. For instance, if a unified, sealed system was required, uncured or partially cured PDMS could be used as an adhesive and be able to form an almost perfectly homogeneous substrate. However, if voids are required for channels which will be filled after lamination, varying the curing ratio of layers or corona discharge could be used to create this laminated assembly at the expense of bond strength. These models allowed the verification of the hypothesis that externally applied loads would not be transferred into rigid silicon dies and discrete components, but be absorbed by the highly conformal PDMS substrate. Silicon cracking was found to be very unlikely to occur due to the incurred stresses being almost negligible with respect to the yield stress of silicon. Delamination however, was identified as a potential threat to devices as the observed pressures reached 25% of the average empirically derived failure pressure possibly resulting in catastrophic failure of the device. Further investigation into bond optimisation and reliability is therefore important to the success of a commercial device.

A secondary research goal was to "identify the limitations of these materials during use and manufacturing processes." This goal was created in order to help assess what problems may arise during manufacture and to set limitations on the designs that utilise this technology. The main limitations come from Galinstan, which due to its liquid state, complicates the design of complex circuits. Liquid metals will form amalgams when they come into contact with other solid metals. In order to combat this conductive passivation, layers will be required on all metallic components that come into contact with the fluid. This will also require that any tooling used in production be a non-metal or passivated as well. Galinstan's conductivity also does not meet performance equivalency of copper or gold, which means there will be limitations on current capacity and switching frequencies of systems that utilise Galinstan interconnects. The main limitation revealed by PDMS is the limited array of permanent bonding and lamination techniques due to its tacky surface and hydrophobic qualities. However, both of these materials have been identified as being able to meet the requirements and parameters of usefulness, though some additional research will be required to reach the mass producible, low cost wearable device that is the target of many researchers and corporations.

7.4 Limitations of this Study and Future Work

7.4.1 Laser Machining of PDMS to Create Predictable Microfluidic Channels Using a Continuous Wave CO_2 Laser

Laser machining is a dynamic and repeatable process, however, there are many variables which can affect the efficacy of the process. Due to this wide range of variable, which include sheath gasses and their flow rates, in addition to material finish, laser power and trace speed among others. Due to the exponentially increasing number of tests required to evaluate all possible combinations for this process, the operation parameters were narrowed to focus on the two most common and easily adjustable variables, trace speed and laser output power.

To further optimise this process for mass production and improve the finish of the machined grooves, alternate sheath gasses should be investigated along with alternative beam focus patterns. It is strongly recommended that research continues in this area as perfecting this process would be of great use for drilling vias in multilayer laminated structures.

7.4.2 Simulating the Deformation of Galinstan Based Interconnects with PDMS Substrates

Assumptions were made in order to reduce the complexity of the simulations, however as is common with assumptions, they reduce the overall fidelity of the model. Assumptions made for this experiment limited the precision of which the internal fluid could be modelled. By modelling the Galinstan as a hydrostatic fluid, it would not be possible to investigate the leaking or movement of fluid within the channels. Simulations were also limited to quasi-steady state and transient analyses, which precludes any information about how impacts would affect the performance of such systems, which is especially important for the use of wearables within sports. The mesh density was also heavily limited due to software licensing, this however, could be overcome relatively easily with a more capable license.

It is also of interest how channel geometry would affect the performance of such systems under deformation and load, as certain geometries such as round shape that would make mould release easier during Roll-to-Roll production processes. Further investigations are recommended to explore more complex interconnect geometries in addition to variation with regard to interconnect cross-sectional geometry.

7.4.3 Simulation Validation

Simulation and modelling is always a great first step into understanding how a system or material will behave under circumstances, however, it is important to verify the models are accurate and precise. This validation grants confidence in the simulations allowing fast iteration during product development and a greater

understanding of the behaviour of the system. Unfortunately, experimental validation was not possible within the confines of this research. It is however recommended that it be carried out and cross referenced with the simulation results presented.

7.4.4 Manufacturing Validation

The manufacturing process for a product is just as important as the architecture and understanding of a product's design. It is especially important for the processes that produce components to be validated and designed for scale. This research often mentioned Roll-to-Roll manufacturing processes, conversely the validation of this as a viable process to manufacture complex multilayer laminated electronics utilising liquid metal interconnects was not proven. It is advisable that knowledge and expertise be created on this topic. This knowledge is a crucial piece of the puzzle that is required to bring these systems to market in the future and must be investigated further.

8 REFERENCES

[1] M. Guarnieri, 'The Age of Vacuum Tubes: Early Devices and the Rise of Radio Communications [Historical]', *IEEE Ind. Electron. Mag.*, vol. 6, no. 1, pp. 41–43, Mar. 2012.

[2] S. McKay, *The Secret Life of Bletchley Park : the History of the Wartime Codebreaking Centre by the Men and Women Who Were There.* Aurum Press, 2011.

[3] IBM, 'IBM Archives: 7090 Data Processing System (continued)'. [Online]. Available: http://www-03.ibm.com/ibm/history/exhibits/mainframe/mainframe_PP7090B.html. [Accessed: 23-May-2017].

[4] J. Wu, H. Li, Z. Lin, and K.-Y. Goh, 'How big data and analytics reshape the wearable device market – the context of e-health', *Int. J. Prod. Res.*, pp. 1–15, Jun. 2015.

[5] C. Erdmier, J. Hatcher, and M. Lee, 'Wearable device implications in the healthcare industry', *J. Med. Eng. Technol.*, vol. 40, no. 4, pp. 141–148, May 2016.

[6] B. H. F. N. C. (BHFNC) and L. U. for Physical Activity and Health, 'Economic costs of Costs of physical inactivity Physical Inactivity', Loughborough, 2013.

[7] D. E. R. Warburton, C. W. Nicol, and S. S. D. Bredin, 'Health benefits of physical activity: the evidence.', *CMAJ*, vol. 174, no. 6, pp. 801–9, Mar. 2006.

[8] 'The MagPie Issue 40', *The MagPie*, Dec-2015.

[9] M. Reardon, 'Nokia demos bendable cell phone - CNET', 2008. [Online].

Jonathan Flowers - July 2019

Available: https://www.cnet.com/news/nokia-demos-bendable-cell-phone/. [Accessed: 24-May-2017].

[10]   P. Sungmee Park *et al.*, 'Enhancing the quality of life through wearable technology', *IEEE Eng. Med. Biol. Mag.*, vol. 22, no. 3, pp. 41–48, May 2003.

[11]   National Institute for Health and Care Excellence, 'Behaviour change: the principles for effective interventions | Guidance and guidelines | NICE', National Institute for Health and Care Excellence, 2007.

[12]   AdvaMed, 'Food and Drug Administration's Impact on U.S. Medical Technology Innovation', 2010.

[13]   G. Berthelot *et al.*, 'Athlete atypicity on the edge of human achievement: performances stagnate after the last peak, in 1988.', *PLoS One*, vol. 5, no. 1, p. e8800, Jan. 2010.

[14]   L. M. Burke, 'Fueling strategies to optimize performance: training high or training low?', *Scand. J. Med. Sci. Sports*, vol. 20 Suppl 2, pp. 48–58, Oct. 2010.

[15]   L. Mertz, 'Making sports safer for kids: using biomechanical devices to prevent injuries.', *IEEE Pulse*, vol. 4, no. 5, pp. 18–21, Sep. 2013.

[16]   A. Alwadi, 'Collision Monitoring and Alarm in Ice-Hockey', Aalto University, 2014.

[17]   A. Jeukendrup and A. VanDiemen, 'Heart rate monitoring during training and competition in cyclists.', *J. Sports Sci.*, vol. 16 Suppl, pp. S91-9, Jan. 1998.

[18]   Würth Elektronik GmbH & Co. KG, 'Flex-Rigid Design Guide'.

[19]   D. Talbot, 'Making Stretchable Electronics', *MIT Technol. Rev.*, vol. 115, no. 5, pp. 84–86, 2012.

[20]   M. Orcutt, 'Electronic Sensors Printed Directly on the Skin', *MIT Technological Review*, 2013. [Online]. Available: http://www.technologyreview.com/news/512061/electronic-sensors-

printed-directly-on-the-skin/.

[21] D.-H. Kim, N. Lu, Y. Huang, and J. a Rogers, 'Materials for stretchable electronics in bioinspired and biointegrated devices', *MRS Bull.*, vol. 37, no. 03, pp. 226–235, Mar. 2012.

[22] S. Choi, H. Lee, R. Ghaffari, T. Hyeon, and D.-H. Kim, 'Recent Advances in Flexible and Stretchable Bio-Electronic Devices Integrated with Nanomaterials', *Adv. Mater.*, vol. 28, no. 22, pp. 4203–4218, Jun. 2016.

[23] B. Macdonald, 'Valuing the Benefits of Cycling : Tees Valley Public Health Shared Service', 2007.

[24] J. Jarrett *et al.*, 'Effect of increasing active travel in urban England and Wales on costs to the National Health Service.', *Lancet*, vol. 379, no. 9832, pp. 2198–205, Jun. 2012.

[25] The NHS Information Centre, 'The Health Survey for England 2008: Physical Activity and Fitness. Summary of Key findings', 2008.

[26] I.-M. Lee, E. J. Shiroma, F. Lobelo, P. Puska, S. N. Blair, and P. T. Katzmarzyk, 'Effect of physical inactivity on major non-communicable diseases worldwide: an analysis of burden of disease and life expectancy.', *Lancet*, vol. 380, no. 9838, pp. 219–29, Jul. 2012.

[27] D. T. Conditions, 'Improving the health and well-being of people with long term conditions', Leeds, 2010.

[28] A. Kingsnorth, 'First year report - Andrew Kingsnorth - B134824', Loughborough, 2014.

[29] L. M. Wankel, 'The importance of enjoyment to adherence and psychological benefits from physical activity.'

[30] L. Green, J. Myerson, and E. Mcfadden, 'Rate of temporal discounting decreases with amount of reward', *Mem. Cognit.*, vol. 25, no. 5, pp. 715–723, Sep. 1997.

[31] L. Green, J. Myerson, D. Lichtman, S. Rosen, and A. Fry, 'Temporal discounting in choice between delayed rewards: the role of age and income.', *Psychol. Aging*, vol. 11, no. 1, pp. 79–84, Mar. 1996.

[32] B. N. Moreira, 'UMass patch would spot stressed out soldiers', *The Boston Globe*, Aug-2014. [Online]. Available: https://www.bostonglobe.com/business/2014/08/03/umass-scientists-working-patch-that-measures-stress/X7MEkIZDz3Mwalb1NY3PNL/story.html. [Accessed: 08-Apr-2014].

[33] N. C. for H. Manufacturing, 'UMass Advanced Roll-to-Roll Manufacturing Facility | Center for Hierarchical Manufacturing'. [Online]. Available: http://chm.pse.umass.edu/node/123. [Accessed: 02-Jun-2015].

[34] Reebok, 'Reebok CHECKLIGHT - Black | Reebok US', *Reebok*, 2015. [Online]. Available: http://www.reebok.com/us/checklight/Z85846.html. [Accessed: 02-Jun-2015].

[35] C. Rafferty *et al.*, 'Electronics for detection of a condition of tissue', US20130245388 A1, 2013.

[36] S. Cheng, A. Rydberg, K. Hjort, and Z. Wu, 'Liquid metal stretchable unbalanced loop antenna', *Appl. Phys. Lett.*, vol. 94, pp. 1–3, 2009.

[37] G. J. Hayes, J.-H. So, A. Qusba, M. D. Dickey, and G. Lazzi, 'Flexible Liquid Metal Alloy (EGaIn) Microstrip Patch Antenna', *TAP_IEEE Trans. Antennas Propag.*, vol. 60, pp. 2151–2156, 2012.

[38] M. J. Lake, 'Development of Liquid Metal Antenna # 1', 2005. [Online]. Available: http://www.hamdomain.com/lm-antenna/development.htm. [Accessed: 24-Nov-2014].

[39] N. Vidal, S. Curto, and J. Lopez-Villegas, 'Detuning study of implantable antennas inside the human body', *Prog. Electromagn. Res.*, vol. 124, no. January, pp. 265–283, 2012.

[40] M. U. Rehman, Y. Gao, X. Chen, C. G. Parini, and Z. Ying, 'Effects of Human Body Interference on the Performance of a GPS Antenna', in *Antennas and Propagation, 2007. EuCAP 2007. The Second European Conference on*, 2007, pp. 1–4.

[41] G. A. Conway, W. G. Scanlon, and S. L. Cotton, 'The performance of on-body wearable antennas in a repeatable multipath environment', in *2008 IEEE Antennas and Propagation Society International Symposium*, 2008, pp. 1–4.

[42] S. Savagatrup, A. D. Printz, T. F. O'Connor, A. V Zaretski, and D. J. Lipomi, 'Molecularly Stretchable Electronics', *Chem. Mater.*, vol. 26, no. 10, pp. 3028–3041, May 2014.

[43] S. Cheng *et al.*, 'Microfluidic stretchable RF electronics', *Lab Chip*, vol. 10, no. 23, p. 3227, 2010.

[44] M. Kaltenbrunner *et al.*, 'An ultra-lightweight design for imperceptible plastic electronics.', *Nature*, vol. 499, no. 7459, pp. 458–63, Jul. 2013.

[45] C. Wang *et al.*, 'Extremely Bendable, High-Performance Integrated Circuits Using Semiconducting Carbon Nanotube Networks for Digital, Analog, and Radio-Frequency Applications', *Nano Lett.*, vol. 12, no. 3, pp. 1527–1533, Mar. 2012.

[46] S. Ishii, M. Nishu, S. Kishimoto, and T. Mizutani, 'Fabrication of Thin-Film Transistor Integrated Circuits on Flexible Substrate by Transfer Technique of Carbon Nanotube Network Using Poly(vinyl alcohol)', *Jpn. J. Appl. Phys.*, vol. 52, no. 10R, p. 108001, Oct. 2013.

[47] D. Shahrjerdi and S. W. Bedell, 'Extremely Flexible Nanoscale Ultrathin Body Silicon Integrated Circuits on Plastic', *Nano Lett.*, vol. 13, no. 1, pp. 315–320, Dec. 2012.

[48] E. Palleau, S. Reece, S. C. Desai, M. E. Smith, and M. D. Dickey, 'Self-healing stretchable wires for reconfigurable circuit wiring and 3D microfluidics.', *Adv.*

Mater., vol. 25, no. 11, pp. 1589–92, Mar. 2013.

[49]   S. Zhu *et al.*, 'Ultrastretchable fibers with metallic conductivity using a liquid metal alloy core', *Adv. Funct. Mater.*, vol. 23, pp. 2308–2314, 2013.

[50]   A. Fassler and C. Majidi, '3D structures of liquid-phase GaIn alloy embedded in PDMS with freeze casting', *Lab Chip*, vol. 13, no. 22, p. 4442, 2013.

[51]   H. Hu, K. Shaikh, and C. Liu, 'Super flexible sensor skin using liquid metal as interconnect', in *IEEE Sensors 2007 Conference*, 2007, pp. 815–817.

[52]   G. Li, M. Parmar, D. Kim, J.-B. J. B. Lee, and D.-W. Lee, 'PDMS based coplanar microfluidic channels for the surface reduction of oxidized Galinstan.', *Lab Chip*, vol. 14, no. 1, pp. 200–9, Jan. 2014.

[53]   A. Koh, J. Sietins, G. Slipher, and R. Mrozek, 'Deformable liquid metal polymer composites with tunable electronic and mechanical properties', 2019.

[54]   L. Francioso *et al.*, 'Flexible thermoelectric generator for wearable biometric sensors', in *2010 IEEE Sensors*, 2010, pp. 747–750.

[55]   S. J. Kim, J. H. We, and B. J. Cho, 'A wearable thermoelectric generator fabricated on a glass fabric', *Energy Environ. Sci.*, vol. 7, no. 6, p. 1959, 2014.

[56]   Y. Qi, N. T. Jafferis, K. Lyons, C. M. Lee, H. Ahmad, and M. C. McAlpine, 'Piezoelectric ribbons printed onto rubber for flexible energy conversion.', *Nano Lett.*, vol. 10, no. 2, pp. 524–8, Feb. 2010.

[57]   S. Xu *et al.*, 'Stretchable batteries with self-similar serpentine interconnects and integrated wireless recharging systems.', *Nat. Commun.*, vol. 4, p. 1543, Jan. 2013.

[58]   S. Choi *et al.*, 'Stretchable Heater Using Ligand-Exchanged Silver Nanowire Nanocomposite for Wearable Articular Thermotherapy', *ACS Nano*, vol. 9, no. 6, pp. 6626–6633, Jun. 2015.

[59]   M. Nathan *et al.*, 'Three-dimensional thin-film Li-ion microbatteries for

autonomous MEMS', *J. Microelectromechanical Syst.*, vol. 14, no. 5, pp. 879–885, Oct. 2005.

[60] Y. Yang *et al.*, 'Liquid-Metal-Based Super-Stretchable and Structure-Designable Triboelectric Nanogenerator for Wearable Electronics', 2018.

[61] K.-I. Jang *et al.*, 'Rugged and breathable forms of stretchable electronics with adherent composite substrates for transcutaneous monitoring.', *Nat. Commun.*, vol. 5, p. 4779, Jan. 2014.

[62] J. Vanfleteren, 'Stretchable Electronics for Smart Textiles'. imec, p. 98, 2012.

[63] F. Leys, 'Large-area stretchable microsystems; potential for food packaging applications', Universiteit Gent, 2012.

[64] A. Jahanshahi, P. Salvo, and J. Vanfleteren, 'Stretchable biocompatible electronics by embedding electrical circuitry in biocompatible elastomers', *Proc. Annu. Int. Conf. IEEE Eng. Med. Biol. Soc. EMBS*, no. c, pp. 6007–6010, 2012.

[65] J. a Fan *et al.*, 'Fractal design concepts for stretchable electronics', *Nat. Commun.*, vol. 5, p. 3266, Feb. 2014.

[66] 'Microstructured electrodes supported on serpentine interconnects for stretchable electronics', 2019.

[67] B. Zhang, Q. Dong, C. E. Korman, Z. Li, and M. E. Zaghloul, 'Flexible packaging of solid-state integrated circuit chips with elastomeric microfluidics', *Sci. Rep.*, vol. 3, no. 1098, Jan. 2013.

[68] Z. Li, M. E. Zaghloul, B. Zhang, and C. E. KORMAN, 'Flexible IC/microfluidic integration and packaging', US 13/715,110, 2013.

[69] S. D. Sheet, G. Medical, A. G. Fahrenheitstra, and G. Telephon, 'Safety Data Sheet acc , to Guideline 93 / 112 / EC Safety Data Sheet acc , to Guideline 93 / 112 EC', 2004.

[70] Wikipedia, 'Polydimethylsiloxane', 2014. [Online]. Available: http://en.wikipedia.org/wiki/Polydimethylsiloxane. [Accessed: 24-Nov-2014].

[71] M. Li, S. Li, J. Wu, W. Wen, W. Li, and G. Alici, 'A simple and cost-effective method for fabrication of integrated electronic-microfluidic devices using a laser-patterned PDMS layer', *Microfluid. Nanofluidics*, vol. 12, no. 5, pp. 751–760, Mar. 2012.

[72] P. Holgerson, D. S. Sutherland, B. Kasemo, and D. Chakarov, 'Patterning and modification of PDMS surface through laser micromachining of silicon masters and molding', *Appl. Phys. A*, vol. 81, no. 1, pp. 51–56, Dec. 2004.

[73] a. D. Stroock and G. M. Whitesides, 'Components for integrated poly (dimethylsiloxane) microfluidic systems', *Electrophoresis*, vol. 23, pp. 3461–3473, 2002.

[74] X. Thomas and Dow Corning Europe, 'Silicones in Medical Applications', *Inorg. Polym.*, vol. Silicones.

[75] G. J. Hayes, A. Qusba, M. D. Dickey, and G. Lazzi, 'Liquid Metal Antennas for Implantable and On-body Systems', in *2012 IEEE*, 2012, no. 1, p. 156.

[76] Q. Zhang, J.-J. Xu, Y. Liu, and H.-Y. Chen, 'In-situ synthesis of poly(dimethylsiloxane)-gold nanoparticles composite films and its application in microfluidic systems.', *Lab Chip*, vol. 8, no. 2, pp. 352–7, Feb. 2008.

[77] D. K. Cai, A. Neyer, R. Kuckuk, and H. M. Heise, 'Optical absorption in transparent PDMS materials applied for multimode waveguides fabrication', *Opt. Mater. (Amst).*, vol. 30, no. 7, pp. 1157–1161, 2008.

[78] F. Schneider, J. Draheim, R. Kamberger, and U. Wallrabe, 'Process and material properties of polydimethylsiloxane (PDMS) for Optical MEMS', *Sensors Actuators A Phys.*, vol. 151, no. 2, pp. 95–99, Apr. 2009.

[79]   matbase, 'PMMA | Commodity Polymers | Thermoplastics | Natural & Synthetic Polymers | Material Categories | Chemical, mechanical, physical and environmental properties of materials | Matbase: the independent online material selection resource'. [Online]. Available: http://www.matbase.com/material-categories/natural-and-synthetic-polymers/commodity-polymers/material-properties-of-polymethyl-methacrylate-extruded-acrylic-pmma.html#properties. [Accessed: 11-Jun-2015].

[80]   MIT, 'PDMS Materiel Properties'. [Online]. Available: http://www.mit.edu/~6.777/matprops/pdms.htm. [Accessed: 11-Jun-2015].

[81]   S. de Mulatier, M. Ramuz, D. Coulon, S. Blayac, and R. Delattre, 'Mechanical characterization of soft substrates for wearable and washable electronic systems', *APL Mater.*, vol. 7, no. 3, p. 031505, Mar. 2019.

[82]   TheraSigma, 'Hydrogel Electrodes', 2015.

[83]   S. Lin *et al.*, 'Stretchable Hydrogel Electronics and Devices.', *Adv. Mater.*, Dec. 2015.

[84]   J. P. Gong, Y. Katsuyama, T. Kurokawa, and Y. Osada, 'Double-Network Hydrogels with Extremely High Mechanical Strength', *Adv. Mater.*, vol. 15, no. 14, pp. 1155–1158, Jul. 2003.

[85]   T. W. Odom, V. R. Thalladi, J. C. Love, and G. M. Whitesides, 'Generation of 30-50 nm structures using easily fabricated, composite PDMS masks.', *J. Am. Chem. Soc.*, vol. 124, no. 41, pp. 12112–3, Oct. 2002.

[86]   MIT, 'PMMA - MIT Material Property Database'. [Online]. Available: http://www.mit.edu/~6.777/matprops/pmma.htm. [Accessed: 11-Dec-2015].

[87]   A. Shamsi, A. Amiri, P. Heydari, H. Hajghasem, M. Mohtashamifar, and M.

Esfandiari, 'Low cost method for hot embossing of microstructures on PMMA by SU-8 masters', *Microsyst. Technol.*, vol. 20, no. 10–11, pp. 1925–1931, Dec. 2013.

[88]   R. Balint, N. J. Cassidy, and S. H. Cartmell, 'Conductive polymers: towards a smart biomaterial for tissue engineering.', *Acta Biomater.*, vol. 10, no. 6, pp. 2341–53, Jun. 2014.

[89]   D.-Y. Kim *et al.*, 'Self-Healing Reduced Graphene Oxide Films by Supersonic Kinetic Spraying', *Adv. Funct. Mater.*, vol. 24, no. 31, pp. 4986–4995, Aug. 2014.

[90]   P. Ahlberg *et al.*, 'Graphene as a Diffusion Barrier in Galinstan-Solid Metal Contacts', *IEEE Trans. Electron Devices*, vol. 61, no. 8, pp. 2996–3000, Aug. 2014.

[91]   E. and C. C. Canada, 'Mercury in the Environment - About Mercury - Chemical Properties - Pollution and Waste - Environment Canada', 08-Dec-2009. [Online].   Available: http://www.ec.gc.ca/mercure-mercury/default.asp?lang=En&n=10C3AF2D-1. [Accessed: 11-Jun-2015].

[92]   T. Liu, P. Sen, and C. J. Kim, 'Characterization of nontoxic liquid-metal alloy galinstan for applications in microdevices', *J. Microelectromechanical Syst.*, vol. 21, no. 2, pp. 443–450, 2012.

[93]   M. R. Khan, C. Trlica, and M. D. Dickey, 'Recapillarity: Electrochemically Controlled Capillary Withdrawal of a Liquid Metal Alloy from Microchannels', *Adv. Funct. Mater.*, vol. 25, no. 5, pp. 671–678, Feb. 2015.

[94]   P. Ralston, M. Oliver, K. Vummidi, and S. Raman, 'Liquid Metal Vertical Interconnects for Flip-Chip Assembly of GaAs C-Band Power Amplifiers onto Micro-Rectangular Coaxial Transmission Lines', in *2011 IEEE Compound Semiconductor Integrated Circuit Symposium (CSICS)*, 2011, pp. 1–4.

[95]   S. Lindersson, 'Reactivity of Galinstan with Specific Transition Metal

Carbides', 2014.

[96] Y.-G. Deng and J. Liu, 'Corrosion development between liquid gallium and four typical metal substrates used in chip cooling device', *Appl. Phys. A*, vol. 95, no. 3, pp. 907–915, Jun. 2009.

[97] Metacollin, *Galinstan - Non-toxic Liquid metal*. YouTube.com, 2015.

[98] Merriam Webster, 'Vital Signs Medical Definition | Merriam-Webster Medical Dictionary', *Medical Dictionary*, 2015. [Online]. Available: http://www.merriam-webster.com/medical/vital signs. [Accessed: 11-Jun-2015].

[99] D. B. McCombie, A. T. Reisner, and H. H. Asada, 'Adaptive blood pressure estimation from wearable PPG sensors using peripheral artery pulse wave velocity measurements and multi-channel blind identification of local arterial dynamics.', *Conf. Proc. ... Annu. Int. Conf. IEEE Eng. Med. Biol. Soc. IEEE Eng. Med. Biol. Soc. Annu. Conf.*, vol. 1, pp. 3521–4, Jan. 2006.

[100] L. Ben Mohammadi *et al.*, 'Noninvasive monitoring of blood pressure using optical Ballistocardiography and Photoplethysmograph approaches', in *Engineering in Medicine and ...*, 2012, no. 0, pp. 84270K-84270K–11.

[101] A. Alzahrani *et al.*, 'Enhancement of absorption and resistance of motion utilizing a multi-channel opto-electronic sensor to effectively monitor physiological signs during sport exercise', in *BiOS SPIE 2015*, 2015, p. 93150O.

[102] T. Tamura, Y. Maeda, M. Sekine, and M. Yoshida, 'Wearable Photoplethysmographic Sensors—Past and Present', *Electronics*, vol. 3, no. 2, pp. 282–302, 2014.

[103] A. Gupta, 'Respiration Rate Measurement Based on Impedance Pneumography', 2011.

[104] Y. Yu, J. Zhang, and J. Liu, 'Biomedical implementation of liquid metal ink as

drawable ECG electrode and skin circuit.', *PLoS One*, vol. 8, no. 3, p. e58771, Jan. 2013.

[105] G. Wang and M. P. Mintchev, 'Development of Wearable Semi-invasive Blood Sampling Devices for Continuous Glucose Monitoring: A Survey', *Engineering*, vol. 05, no. 05, pp. 42–46, 2013.

[106] E. Cengiz and W. V Tamborlane, 'A tale of two compartments: interstitial versus blood glucose monitoring.', *Diabetes Technol. Ther.*, vol. 11 Suppl 1, no. s1, pp. S11-6, Jun. 2009.

[107] Euro Circuits, 'Making a PCB - PCB Manufacture step by step'. [Online]. Available: http://www.eurocircuits.com/making-a-pcb-pcb-manufacture-step-by-step. [Accessed: 23-Jun-2015].

[108] AT&S, 'HDI Rigid Flex PCBs | AT&S PCBs', 2015. [Online]. Available: http://www.ats.net/products-technology/product-portfolio/flexible-rigid-flexible-pcbs/hdi-rigid-flex-pcbs/. [Accessed: 23-Jun-2015].

[109] C.-G. Choi, 'Fabrication of optical waveguides in thermosetting polymers using hot embossing', *J. Micromechanics Microengineering*, vol. 14, no. 7, pp. 945–949, Jul. 2004.

[110] R. Liedert *et al.*, 'Disposable roll-to-roll hot embossed electrophoresis chip for detection of antibiotic resistance genemecA in bacteria', *Lab Chip*, vol. 12, no. 2, pp. 333–339, 2012.

[111] A. Hagman, 'Print and roll technique for rapid production of stretchable liquid alloy circuits', Uppsala Universitet, 2010.

[112] Y. Zheng, Z. He, J. Yang, and J. Liu, 'Fully Automatic Liquid Metal Printer towards Personal Electronics Manufacture', Beijing, 2013.

[113] Q. Zhang, Y. Gao, and J. Liu, 'Atomized spraying of liquid metal droplets on desired substrate surfaces as a generalized way for ubiquitous printed

electronics', Beijing, 2013.

[114] B. Kirby, *Micro- and Nanoscale Fluid Mechanics*. Cambridge: Cambridge University Press, 2010.

[115] J. Monahan, A. A. Gewirth, and R. G. Nuzzo, 'A Method for Filling Complex Polymeric Microfluidic Devices and Arrays', *Anal. Chem.*, vol. 73, no. 13, pp. 3193–3197, Jul. 2001.

[116] M. D. Dickey, R. C. Chiechi, R. J. Larsen, E. A. Weiss, D. A. Weitz, and G. M. Whitesides, 'Eutectic Gallium-Indium (EGaIn): A Liquid Metal Alloy for the Formation of Stable Structures in Microchannels at Room Temperature', *Adv. Funct. Mater.*, vol. 18, no. 7, pp. 1097–1104, Apr. 2008.

[117] R. C. Gough, A. M. Morishita, J. H. Dang, W. Hu, W. A. Shiroma, and A. T. Ohta, 'Continuous Electrowetting of Non-toxic Liquid Metal for RF Applications', *IEEE Access*, vol. 2, pp. 874–882, 2014.

[118] M. a Eddings, M. a Johnson, and B. K. Gale, 'Determining the optimal PDMS– PDMS bonding technique for microfluidic devices', *J. Micromechanics Microengineering*, vol. 18, no. 6, p. 067001, Jun. 2008.

[119] M. Stoppa and A. Chiolerio, 'Wearable Electronics and Smart Textiles: A Critical Review', *Sensors*, vol. 14, no. 7, pp. 11957–11992, Jul. 2014.

[120] Resistat, 'Home Page for Jarden Applied Materials - Resistat Fiber Collection', *Resistat Fiber Collection*, 2008. [Online]. Available: http://www.resistat.com/. [Accessed: 25-Nov-2015].

[121] lessEMF.com, 'Electromagnetic Field Shielding Fabrics'. [Online]. Available: http://www.lessemf.com/fabric.html. [Accessed: 25-Nov-2015].

[122] Sophitex, 'Sophitex ESD Fabrics , Antistatic Fabrics , antistatic garments and ESD wear'. [Online]. Available: http://www.sophitex.com/. [Accessed: 25-Nov-2015].

[123] Sensoria Fitness, 'Sensoria Fitness'. [Online]. Available: http://www.sensoriafitness.com/. [Accessed: 25-Nov-2015].

[124] Y. Enokibori, A. Suzuki, H. Mizuno, Y. Shimakami, and K. Mase, 'E-textile pressure sensor based on conductive fiber and its structure', in *Proceedings of the 2013 ACM conference on Pervasive and ubiquitous computing adjunct publication - UbiComp '13 Adjunct*, 2013, pp. 207–210.

[125] H. Mattila, *Intelligent Textiles and Clothing*. Elsevier Science, 2006.

[126] M. Hamedi, R. Forchheimer, and O. Inganäs, 'Towards woven logic from organic electronic fibres.', *Nat. Mater.*, vol. 6, no. 5, pp. 357–62, May 2007.

[127] T. Acti *et al.*, 'High performance flexible fabric electronics for megahertz frequency communications', in *2011 Loughborough Antennas & Propagation Conference*, 2011, pp. 1–4.

[128] Y. Y. Lim, Y. M. Goh, and C. Liu, 'Surface Treatments for Inkjet Printing onto a PTFE-Based Substrate for High Frequency Applications', *Ind. Eng. Chem. Res.*, vol. 52, no. 33, pp. 11564–11574, Aug. 2013.

[129] A. Sridhar, J. Reiding, H. Adelaar, F. Achterhoek, D. J. van Dijk, and R. Akkerman, 'Inkjet-printing- and electroless-plating- based fabrication of RF circuit structures on high-frequency substrates', *J. Micromechanics Microengineering*, vol. 19, no. 8, p. 085020, Aug. 2009.

[130] I. Locher, M. Klemm, T. Kirstein, and G. Trster, 'Design and Characterization of Purely Textile Patch Antennas', *IEEE Trans. Adv. Packag.*, vol. 29, no. 4, pp. 777–788, Nov. 2006.

[131] P. Tiberto *et al.*, 'Magnetic properties of jet-printer inks containing dispersed magnetite nanoparticles', *Eur. Phys. J. B*, vol. 86, no. 4, p. 173, Apr. 2013.

[132] V. Camarchia *et al.*, 'Demonstration of inkjet-printed silver nanoparticle microstrip lines on alumina for RF power modules', *Org. Electron.*, vol. 15, no.

1, pp. 91–98, Jan. 2014.

[133] Conductive Compounds, 'Conductive Compounds Ink Matrix and Product Comparison Tool', *For Your Functional Ink & Coating Requirements*, 2015. [Online]. Available: http://www.conductivecompounds.com/product-matrix/silver-inks.html. [Accessed: 30-Nov-2015].

[134] T. Lu, L. Finkenauer, J. Wissman, and C. Majidi, 'Rapid Prototyping for Soft-Matter Electronics', *Adv. Funct. Mater.*, vol. 24, no. 22, pp. 3351–3356, Jun. 2014.

[135] W. Honda, S. Harada, T. Arie, S. Akita, and K. Takei, 'Wearable, Human-Interactive, Health-Monitoring, Wireless Devices Fabricated by Macroscale Printing Techniques', *Adv. Funct. Mater.*, vol. 24, no. 22, pp. 3299–3304, Jun. 2014.

[136] J. Hruska, 'Atom Everywhere: Intel breaks ground on first 450mm fab | ExtremeTech', *ExtremeTech*, 2013. [Online]. Available: http://www.extremetech.com/extreme/163372-atom-everywhere-intel-breaks-ground-on-first-450mm-fab. [Accessed: 02-Dec-2015].

[137] Riddell, 'Riddell SpeedFlex Helmet - Helmets - On-Field Equipment - Shop', 2015. [Online]. Available: http://www.riddell.com/shop/on-field-equipment/helmets/riddell-speedflex-helmet.html. [Accessed: 18-Dec-2015].

[138] Riddell, 'InSite - Shop Riddell'. [Online]. Available: http://www.riddell.com/InSite. [Accessed: 01-Dec-2015].

[139] D. Ecker, 'Riddell continues tech helmet push with SpeedFlex - Blogs On Sports - Crain's Chicago Business'. [Online]. Available: http://www.chicagobusiness.com/article/20140819/BLOGS04/140819838/riddell-continues-tech-helmet-push-with-pricey-speedflex. [Accessed: 01-Dec-2015].

[140] Brands Cycle & Fitness, 'Polar H7 Heart Rate Sensor - Brands Cycle and Fitness', 2015. [Online]. Available: http://brandscycle.com/product/polar-h7-heart-rate-sensor-34491.htm?gclid=CjwKEAiAp_WyBRD37bGB_ZO9qAYSJAA72IkghIrqSxnCMzVzXYV8j49AmpXDGHvAsLrN5QtO6orL8hoCNojw_wcB. [Accessed: 01-Dec-2015].

[141] Longstreth, 'Gryphon Goalkeeping Bodyguard-longstreth.com'. [Online]. Available: http://www.longstreth.com/Gryphon-Goalkeeping-Bodyguard/productinfo/HGGRBG/. [Accessed: 01-Dec-2015].

[142] Texas Instruments, 'Selecting antennas for low-power wireless applications', 2008.

[143] H.-B. Liu and H.-Q. Gong, 'Templateless prototyping of polydimethylsiloxane microfluidic structures using a pulsed CO2 laser', *J. Micromechanics Microengineering*, vol. 19, no. 3, p. 037002, Mar. 2009.

[144] G. Camino, S. M. Lomakin, and M. Lageard, 'Thermal polydimethylsiloxane degradation. Part 2. The degradation mechanisms', *Polymer (Guildf).*, vol. 43, no. 7, pp. 2011–2015, 2002.

[145] I. D. Johnston, D. K. McCluskey, C. K. L. Tan, and M. C. Tracey, 'Mechanical characterization of bulk Sylgard 184 for microfluidics and microengineering', *J. Micromechanics Microengineering*, vol. 24, p. 035017, 2014.

[146] R. C. Huang and L. Anand, 'Non-linear mechanical behavior of the elastomer polydimethylsiloxane (PDMS) used in the manufacture of microfluidic devices'.

[147] H. C. Jung *et al.*, 'CNT/PDMS composite flexible dry electrodesfor long-term ECG monitoring', *IEEE Trans. Biomed. Eng.*, vol. 59, no. 5, pp. 1472–1479, May 2012.

[148] J. Park and B. Kim, 'Fabrication of a roller type PDMS stamp using SU-8

concave molds and its application for roll contact printing', *J. Micromechanics Microengineering*, vol. 26, no. 3, p. 035007, Mar. 2016.

[149] X. Lv *et al.*, 'Route to one-step microstructure mold fabrication for PDMS microfluidic chip', *AIP Adv.*, vol. 8, p. 45207, 2018.

[150] F. Zahir, S. J. Rizwi, S. K. Haq, and R. H. Khan, 'Low dose mercury toxicity and human health', *Environ. Toxicol. Pharmacol.*, vol. 20, no. 2, pp. 351–360, Sep. 2005.

[151] G. Speckbrock, S. Kamitz, M. Alt, and H. Schmitt, 'Low melting gallium, indium, and tin eutectic alloys, and thermometers employing same', CN1039162C, CN1092163A, DE4227434A1, DE4227434C2, EP0657023A1, EP0657023B1, US5800060, WO1994004895A1, 1997.

[152] E. Senel, J. C. Walmsley, S. Diplas, and K. Nisancioglu, 'Liquid metal embrittlement of aluminium by segregation of trace element gallium', *Corros. Sci.*, vol. 85, pp. 167–173, 2014.

[153] M. Rajagopalan, M. A. Bhatia, M. A. Tschopp, D. J. Srolovitz, and K. N. Solanki, 'Atomic-scale analysis of liquid-gallium embrittlement of aluminum grain boundaries', *Acta Mater.*, vol. 73, pp. 312–325, 2014.

[154] J. Hiltunen *et al.*, 'Roll-to-roll fabrication of integrated PDMS–paper microfluidics for nucleic acid amplification', *Lab Chip*, vol. 18, no. 11, pp. 1552–1559, May 2018.

[155] J. Flowers, C. Liu, S. Mitchell, A. Harland, and D. Esliger, 'Conductive Microfluidic Interconnects to Enable Scalable 3D Manufacturing of Wearable Electronics', in *Proceedings - Electronic Components and Technology Conference*, 2016, vol. 2016-Augus.

[156] R. Bringans, 'Challenges and opportunities for the flexible electronics industry'. Palo Alto.

[157] M. K. Armstrong, 'PCB design techniques for lowest-cost EMC compliance. Part 1', *Electron. Commun. Eng. J.*, vol. 11, no. 4, pp. 185–194, Aug. 1999.

[158] K. Ren, J. Zhou, and H. Wu, 'Materials for Microfluidic Chip Fabrication'.

[159] S. M. Westwood, S. Jaffer, and B. L. Gray, 'Enclosed SU-8 and PDMS microchannels with integrated interconnects for chip-to-chip and world-to-chip connections', *J. Micromechanics Microengineering*, vol. 18, no. 6, p. 064014, Jun. 2008.

[160] J. A. Rogers and R. G. Nuzzo, 'Recent progress in soft lithography', *Mater. Today*, vol. 8, no. 2, pp. 50–56, 2005.

[161] C. K. Chung, Y. C. Lin, and G. R. Huang, 'Bulge formation and improvement of the polymer in CO 2 laser micromachining', *J. Micromechanics Microengineering*, vol. 15, no. 10, pp. 1878–1884, Oct. 2005.

[162] N. S. Shanmugam, G. Buvanashekaran, K. Sankaranarayanasamy, and K. Manonmani, 'Influence of Beam Incidence Angle in Laser Welding of Austenitic Stainless Steel using Finite Element Analysis', *Multidiscip. Model. Mater. Struct.*, Jul. 2013.

[163] The British Standards Institution, 'BS EN ISO 4287 - Geometrical product specification (GPS). Surface texture: Profile method. Terms, definitions and surface texture parameters'. The British Standards Institution, 2000.

[164] J. Haq, B. D. Vogt, G. B. Raupp, and D. Loy, 'Finite element modeling of temporary bonding systems for flexible microelectronics fabrication', *Microelectron. Eng.*, vol. 94, pp. 18–25, 2012.

[165] V. Damić, 'Modelling flexible body systems: a bond graph component model approach', *Math. Comput. Model. Dyn. Syst.*, vol. 12, no. 2–3, pp. 175–187, Apr. 2006.

[166] D.-W. Lee and Y.-S. Choi, 'A novel pressure sensor with a PDMS diaphragm',

Microelectron. Eng., vol. 85, no. 5–6, pp. 1054–1058, May 2008.

[167] ANSYS Inc., 'ANSYS Mechanical User's Guide 18.2', *2017*. [Online]. Available: https://support.ansys.com/portal/site/AnsysCustomerPortal/template.MA XIMIZE/menuitem.2884af70ee553994a6f26c10639c97a0/?javax.portlet.tps t=79fa7a6e32edb10c85fbb010639c97a0_ws_MX&javax.portlet.prp_79fa7a6 e32edb10c85fbb010639c97a0=wcproxyurl%3Dhttp%25253A%25. [Accessed: 13-Nov-2017].

[168] F. J. Harewood and P. E. McHugh, 'Comparison of the implicit and explicit finite element methods using crystal plasticity', *Comput. Mater. Sci.*, vol. 39, no. 2, pp. 481–494, 2007.

[169] J. L. Chenot, R. D. Wood, and O. C. Zienkiewicz, *Numerical methods in industrial forming processes : proceedings, 4th International Conference on Numerical Methods in Industrial Forming Processes, NUMIFORM '92 : Valbonne, France, 14-18 September 1992*. A.A. Balkema, 1992.

[170] J. S. Sun, K. H. Lee, and H. P. Lee, 'Comparison of implicit and explicit finite element methods for dynamic problems', *J. Mater. Process. Technol.*, vol. 105, no. 1, pp. 110–118, 2000.

[171] M. Mashayekhi, 'Element Selection Criteria'. Isfahan University of Technology.

[172] 'SOLID187'. [Online]. Available: https://www.sharcnet.ca/Software/Ansys/17.0/en-us/help/ans_elem/Hlp_E_SOLID187.html. [Accessed: 20-Nov-2017].

[173] '13.186. SOLID186 - 3-D 20-Node homogeneous/Layered Structural Solid'. [Online]. Available: https://www.sharcnet.ca/Software/Ansys/16.2.3/en-us/help/ans_thry/thy_el186.html. [Accessed: 19-Nov-2017].

[174] G. R. Joldes, A. Wittek, and K. Miller, 'Suite of finite element algorithms for accurate computation of soft tissue deformation for surgical simulation.', *Med. Image Anal.*, vol. 13, no. 6, pp. 912–9, Dec. 2009.

[175] E. Q. Sun, 'Shear Locking and Hourglassing in MSC Nastran, ABAQUS, and ANSYS'.

[176] '13.242. HSFLD242 - 3-D Hydrostatic Fluid'. [Online]. Available: https://www.sharcnet.ca/Software/Ansys/16.2.3/en-us/help/ans_thry/thy_el242.html. [Accessed: 19-Nov-2017].

[177] 'Ansys License Type'.

[178] T. Payne, 'Improved Human Soft Tissue Thigh Surrogates for Superior Assessment of Sports Personal Protective Equipment', Loughborough University, 2015.

[179] '2. Semiconductor Doping Technology'. [Online]. Available: http://www.iue.tuwien.ac.at/phd/wittmann/node7.html. [Accessed: 02-Jun-2017].

[180] Granta Design, 'GRANTA MI:Materials Gateway for ANSYS', 2018. [Online]. Available: https://www.grantadesign.com/products/mi/ansys/. [Accessed: 27-Oct-2018].

[181] L. Kersey, V. Ebacher, V. Bazargan, R. Wang, and B. Stoeber, 'The effect of adhesion promoter on the adhesion of PDMS to different substrate materials', *Lab Chip*, vol. 9, no. 7, pp. 1002–1004, Apr. 2009.

[182] L. Guo, Y. Lv, Z. Deng, Y. Wang, and X. Zan, 'Tension testing of silicone rubber at high strain rates', *Polym. Test.*, vol. 50, pp. 270–275, Apr. 2016.

[183] 'What is von Mises Stress? — SimScale Documentation'. [Online]. Available: https://www.simscale.com/docs/content/simwiki/fea/what-is-von-mises-stress.html. [Accessed: 01-Jul-2019].

[184] Y. V. Milman, I. V. Gridneva, and A. A. Golubenko, 'Construction of stess-strain curves for brittle materials by indentation in a wide temperature range', *Sci. Sinter.*, vol. 39, no. 1, pp. 67–75, 2007.

[185] D. Graham-Rowe, 'Bendable Microchips Could Make Smarter Sensors', *MIT Technological Review*, 2012. [Online]. Available: http://www.technologyreview.com/news/429344/bendable-microchips-could-make-smarter-sensors/. [Accessed: 12-Nov-2014].

[186] EL-CAT Inc, 'Properties of Silicon - El-Cat.com', *Properties of silicon and silicon wafers*, 2015. [Online]. Available: https://www.el-cat.com/silicon-properties.htm. [Accessed: 03-Jul-2015].

[187] D. Y. R. Chong, W. E. Lee, B. K. Lim, J. H. L. Pang, and T. H. Low, 'MECHANICAL CHARACTERIZATION IN FAILURE STRENGTH OF SILICON DICE'.

[188] T. Mizuno and T. Kamae, 'Mechanical Strength of Silicon wafers', 2000.

[189] K. E. Petersen, 'Silicon as a Mechanical Material', 1982.

[190] K. E. Petersen, 'Silicon as a mechanical material', *Proc. IEEE*, vol. 70, no. 5, pp. 420–457, 1982.

[191] P. Sunilkumar, C. Patil, B. H, K. Putturaj, V. C. Sangolgi, and K. Jayasudha, 'A Comparative Study of the Shear and Tensile Bond Strength using three types of Direct Bonding Adhesives on Stainless Steel Brackets - An In Vitro Study.', *J. Int. oral Heal. JIOH*, vol. 5, no. 4, pp. 26–9, Aug. 2013.

[192] Z. Zhu *et al.*, 'A Versatile Bonding Method for PDMS and SU-8 and Its Application towards a Multifunctional Microfluidic Device', *Micromachines*, vol. 7, no. 12, p. 230, Dec. 2016.

[193] G. K. Stylios, 'Interactive SMART textiles: innovation and collaboration in Japan and South Korea', *Int. J. Cloth. Sci. Technol.*, vol. 17, no. 1, Feb. 2005.

9 APPENDICES

APPENDIX 1 – IEEE ECTC 2016 FULL PAPER

The following is the full paper that was submitted and published as part of the ECTC conference proceedings.

Conductive Microfluidic Interconnects to Enable Scalable 3D Manufacturing of Wearable Electronics

Jonathan Flowers[1], Changqing Liu[1], Sean Mitchell[1], Andy Harland[1], Dale Esliger[2]

[1]Wolfson School of Mechanical, Manufacturing and Electrical Engineering
[2]School of Sport, Exercise and Health Sciences
Loughborough University, Loughborough, Leicestershire, LE11 3TU, UK
e-mail: j.b.flowers@lboro.ac.uk, c.liu@lboro.ac.uk

Abstract—**This paper seeks to investigate the geometry and surface finish of channels machined into polydimethylsiloxane using a continuous wave CO_2 laser with respect to the configurations used when creating these channels. It has been found that there is a very strong correlation between both power and speed with regard to depth. However, at higher energy levels this relationship appears to break down and the depth of the cut reduces when compared to similar laser configurations at a lower power level. In order to investigate the various mechanisms, that could affect the channel geometry, both the laser power and trace speed were varied in conjunction with the use of a fixed focal size to allow comparison between configurations. It was discovered that as the power level increases repeatability decreases while dimensional variability of the channel along its length and multiple iterations increases. It was found that the power output of the laser has a greater effect on the dimensions of the channels than the total energy input into the material.**

Keywords – laser machining; microfluidics manufacture; galinstan;

I. INTRODUCTION

Wearable electronics are a set of technologies and devices that can be worn to track information related to health and fitness markers and sometimes even include location and activity data. These wearable devices must be thin, flexible, stretchable and conformal to the human body [1]. Low cost and scalable conformal electronics are currently seen as the gold standard for on-body sensor networks; however, their manufacture has remained elusive, it demands abrupt changes to technologies when compared to conventional electronics, which are usually rigid. In order to achieve this, various challenges and bottlenecks exist with regard to both the design and manufacture of electronics [2]. Conventional interconnect materials such as copper, gold and tin alloys can become the victims of their own mechanical properties, as for a device to be flexible and stretchable, these materials need to be capable of repeated elastic and plastic deformation, which will quickly lead to metal fatigue jeopardizing the reliability of the products [3]. To solve this problem unique high conductivity metallic interconnects are proposed, which can be deformed without inducing fatigue through the use of a room temperature liquid metal called Galinstan in this study [4].

The use of Galinstan as a conductor does introduce a new set of hurdles that would need to be overcome in order to bring these technologies to tangible applications. Due to Galinstan being a liquid, it must be fully encapsulated within a confined channel in order to prevent any change in geometry of the conductors. For the channels that have to be fabricated to carry Galinstan liquid, the manufacturing method must be capable of varying channel geometry across the length of the channel. An additional challenge that requires a solution is to include vertical vias that are able to form a three dimensional electronic interconnect structure or circuit design [5]. Conventional methods that are used to create these channels for Lab on Chip applications normally involve the use of complex lithography, molding or embossing techniques [6], which can introduce problems when creating holes directly through the substrate in order to enable vertical interconnects. One of these issues is requiring sacrificial layers in order to create a single component, which when scaled can lead to increased costs [7].

The use of conductive fluids such as Galinstan for interconnects contained within a soft, flexible substrate has been shown to be a promising direction for the manufacture of such devices, which, can fit well with existing Roll2Roll approach for scalable manufacturing of fluidic channels. It is desirable to have the ability to fabricate 3D interconnected channels on a suitable flexible substrate, for which the process is capable of high throughput, and is scalable at reasonable costs for production and mass manufacture of low cost devices. In this work, several potential scalable methods for creating the channels have been investigated for the direct fabrication of microfluidic channels within a Polydimethylsiloxane (PDMS) substrate. The use of lasers as a processing tool allows the creation of a varied channel sizes in addition to drilling and cutting directly through the material.

This paper seeks to identify the optimal laser cutting parameters using a continuous wave Carbon Dioxide laser for the cutting and engraving of a PDMS substrate. The use of a CW CO_2 laser allows the low cost, continuous manufacture of PDMS based microfluidic devices with few if any restrictions on channel geometry, while being capable of small-scales and high precision. Various laser parameters such as power levels, trace speed and repetitions were tested to narrow down the optimal combination in order to create a uniform high quality cut and surface finish. This has led to a data set that was produced to enable the correct selection of parameters when machining PDMS with a CW CO2 laser. An evaluation of the quality of the obtained channels was

subsequently carried out using various metrology tools to provide a clear understanding of the effects of laser processing parameters on the surface finish, depth and geometry of the machined channel in the PDMS substrate. It is envisaged that the use of low cost CW CO2 lasers in both the small-scale prototyping and mass manufacture of microfluidic channels on PDMS substrates will be viable for scalable 3D manufacturing of wearable electronics. A tangible wearable device will be designed at a later stage, to demonstrate the processes being developed in this study.

II. METHODS AND MATERIALS

A. Polydimethylsiloxane (PDMS) Substrate

PDMS has been selected as the substrate which was supplied by Dow Corning Sylgard 184 blended in a 10:1 ratio of resin to hardener. Sheets with a nominal thickness of 4mm were produced in 200mm by 200mm squares and cured at 22°C for 48 hours.

B. Laser Set-up

The laser used for the fabrication of via holes and channels was a 100W Synrad CO_2 Marking Laser with an FH Flyer Marking head, also manufactured by Synrad. The laser was configured with a focal point of 300μm and has a characteristic wavelength of 10.6μm. A CO2 laser was chosen due to its ability to easily cut the polymer substrate, other types such as Nd:YAG and Excimer lasers were tested but either were not able to cut the polymer due to incompatible emission and absorption spectra or were too slow to be used in a viable continuous production process. The laser is a continuous wave unit that uses Pulse Width Modulation to adjust the power level of the laser. The configuration settings exposed to the user include the power output, as a percentage of 100W and trace speed, up to a maximum value of 990mm/s.

C. Channel Fabrication

To quantify the effect of the laser configuration on channel geometry and quality, a range of parameters were

Figure 1. a) Channel Texture bitmap and b) depth map (Sample 1 - 80W at 100mm/s)

tested. These include three power settings (60W, 80W 100W) in combination with nine speed settings between 250mm/s and 50mm/s in 25mm/s intervals for comparison and evaluation. They are summarized in Table 1. Each combination of parameters was tested three times in order to identify the repeatability of the process. Eighty-one lines, 20mm in length and with 10mm spacing between each line were marked onto the pre-prepared PDMS substrate. Once all cuts were made, the sample was diced into groups of three lines and washed with isopropyl alcohol, then dried with clean air blasts. Once dried the samples were then sputtered with a 12nm AuPd layer in order to facilitate imaging and surface profiling.

TABLE I.   LASER CONFIGURATIONS USED

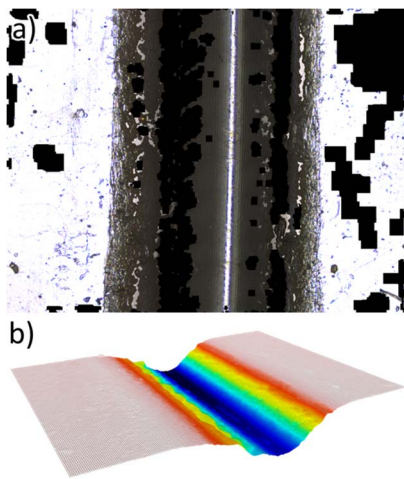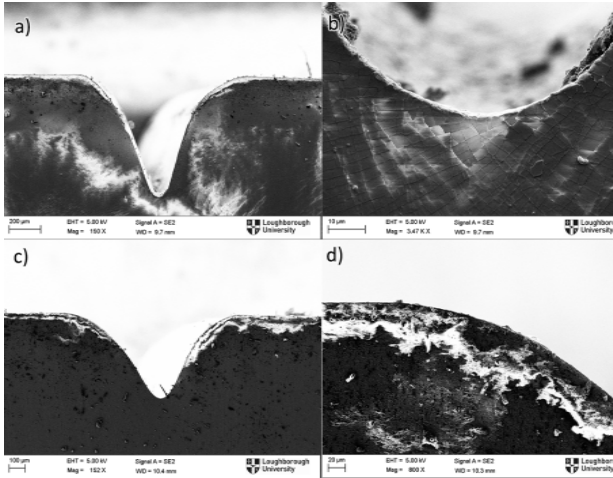| Laser Power Levels	Focal Diameter	Trace Speed	Energy Output per m^2
100W		250 mm/s	1333.33
		225 mm/s	1481.48
		200 mm/s	1666.67
		175 mm/s	1904.76
		150 mm/s	2222.22
		125 mm/s	2666.67
		100 mm/s	3333.33
		75 mm/s	4444.44
		50 mm/s	6666.67
80W	0.3mm	250 mm/s	1066.67
		225 mm/s	1185.19
		200 mm/s	1333.33
		175 mm/s	1523.81
		150 mm/s	1777.78
		125 mm/s	2133.33
		100 mm/s	2666.67
		75 mm/s	3555.56
		50 mm/s	5333. 33
60W		250 mm/s	800.00
		225 mm/s	888.89
		200 mm/s	1000.00
		175 mm/s	1142.86
		150 mm/s	1333.33
		125 mm/s	1600.00
		100 mm/s	2000.00
		75 mm/s	2666.67
		50 mm/s	4000.00

Figure 2. FEGSEM Images of two samples, which demonstrate some of the artifacts that are left around the channel after processing. Images a) and b) are from a 100W exposure at 50mm/s and demonstrate what appears to be thermal induced fracture of the material. Images c) and d) are from a 100W exposure at 75mm/s and clearly show re-deposition along the edges of the groove.

D. Characteriasation: Data Acquisition

Each of the diced segments was imaged using an Alicona InfiniteFocus with a 10x magnification lens, however, the lines cut at 100W 50mm/s-100mm/s were imaged with 5x magnification. The system was configured to acquire a lateral resolution of 3μm and a vertical resolution of 750nm.

The system produced both texture images and three-dimensional depth profile maps, which can be typically seen in Figure 1.

Field Emission Gun Scanning Electron Microscope (FEGSEM) images were taken of a selection of cross section from some samples in order to observe any changes to the material structure and any re-deposition that may be
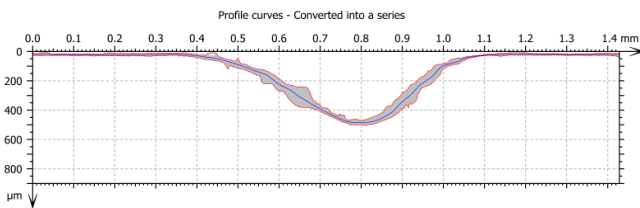

Figure 3. Profile curve stack (grey) showing upper and lower envelopes (red) and mean (blue) for Sample 1 - 80W at 100mm/s
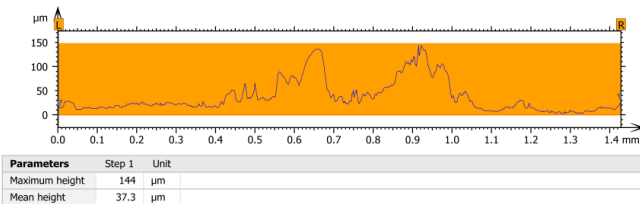

Figure 4. Profile curve range calculated as the difference between upper and lower envelopes as seen in Figure .

occurring. These cross sections also allowed observation of some of the surface qualities of the channels as well as any kind of thermal fracture that may be occurring. A selection of these images can be seen in Figure 2. These images include a close up of the entire channels as well as some of the artifacts that could be seen occurring around the channel itself like in Figures 2(b) and 2(d).

E. Characteriasation: Data Analysis

Depth profile maps were imported into Digital Surf MountainsMap Premium 7.2, where various analysis tools can be accessed to carry out and extract various metrics for the channels that were laser machined. Channel depth was measured using two methods: i) by calculating the maximum depth using every profile across the 1.4mm imaged sample, ii) by using the "Valley Depth Tool" which intelligently identifies the bottom of the valley and averages only those points. The latter was the preferable to the profile tool, as the deepest part of the channel may not always be
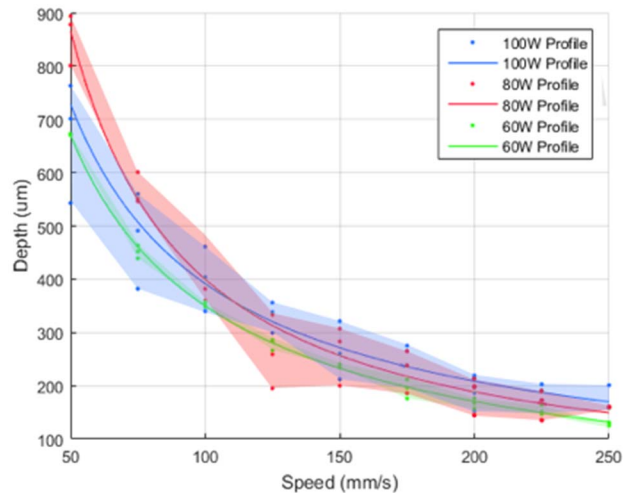

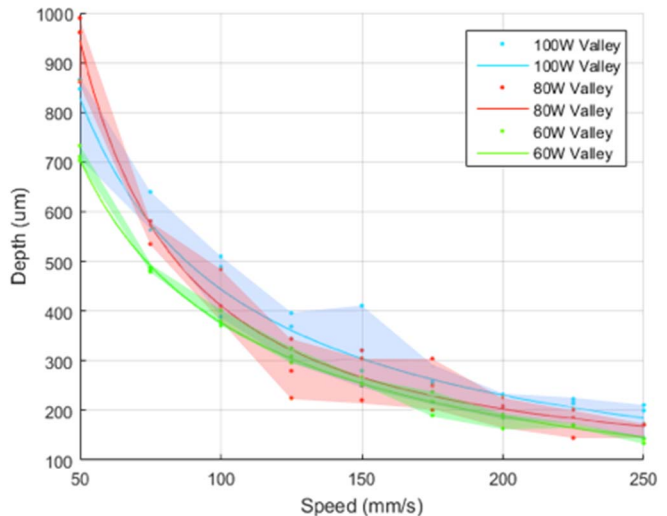Figure 2. Depth vs Speed using mean maximum profile depth

Figure 3. Depth vs Speed using Valley Depth Tool

vertically aligned. Channel quality was evaluated using the upper and lower envelopes of all the profiles (Figure 3) and a difference calculated at each point as can be seen in Figure 4.

The channel edge shape was identified qualitatively as either having a smooth or blunt transition. An example of smooth transitions can be seen in Figure . A blunt transition is a sharper transition that actually has a ridge; edges of this type were quite uncommon.

III. RESULTS AND DISCUSSION

The results can be divided into two categories, channel profile shape and surface finish. Profile shape covers the channel geometry such as channel depth, channel quality, slope angle and edge transition type. Surface finish covers the waviness and surface roughness of the channel.

A. Channel Profile: Depth Analysis

Data for the channel depth displayed in Figures 5 and 6. It can be seen that when the cut was made using 100W power at speeds below 125mm/s the depth did not increase as expected. The expected result was that as the power level increases the channel depth increases and as the trace speed decreases, the channel depth increases as well. This therefore means that the 100W channels traced at 50mm/s should be the deepest channels. It was seen in the depth maps that the shape of the groove no longer followed the Gaussian profile as all the other lines did in addition to being much wider. This can possibly be attributed the increased energy, a higher energy input concentration and longer exposure time, thus creating a larger heat effected zone which may possibly be recasting the burnt, ejected mass. Another possibility is when the material is burnt, boiled or vaporized, due to the high energy levels involved, there is a possibility the ejected mass is obstructing the beam and absorbing a significant portion of the energy from the laser. During the experimentation and the cutting of the channels, large amounts of burnt material were observed being ejected from the material and b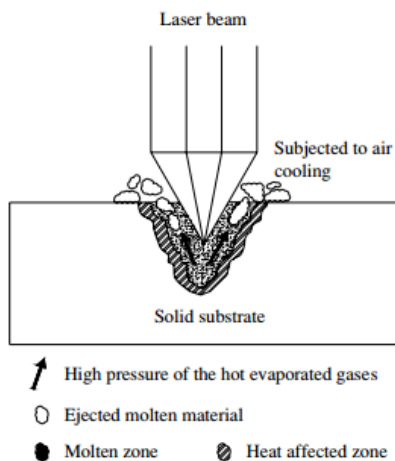eing blown around the containment vessel of the laser. Figure 7 shows schematically the process which material goes through as it is being exposed to a laser beam. The material ejected is done through the rapid expansion of high temperature vaporized and molten material. This can cause the material to be recast along the edges, which is visible Figure 4(d). This would also explain why the repeatability and quality of the channel is drastically reduced. These hypotheses will need to be investigated further incorporating SEM imagery and high-speed imaging of the process itself. Investigation of the material structure within the groove can then be carried out in addition to observing the behavior of ejected mass. The observed behavior however, does indicate a loss of control of the process at higher energy levels. A loss of control is evident when the dramatic increase in max variance with respect to the channel depth, as seen in Figure 8, is investigated in addition to energy level. The ribbon plots in Figures 5 and 6 demonstrate that as laser power increases the variation in depth increases as repeatability decreases, regardless of trace speed or overall cut depth.

Besides this observation, the data had R^2 values of between 0.926 and 0.997 indicating an extremely strong correlation between trace speed and channel depth.

B. Channel Profile: Evaluation of Channel Quality

The groove quality can be quantified using the variance graph produced for each sample as seen in Figure . These values were then plotted in Figure 8. It can be seen that above 125mm/s there is no major relationship between speed, power and channel quality. However, as the amount of energy input into the material increases and the exposure time is extended, the channel quality is further reduced evidenced by Figure 8. It shows a strong negative correlation between both trace speed and variance. Some of this increase can be attributed to the increased channel depth, however, the same trend still exists when running this comparison with the variance as a percentage of the channel depth.

C. Channel Profile: Slope Angle

Due to the configuration of the laser, the slope angles

Figure 7. The schematic model of the formation of bulges and the material ejection process during polymer machining by laser [10]
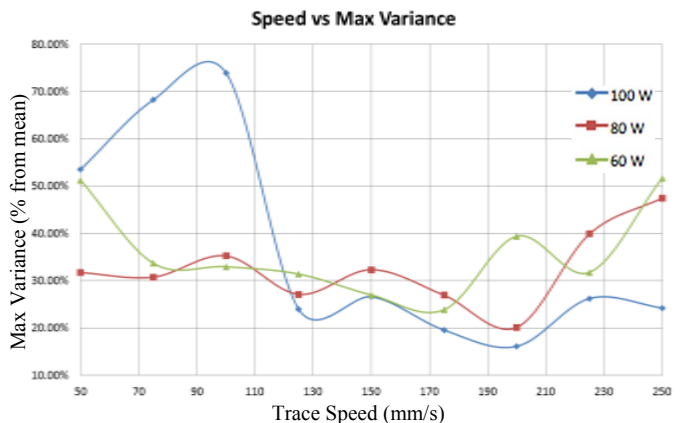

Figure 8. Speed vs Max Variance of the channel

produced are largely dependent on the incidence of the beam. The laser used a scanning head configuration, which uses an articulated mirror to redirect the beam. This means that the incidence angle between the beam and material surface changes as the beam follows its programmed cutting paths[8]. This angle is, at its maximum will be approximately 10° away from vertical. This angle is not enough to cause any noticeable effect to the depth as seen in the relatively consistent depths achieved across multiple samples. It will however affect the slope angle of the grooves. The advantages of using a scanning head such as this enable the ability to achieve much higher trace speeds than a conventional Cartesian bed laser. In addition to higher trace speeds, scanning heads are less affected by speed ramping due to the much lower mass and thus the inertial effects generated during acceleration and deceleration of the laser when compared to an equivalent Cartesian bed system.

D. Channel Profile: Edge Transition Type

Two types of edge transition exist within the scope of this experiment, smooth and blunt. A blunt transition is defined as having a sharp drop-off from the surface to the bottom of the channel is narrower than the depth. A smooth transition is one that is wider than the depth. It was found that there was no correlation between transition type and either power nor speed. The link between the power and transition produced a spearman coefficient of 0.068, and for the speed and transition link a value of -0.582. This shows there is a slight correlation between speed and the likelihood of a specific transition occurring, however it is far from a strong link. The transition depth is more likely affected by the angle of incidence, for which the laser interacts with the material; this was not a controlled variable for this experiment. This is due to the way a scanning head operates.
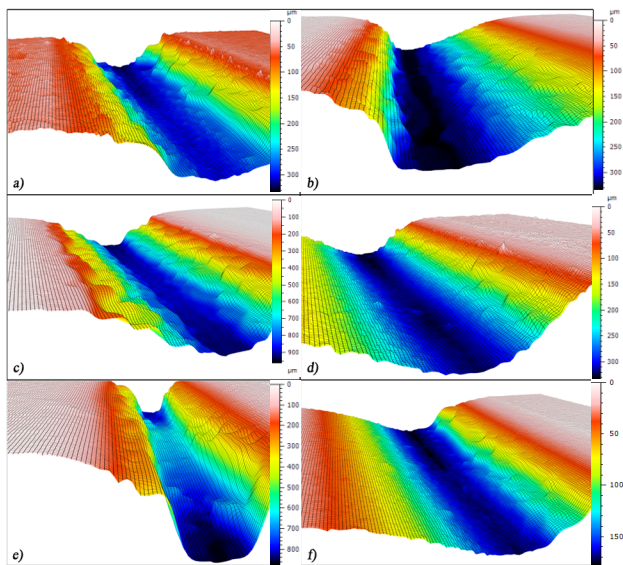

Figure 9. Surface maps of samples used to investigate surface finish a) 60W at 50mm/s b) 60W at 250mm/s c) 80W at 50mm/s d) 80W at 250mm/s e) 100W at 50mm/s f) 100W at 250mm/s (All scales are in

E. Material Integrity

It can be seen in Figure(b) that cracking has occurred at the bottom of the channel likely due to the high thermal stresses induced within the material. These stresses are caused by the extremely rapid temperature rise and steep thermal gradient between the areas of material exposed to the laser and the immediate surrounding areas, both on the surface and below the penetration depth of the beam. As of yet it is unknown if this structure of cracks which are less than 200nm in width will have an effect on the surface wettability with Galinstan or more importantly absorb the fluid and allow penetration of the fluid into the material.

F. Surface Finish

Surface texture is a significant part of overall surface finish and can be quantified using various metrics that are
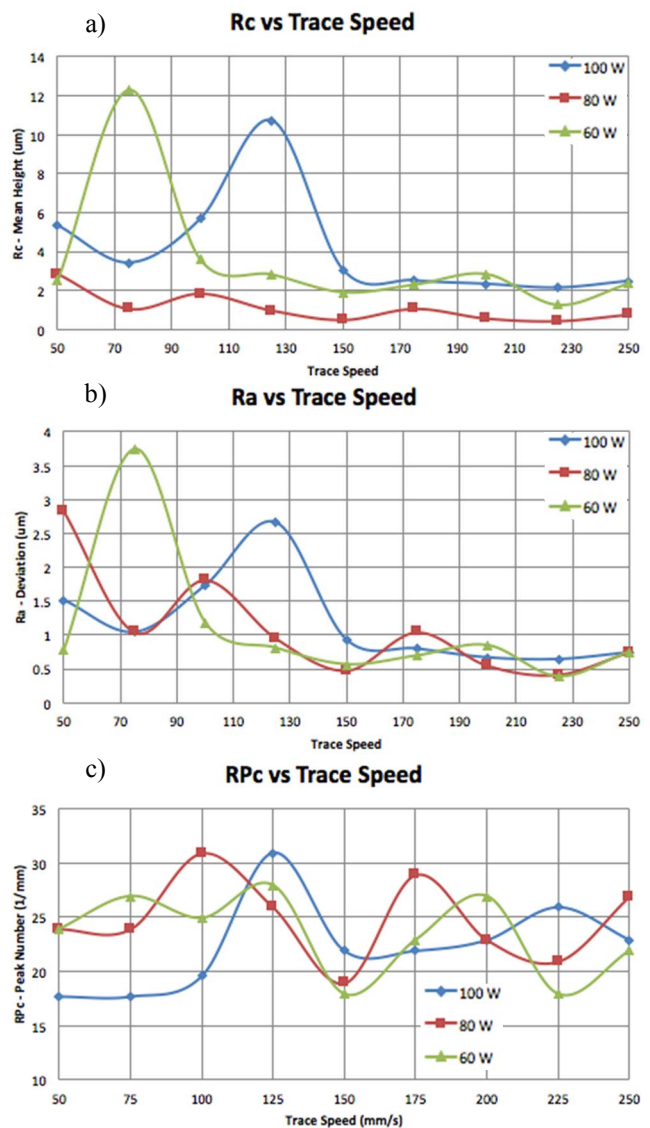

Figure 10. Data extracted from each samples surface profile report presented above. a) Mean peak height vs trace speed. b) Arithmetical mean deviation of the mean height vs trace speed. c) Average number of peaks per mm vs trace speed

defined by various standards, specifically BS EN ISO 4287 [9]. From this standard, a specific set of metrics can quantifiably allow the comparison of a set of surfaces. These indicators are Mean Peak Height (Rc), Arithmetical Mean Deviation (Ra) and the number of peaks per millimeter (RPc). The use of these metrics defines the height and frequency of peaks and troughs on the surface as well as defining their deviation from the maximum value. A typical report generated by Mountains Map from each depth map as seen in Figure 9, can be created and plots of these values from the samples can be seen in Figure 10. The only drawback to using these values is that they can only be generated for a single profile extracted from the three dimensional depth maps. Each profile was selected from the deepest part of the channel.

It can be seen from Figure 10(a) that Mean Peak height appears to be affected by the amount of power input into the material but not by the trace speed. However, the 80W power output appeared to generate the smoothest channels with the overall lowest mean peak heights, however when this value is paired with the mean deviation shown in Figure 10(b), this relationship becomes far less significant as there is discernable relationship between power and the deviation of peak height. There is however, a correlation between the deviation and trace speed (R^2 = -0.581), with higher trace speeds producing a more even and nominal channel surface. This is likely due to shorter exposure times to the laser and thus reducing the thermal stresses on the material and resulting in less thermal fracture and additional burning, where the material does not have the required energy to be ejected from the exposed zone. As for the number of peaks that appear over the measured length, there is no correlation to trace speed or power, which is apparent when the R^2 values of -0.011 and -0.116 are examined. This can clearly be seen in the chaotic nature of Figure 10(c). This is very likely due to the chaotic and violent nature of the burning and vaporization process that occurs within the laser's focal point on the surface.

IV. CONCLUSION

From the results obtained, it can be seen there is a strong correlation to laser power, trace speed and channel depth. However, increases in power can negatively affect the channel quality and geometry creating channels that are less repeatable and have increased variability across their length; this makes higher laser powers unsuitable for the manufacture Galinstan carrying channels as it will create current bottlenecks in addition to increasing the channel resistance. In addition to higher power levels negatively affecting channel quality, lower trace speeds also had this effect. This effectively places a limitation on channel dimensions as in order to create deeper channels, repeatability and channel quality would need to be sacrificed. Further testing of the channel surface with respect to its interaction with the fluid Galinstan is currently being carried out to investigate how the material flows through and wets to the channel wall surface. Simulation and experimental work is also being carried out to investigate how the channels deform when undergoing mechanical stress, which is a vital piece of knowledge to know how the conductors would perform when in use.

VI. REFERENCES

[1] *Wearable Electronics Sensors: For Safe and Healthy Living*. Springer, 2015.

[2] R. Bringans, "Challenges and opportunities for the flexible electronics industry." Palo Alto.

[3] J. a Fan, W.-H. Yeo, Y. Su, Y. Hattori, W. Lee, S.-Y. Jung, Y. Zhang, Z. Liu, H. Cheng, L. Falgout, M. Bajema, T. Coleman, D. Gregoire, R. J. Larsen, Y. Huang, and J. a Rogers, "Fractal design concepts for stretchable electronics," *Nat. Commun.*, vol. 5, p. 3266, Feb. 2014.

[4] T. Liu, P. Sen, and C. J. Kim, "Characterization of nontoxic liquid-metal alloy galinstan for applications in microdevices," *J. Microelectromechanical Syst.*, vol. 21, no. 2, pp. 443–450, 2012.

[5] M. K. Armstrong, "PCB design techniques for lowest-cost EMC compliance. Part 1," *Electron. Commun. Eng. J.*, vol. 11, no. 4, pp. 185–194, Aug. 1999.

[6] K. Ren, J. Zhou, and H. Wu, "Materials for Microfluidic Chip Fabrication."

[7] S. M. Westwood, S. Jaffer, and B. L. Gray, "Enclosed SU-8 and PDMS microchannels with integrated interconnects for chip-to-chip and world-to-chip connections," *J. Micromechanics Microengineering*, vol. 18, no. 6, p. 064014, Jun. 2008.

[8] N. S. Shanmugam, G. Buvanashekaran, K. Sankaranarayanasamy, and K. Manonmani, "Influence of Beam Incidence Angle in Laser Welding of Austenitic Stainless Steel using Finite Element Analysis," *Multidiscip. Model. Mater. Struct.*, Jul. 2013.

[9] The British Standards Institution, "BS EN ISO 4287 - Geometrical product specification (GPS). Surface texture: Profile method. Terms, definitions and surface texture parameters." The British Standards Institution, 2000.

[10] C. K. Chung, Y. C. Lin, and G. R. Huang, "Bulge formation and improvement of the polymer in CO 2 laser micromachining," *J. Micromechanics Microengineering*, vol. 15, no. 10, pp. 1878–1884, Oct. 2005.

Appendix 2 – ADPL Commands for 3D Contained Hydrostatic Fluids

```
!   Commands inserted into this file will be executed just after material definitions in /PREP7.
!   Active UNIT system in Workbench when this object was created:  Metric (m, kg, N, s, V, A)
!   NOTE:  Any data that requires units (such as mass) is assumed to be in the consistent solver unit system.
! It is assumed that NO SYMMETRY effects are in this model.

fini
/prep7
*get,typemax,ETYP,,NUM,MAX     ! max defined element type
*get,realmax,RCON,,NUM,MAX     ! max defined real constant
*get,mat_max,MAT,,NUM,MAX      ! max defined material
*get,nodemax,NODE,,NUM,MAX     ! highest numbered node in model

! Create a new higher number for element type, real, and material
newnode=nodemax+1000           ! number for pressure node for HSFLD242
newnumber=typemax+1
*if,realmax,ge,newnumber,then
    newnumber=realmax+1
*endif
*if,mat_max,ge,newnumber,then
    newnumber=mat_max+1
*endif

et,newnumber,HSFLD242          ! 3-D Hydrostatic Fluid Element
keyopt,newnumber,1,0           ! UX, UY, UZ, plus HDSP at pressure node
keyopt,newnumber,5,1           ! Fluid mass calculated based on the volume of the fluid element
keyopt,newnumber,6,1           ! Incompressible
mp,dens,newnumber,6440         ! Density of Galinstan, kg/m^3
                                    ! Ignoring thermal expansion in this example
type,newnumber                 ! Ignoring TB,FLUID in this example
mat,newnumber                  ! Ignoring Reference pressure for compressible gas
r,newnumber,0.10156            ! Applying intitial atomospheric Pressure = 0.10156 N/mm^2
real,newnumber                 !

cmsel,s,FluidSurfaces1         ! Select nodes on interior
esln                               ! Select elements that touch these nodes
n,newnode,0,0,1.2e-002         ! Pressure node at 0,0,400 (automatically moved to centroid?)
ESURF,newnode                      ! ESURF HSFLD242 elements over solid element faces
                                   !     Extra node "newnode" with ESURF with HSFLD242
allsel
fini
/solu                              ! return to solving
```

Figure 9-1 ADPL Command to enable the generation of three dimensional hydrostatic elements required to simulate filled Galinstan Channels